H_2S AND CO_2 CORROSION OF SA-543 AND X65 STEELS IN OIL/WATER EMULSION

BY

MUHAMMAD NAUMAN ZAFAR

A Thesis Presented to the
DEANSHIP OF GRADUATE STUDIES

KING FAHD UNIVERSITY OF PETROLEUM & MINERALS

DHAHRAN, SAUDI ARABIA

In Partial Fulfillment of the
Requirements for the Degree of

MASTER OF SCIENCE

In

MECHANICAL ENGINEERING

MARCH 2014

KING FAHD UNIVERSITY OF PETROLEUM & MINERALS

DHAHRAN- 31261, SAUDI ARABIA

DEANSHIP OF GRADUATE STUDIES

This thesis, written by **MUHAMMAD NAUMAN ZAFAR** under the direction his thesis advisor and approved by his thesis committee, has been presented and accepted by the Dean of Graduate Studies, in partial fulfilment of the requirements for the degree of **MASTER OF SCIENCE IN MECHANICAL ENGINEERING.**

Dr. Luai M. Al-Hadhrami
(Advisor)

Dr. Rihan O. Rihan
(Co-Advisor)

Dr. Zuhair M. A. Gasem
Department Chairman

Dr. Zuhair M. A. Gasem
(Member)

Dr. Salam A. Zummo
Dean of Graduate Studies

Dr. Ihsan ul Haq Toor
(Member)

15/5/14

Date

Dr. Rami K.M. Suleiman
(Member)

Dedicated to my beloved parents, grandmother, brothers and my fiancé

ACKNOWLEDGEMENT

First of all I would like to thank Almighty ALLAH for bestowing me strength and knowledge to undertake this research and guiding me step by step till its completion. I am grateful to my parents and brothers for their untiring support and prayers. They were a source of inspiration and continuous support for me. I would like to thank to my fiancé for being on my side and encouraging me to finish my thesis.

I would like to thank my advisor Dr. Luai Al Hadhrami and my co-advisor Dr. Rihan O. Rihan for their continuous support and encouraging me to uptake this challenge and guiding me till the end of this research. I would like to thank my committee members, Dr. Zuhair, Dr. Ihsan and Dr. Rami for their guidance in this research work.

I would like to thank all my colleagues at Center of Research Excellence in Corrosion, Research Institute. Special thanks to my roommate Farooq Riaz for bearing me for 3 years and encouraging me to complete my write up. I would like to acknowledge the support of Ahmad Rafiq, Hussain Ali, Umar Khan, Omer bin Sohail, Mudassar Imam, Amir Hamza, Khobeb Muslim, Pamir Aly and Haroon Ashraf for making this journey memorable.

Finally I would like to acknowledge the support provided by Mr. Siddiqui, Mr. Abdul Quddus, Mr. Muneer, Mr. Hatim, Mr. Lateef and Mr. Sadaqat for helping me out during my experimental work.

TABLE OF CONTENTS

ACKNOWLEDGEMENT ..... **v**

TABLE OF CONTENTS ..... **vi**

LIST OF FIGURES ..... **viii**

LIST OF TABLES ..... **xii**

LIST OF ABBREVIATIONS ..... **xiii**

ABSTRACT ..... **xiv**

ABSTRACT ARABIC..... **xvi**

CHAPTER 1 INTRODUCTION **1**

1.1 Introduction 1

1.2 Thesis objective 6

1.3 Thesis structure 6

CHAPTER 2 LITERATURE REVIEW **7**

2.1 Literatures 7

2.1.1 H_2S and CO_2 corrosion 7

2.1.2 Rotating Cylinder 13

2.1.3 Flow Loop 18

2.2 University Research 23

2.3 Research Motivation 24

CHAPTER 3 EXPERIMENTAL APPARATUS **25**

3.1 Rotating cylinder electrode 25

3.1.1 Experimental setup 25

3.1.2 Procedure 26

3.1.3 Data reduction 30

3.2 Novel emulsion flow loop 32

3.2.1 Experimental setup 32

3.2.2 Procedure 56

3.2.3 Data reduction 64

3.3 Test material 66
3.3.1 Test area of RCE 68
3.3.2 Test area for flow loop 68
CHAPTER 4 RESULTS AND DISSCUSSIONS 71
4.1 Rotating cylinder electrode 71
4.1.1 Effect of $Na_2S_2O_3$, CO_2 and NaCl 71
4.1.2 Emulsion at different oil percentages 78
4.1.3 Effect of Velocities 82
4.1.4 Effect of Temperature 85
4.2 Flow loop 88
4.2.1 Effect of CO_2 emulsion corrosion 88
4.2.2 Emulsion at different oil percentages 92
4.2.3 Effect of velocity on corrosion 95
4.2.4 Effect of temperature on corrosion 98
4.2.5 Corrosion behaviour along the pipe length with D80 oil 101
4.2.6 Effect of oil viscosity on corrosion 105
CHAPTER 5 CONCLUSIONS AND RECOMMENDATIONS 109
5.1 Conclusion 109
5.1.1 Rotating Cylinder Electrode 109
5.1.2 Flow Loop 110
5.2 Recommendation 111
REFERENCES 112
VITAE 120

LIST OF FIGURES

Figure 3.1 Rotating shaft with working samples and impeller. 28

Figure 3.2 The experimental apparatus. 29

Figure 3.3 Emulsion flow loop. 33

Figure 3.4 Flow loop front view. 35

Figure 3.5 Flow loop test sections. 36

Figure 3.6 Electrodes positioning in test section. 37

Figure 3.7 Test sections dimensions in mm. 38

Figure 3.8 Preparation tank and mixer. 40

Figure 3.9 Autoclave. 41

Figure 3.10 Pumps. 44

Figure 3.11 Dosing Pumps. 44

Figure 3.12 pH chamber. 45

Figure 3.13 pH probe. 46

Figure 3.14 Control panel. 47

Figure 3.15 Flow meters. 48

Figure 3.16 A detailed drawing of the sample/specimen holder. 52

Figure 3.17 The electrode surface through a cross section of a test section. 52

Figure 3.18 Potentiostat. 53

Figure 3.19 Multiplexer. 54

Figure 3.20 Reference chamber. 55

Figure 3.21 A diagram illustrating the direction the flow (front view). 58

Figure 3.22 A diagram illustrating the direction the flow (top view). 59

Figure 3.23 A photograph illustrating the direction the flow (top view). 60

Figure 3.24 A photograph illustrating the direction the flow in the primary circulating loop. 61

Figure 3.25 Piping and instrumentation diagram (PID) of emulsion flow loop. 62

Figure 3.26 Milky emulsion in transparent pipe. 63

Figure 3.27 The microstructure of SA-543 steel. 67

Figure 3.28 The microstructure of X-65 steel. 67

Figure 3.29 Sample mounting. 69

Figure 3.30 Diagram to calculate exposed electrode area. 70

Figure 4.1 The potentiodynamic polarization curves of SA-543 and X65 steels in 0.01 M $Na_2S_2O_3$ solution with 30% oil at 1 m/s, and 25^{o}C after 24 hours. 73

Figure 4.2 Polarization resistance of SA-543 and X65 steels with time in 0.01 M $Na_2S_2O_3$ solution with 30% oil at 1 m/s, and 25^{o}C. 75

Figure 4.3 Corrosion rate measurement of SA-543 and X65 steels using the weight loss method in 0.01 M $Na_2S_2O_3$ solution with 30 % oil at 25^{o}C and 1 m/s. 77

Figure 4.4 The potentiodynamic polarization curves of SA-543 steel in different oil percentages with 0.01 M $Na_2S_2O_3$ solution at 25^{o}C and 1 m/s. 80

Figure 4.5 Polarization resistance of SA-543 steel with time in 0.01 M $Na_2S_2O_3$ solution with 30% oil at different oil percentages. 80

Figure 4.6 Corrosion rate measurement of SA-543 steel at different oil concentrations using the weight loss method. 81

Figure 4.7 The potentiodynamic polarization curves of SA-543 steel in 0.01 M $Na_2S_2O_3$ solution with 30% oil at 25^{o}C and different velocities. 83

Figure 4.8 R_P of SA-543 steel with time in 0.01 M $Na_2S_2O_3$ solution with 30% oil at 25°C and different velocities. 83

Figure 4.9 Corrosion rate measurement of SA-543 steel at different velocities using the weight loss method. 84

Figure 4.10 The potentiodynamic polarization curves of SA-543 steel in 0.01 M $Na_2S_2O_3$ solution with 30% oil at 1 m/s and different temperatures..... 86

Figure 4.11 R_P of SA-543 steel with time in 0.01 M $Na_2S_2O_3$ solution with 30% oil at 1 m/s and different temperatures..... 86

Figure 4.12 Corrosion rate measurement of SA-543 steel at 1 m/s and different temperatures using the weight loss method..... 87

Figure 4.13 The potentiodynamic polarization curves of SA-543 and X65 steels in 0.01 M $Na_2S_2O_3$ solution with 30% oil at 1 m/s and 25°C..... 89

Figure 4.14 R_p of SA-543 and X65 steels with time in 0.01 M $Na_2S_2O_3$ solution with 30% oil at 1 m/s and 25°C. 91

Figure 4.15 Corrosion rate measurement of SA-543 and X65 steels in 0.01 M $Na_2S_2O_3$ solution with 30 % oil at 25°C and 1 m/s..... 91

Figure 4.16 The potentiodynamic polarization curves of SA-543 steel in different oil percentages with 0.01 M $Na_2S_2O_3$ + CO_2 solution at 25°C and 1 m/s..... 93

Figure 4.17 R_p of SA-543 steel with time in 0.01 M $Na_2 S_2O_3$ + CO_2 solution at different oil percentages. 93

Figure 4.18 Corrosion rate measurement of SA-543 and X65 steels at different oil percentages. 94

Figure 4.19 The potentiodynamic polarization curves of SA-543 steel in 0.01 M $Na_2S_2O_3$ + CO_2 solution with 30% oil at 25°C and different velocities. 96

Figure 4.20 R_P of SA-543 steel with time in 0.01 M $Na_2S_2O_3$ + CO_2 solution with 30% oil at 25°C and different velocities..... 97

Figure 4.21 Corrosion rate measurement of SA-543 steel at different velocities..... 97

Figure 4.22 The potentiodynamic polarization curves of SA-543 steel in 0.01 M $Na_2S_2O_3$ + CO_2 solution with 30% oil at 1 m/s and different temperatures. 99

Figure 4.23 R_P of SA-543 steel with time in 0.01 M $Na_2S_2O_3$ + CO_2 solution with 30% oil at 1 m/s and different temperatures. 99

Figure 4.24 Corrosion rate measurement of SA-543 steel at 1 m/s and different temperatures. 100

Figure 4.25 Vena contracta demonstration. 102

Figure 4.26 The potentiodynamic polarization curve for Exxsol D80 oil at 30% Oil and 70 % 0.01 M $Na_2S_2O_3$. 103

Figure 4.27 Corrosion rate trend for Exxsol D80 oil at 30% Oil and 70% 0.01 M $Na_2S_2O_3$. 103

Figure 4.28 Corrosion rate of D80 oil at different electrode positions. 104

Figure 4.29 The potentiodynamic polarization curve for Exxsol D80 and D130 oils at 30% Oil and 70% 0.01 M $Na_2S_2O_3$. 106

Figure 4.30 Corrosion rate trend for Exxsol D80 and D130 oils at 30% Oil and 70% 0.01 M $Na_2S_2O_3$. 108

Figure 4.31 Corrosion rate of D80 and D130 oils at different electrode positions..... 108

LIST OF TABLES

Table 3.1 Chemical and physical properties of Exxsol D80 and D130 oils. 31

Table 3.2 Pumps specification. 43

Table 3.3 Flow-meter specification. 49

Table 3.4 Chemical Composition of SA-543 and X65 steels. 66

Table 3.5 Exposed area of test electrodes in different test sections. 70

Table 4.1 Tafel extrapolation data. 72

Table 4.2 Experimental series chart. 78

Table 4.3 Tafel extrapolation for different oil percentages 79

Table 4.4 Tafel extrapolation for different velocities. 82

Table 4.5 Tafel extrapolation for different temperatures. 85

Table 4.6 Tafel extrapolation for $Na_2S_2O_3$ and CO_2 89

Table 4.7 Tafel extrapolation for different oil percentages 92

Table 4.8 Tafel extrapolation for different velocities. 96

Table 4.9 Tafel extrapolation for different temperatures. 98

Table 4.10 Tafel extrapolation along the pipe length. 102

Table 4.11 Tafel extrapolation for different oils. 105

LIST OF ABBREVIATIONS

I_{corr}	:	Corrosion current
E_{corr}	:	Corrosion potential
βa	:	Anodic Tafel constant
βc	:	Cathodic Tafel constant
$Na_2S_2O_3$	:	Sodium thiosulphate
CO_2	:	Carbon dioxide
O/W	:	Oil-in-water emulsion
W/O	:	Water-in-oil emulsion
H_2S	:	Hydrogen sulphide
R_p	:	Polarization resistance
J_{corr}	:	Current density
RCE	:	Rotating cylinder electrode
FAC	:	Flow accelerated corrosion

ABSTRACT

Full Name : Muhammad Nauman Zafar

Thesis title : H_2S and CO_2 corrosion of SA-543 and X65 steels in oil/water emulsion corrosion

Major Field : Mechanical Engineering

Date of Degree : March, 2014

An experimental study was performed using rotating cylinder electrode and a novel emulsion flow loop to investigate the corrosion behaviour of SA-543 and X65 steels when exposed to emulsion containing oil and sodium thiosulphate ($Na_2S_2O_3$) solution along with carbon dioxide (CO_2). This study aimed at understanding the effects of hydrodynamics on corrosion. $Na_2S_2O_3$ was used to generate the hydrogen sulphide (H_2S). The emulsions were formed using 0.01 M $Na_2S_2O_3$ and Exxsol D80 oil. To mimic the well conditions, CO_2 was purged in order to maintain a pH of 5. Experiments were performed for different ranges of oil content, velocity, temperature, viscosity, and pipe diameter. Individual and combined effects of thiosulphate and CO_2 were also studied. It was observed that SA-543 steel was more corrosion resistant than X65 steel in the emulsion solution. Similar corrosion trend was found for both RCE and flow loop under the same test conditions. Iron sulphide film was formed on all the samples. Corrosion rates were reduced upon the introduction of CO_2 in the flowing fluid. The presence of oily phase dwindled the corrosion due to its inertness as oil is adsorbed on the steel surface. Increasing the velocity augmented the kinetics of reduction reaction thus forming sulphide film at higher rate and hence inhibiting the corrosion. Varying the temperature had a similar effect; corrosion dwindled by increasing the temperature due to the formation of stable sulphide films that are formed at higher temperatures. The corrosion

rate at downstream was less than at upstream due to higher perturbations at the inlet. The increase in oil viscosity led to increase in the corrosion rate and this is due to the higher shear stresses.

MASTER OF SCIENCE DEGREE

KING FAHD UNIVERSITY OF PETROLEUM AND MINERALS

Dhahran, Saudi Arabia

الخلاصة

الاسم: محمد نعمان ظفر

عنوان الرسالة: تسبب كبريتيد الهيدروجين وثاني أكسيد الكربون في تآكل الفولاذ SA-543و X65 في المستحلبات المائية / النفطية

التخصص الرئيسي: الهندسة الميكانيكية

تاريخ الدرجة العلمية: مارس 2014

تم إجراء دراسة تجريبية باستخدام قطب اسطواني دوار و جهاز تدفق حلقي جديد لم يتم إستخدامه من قبل لدراسة سلوك تآكل الفولاذ SA-543 و X65 ، عند التعرض لمستحلب يحتوي على النفط ومحلول ثيوكبريتات الصوديوم ($Na_2S_2O_3$) بالإضافة إلى ثاني أكسيد الكربون (CO_2). وتستهدف هذه الدراسة فهم آثار قوى الموائع على التآكل. وقد أستخدم ثيوكبريتات الصوديوم لتوليد كبريتيد الهيدروجين (H_2S). وتم تشكيل المستحلبات باستخدام 0.01 مل من ثيوكبريتات الصوديوم ($Na_2S_2O_3$) ، و الزيت Exxsol D80. ولمحاكاة ظروف البئر تم إضافة ثاني أكسيد الكربون (CO_2) من أجل الحفاظ على درجة 5 للأس الهيدوجيني. وقد أجريت التجارب على نطاقات مختلفة من محتوى الزيت ، والسرعة ، ودرجة الحرارة ، واللزوجة ، وقطر الأنبوب. وقد تم أيضا دراسة التأثير الفردي و الجماعي للثيوكبريتات وثاني أكسيد الكربون. ولوحظ أن فولاذ SA-543 كان أكثر مقاومة للتآكل من فولاذ X65 في محلول المستحلب. وقد تبين وجود نفس سلوك التآكل في كل من القطب الاسطواني الدوار و جهاز التدفق الحلقي في ظل نفس ظروف الإختبار. وتشكلت طبقة من كبريتيد الحديد على جميع العينات. وظهر تثبيط أكثر في عملية التآكل في التجارب اللتي تم إضافة ثاني أكسيد الكربون إليها. و أدى وجود الزيت إلى تضاءل التآكل بسبب وجود طبقة من الزيت على سطح الفولاذ. وتسببت زيادة السرعة في زيادة حركية تفاعل الاختزال وبالتالي تشكلت طبقة من الكبريتيد بمعدل أعلى مما ثبط التآكل. وقد كان لتغيير درجة الحرارة تأثير مماثل ، حيث تضاءل التآكل مع زيادة درجة الحرارة بسبب تشكل طبقات مستقرة من الكبريتيد والتي تتشكل عند درجات الحرارة العالية. وكان معدل التآكل في العينة الموجودة بالقرب من مدخل قناة الإختبار أكثر من العينة الموجودة بالقرب من مخرج قناة الإختبار بسبب زيادة الاضطرابات التدفقية عند المدخل. وأدت الزيادة في لزوجة النفط إلى الزيادة في معدل التآكل وذلك بسبب إرتفاع إجهادات القص.

درجة الماجستير في العلوم

جامعة الملك فهد للبترول والمعادن

الظهران - المملكة العربية السعودية

CHAPTER 1

INTRODUCTION

1.1 Introduction

Corrosion is defined as the degradation of metals through electrochemical processes. Losses due to corrosion are worth multi-billion dollars, with an estimated figure of $200 billion per year [1]. Corrosion has to occur as every element has tendency to go back to its stable state. One can not eliminate corrosion but can take measures to slow down the corrosion process. Corrosion of materials poses threat to plant safety and also affects the smoothness of production process. Corrosion is further classified according to the media they are exposed to, either it is dry or wet corrosion. There are multiple types of corrosion, but we will mainly focus on flow accelerated corrosion. This type of corrosion depends highly on flow conditions. In flow accelerated corrosion, the scale on the surface is eroded by the flow and thus exposing the bare metal to corrosion.

Flow in petrochemical, pharmaceutical, and process industries is usually a multiphase flow. Multiphase flow means that two or more phases are flowing at a moment. The characteristics of multiphase flow are different from single phase flow. Multiphase flow has certain flow patterns which are formed according to the two fluid velocities. Emulsion is a sort of multiphase flow, but the difference is that emulsions are formed by agitation. Emulsion exists in a metastable state, formed by mechanical agitation and the presence of surfactant molecules that diminish interfacial tension [2]. If you flow two fluids with different densities, they will remain separated during the flow. In case of emulsion, they will be usually mixed up. Emulsion is a mixture of two or more fluids that

are immiscible and remain suspended as dispersed particles. They are further classified into two types. i.e. i) Oil-in-water emulsion (O/W), ii) Water-in-oil emulsions (W/O). Their classification is dependent upon the dispersed phase. When oil is dispersed in water phase, this is known as oil-in-water emulsion and when water particles are dispersed in oil phase it is known as water-in-oil emulsions. The properties of the above two mentioned emulsions are different from each other. The type of emulsion is dependent on the fraction of one fluid into the other.

Emulsions are one of the essentials of our life, ranging from foods, cosmetics, pesticides, medicines, paints etc. Emulsions are usually formed to ease the extraction of oil and on the other hand emulsions form at the valves, flanges poses threat to the life of equipment. The corrosion and mechanical properties of emulsion are different from their constituent fluids. Emulsion corrosion has been observed to have higher corrosion rate as compared to individual oil water corrosion [3]. In this study we will mainly focus on oil-in-water emulsion, where water is present as a continuous phase; metallic corrosion is expected due to water. Since oil is known to wet metals, the destabilization of the emulsion at the interface could significantly alter the corrosion behaviour compared with aqueous water phase alone **[**4**,**5]. The corrosion rate may be affected also by changes in the rate of transport of oxygen from reactants to the metal surface, as a result to the presence of oil in the system [2,6-9].

CO_2 and H_2S gases are type of gases that exist in crude oil wells. Both gases form acids when combined with moisture. Corrosion due to CO_2 is known as sweet corrosion and sour corrosion is due to H_2S. The extraction of oil from sour wells is relatively expensive due to the higher refining costs in removing sulphur. But the high oil demands make the

extraction of H_2S containing oil highly essential. H_2S is a toxic gas with a rotten egg smell, and its exposure up to 15 ppm is considered hazardous. It is a poisonous, corrosive, heavier than air, and explosive gas [10]. H_2S is known to cause stress corrosion cracking (SCC) due to the brittlement of material via hydrogen ingress **[**11**,**12**]**. Corrosion in sour environment is usually initiated with the formation of iron sulphide film [11]. Iron sulphide scales are usually formed inside the sour well pipelines, and observed to have both corrosive and inhibitive properties. The film formation depends on temperature, where stable adherent films are formed at higher temperatures (> 80^oC) **[**11**,**13].

In petroleum industry, the sulphur present in sour crude oil, which is sometimes used as a feedstock for hydrocrackers, produces iron sulphide scale. The scale subsequently reacts with water and oxygen during shutdowns to form polythionic acids ($H_2S_xO_6$) and other oxyanions such as thiosulphate ($S_2O_3^{2-}$). Analogies have been established between polythionic acid cracking, where the most aggressive sulphur species is considered to be S_4O_6, and SCC in thiosulphate solution [14].

Corrosion due to CO_2 is known as sweet corrosion as it has no smell. CO_2 forms weak acid in aqueous media which causes internal corrosion in oil/gas pipelines. CO_2 has certain advantages along with its some detrimental effects. CO_2 is injected into the well to reduce the viscosity of oil and to increase the production of well [15-17]. This process is known as enhanced oil recovery. CO_2 corrosion usually involved the formation of iron carbide (Fe_3C) and iron carbonate ($FeCO_3$) with the evolution of H_2. Corrosion is substantially reduced when $FeCO_3$ is precipitated on the steel surface due to its dense and protective corrosion product film which acts as a diffusion barrier for corrosive species to travel to metal surfaces **[**15**,**18**]**. The nature of carbonate film is dependent upon alloy,

temperature, CO_2 partial pressure, and pH [19-25]. The increase in pH favors the formation of $FeCO_3$.

A new approach has been adapted in this research by using sodium thiosulphate ($Na_2S_2O_3$) instead of H_2S, since H_2S is a toxic and flammable gas, and requires special safety measures for its usage. This replacement made the study of H_2S effects at laboratory scale practically feasible. Thiosulphate is a non-toxic anion and found to be a good substitutent for H_2S. This idea was first proposed by Tsujikawa et al. [26] where he used sodium thiosulphate for stress corrosion cracking of low alloy steels. The results were in good agreement with the solutions containing H_2S. $S_2O_3^{2-}$ being metastable anion reduces to form H_2S gas at the metal surface. This reaction is spontaneous at open circuit potential of steel [11]. The exact disproportion reaction of thiosulphate is still ambiguous, but it is believed that the reduction of thiosulphate anion produces elemental sulphur and this elemental sulphur further combines with proton to form H_2S [11,15,27]. The formation of FeS on the surface is done from both elemental sulphur and H_2S. Mackinawite (FeS) is formed initially on the metal surface because the kinetics of Mackinawite formation are faster than any other FeS species [15,28-31]. This surface is loose, less adherent and rich in defects which contributes to good electron conductivity and sometimes also inhibits the anodic dissolution by hindering the movement of iron ions [11,15,32]. The formation of sulphide film on surface is dependent upon pH; with an increase in pH, the solubility of sulphide film is reduced, and the maximum sulphide precipitation occurs at pH 4. However the amount of mackinawite augments with time due to high stability [11].

Kappes et al. **[**27**,**33] quoted in his study that the H_2S generation rate was maximum for the 0.01 M $Na_2S_2O_3$. Increasing the concentration resulted in reducing the H_2S generation rate due to thick formation of sulphide film. The sulphide film was good catalyst for cathodic reactions. The film growth rate was also higher in thiosulphate solutions as compared to H_2S containing solutions **[**11**]**.

Pipelines at oil and gas facilities are affected by flow accelerated corrosion (FAC). FAC results in totally or partially removal of protective surface films and higher wear rate resulting in thinning of pipelines [34]. Most affected piping components by FAC are usually sudden expansion or contraction, orifice, valves, tees, elbows. This is due to severe changes in flow direction as well as the development of secondary flow instabilities downstream of these components [34-36]. The changes in fluid hydrodynamics, turbulence, wall shear stress, the formation and destruction of corrosion product film are all related to hydrodynamic boundary layer in the vicinity of metal substrate **[**37**]**.

Increasing demands leads to an increase in productions, and the increase in production requires high strength corrosion resistant materials in order to reduce the maintenance downtime. SA-543 is a high strength quenched and tempered steel. It is recently introduced in the construction of reactors in petrochemical plants. Usage of these types of materials will reduce the corrosion allowance to the wall and, reducing weight and increasing the capacity of equipment. SA-543 comprises of nickel, chromium and molybdenum. These three elements provide high corrosion resistance and enhance the performance. Chromium helps in formation of highly corrosion resistant stable oxide layer and molybdenum is used to augment pitting and crevice corrosion resistance **[**38**]**.

1.2 Thesis objective

The main objective of this thesis is to investigate the corrosion of SA-543 and X65 steels in hydrodynamic H_2S and CO_2 environments. Initial study will be performed using rotating cylinder electrode with oil/water emulsion. The emulsion corrosion will be studied for different oil percentages, velocities and temperatures. Once the trend of emulsion corrosion will be at hand, similar experiments will be performed using emulsion flow loop. Using flow loop, the effect of viscosity, pipe diameter, and corrosion along the length of vertical pipe will be investigated. Finally, a comprehensive analysis will be given for the above two techniques.

1.3 Thesis structure

This thesis is splited into 5 chapters started with introduction in which a brief introduction on emulsion, CO_2 and H_2S corrosion are highlighted. The second chapter provides a comprehensive literature review on emulsion corrosion, H_2S and CO_2 corrosion, using RCE and flow loop, with some of the renowned institutes that are working on erosion-corrosion. Third chapter comprises of a description for the rotating cylinder electrode setup and flow loop setup. Results and discussion is given in chapter four. At the end of thesis conclusions were listed in chapter 5 with some recommendations followed by references.

CHAPTER 2

LITERATURE REVIEW

A thorough literature survey was performed ranging from the H_2S and CO_2 corrosion in multiphase to the discovery of thiosulphate as H_2S replacement. Each aspect of $Na_2S_2O_3$ and CO_2 corrosion were meticulously gathered. The effect of pipe diameters, inlet sharpness, contraction, expansion, each and every aspect of pipeline corrosion was reviewed. This literature review is divided into two sections; first section deals with the published literature, and the second section highlights the current multiphase corrosion facilities around the globe.

2.1 Literatures

2.1.1 H_2S and CO_2 corrosion

Hamzah et al. [39] setup an experimental test for the erosion-corrosion of C-Mn steel. This steel is heavily used in petroleum industry. The C-Mn was tested with wet and dry carbon dioxide conditions with varying impact angles and insertion of sand particles. Material loss was augmented with the insertion of sand particles. For velocities below 50 m/s the erosion was dominated by scale setup and its removal and by substrate erosion for velocities greater than 50 m/s. The ferric carbonate scale formed due to wet carbon dioxide is weak in strength at temperature between 20 - 80ºC.

Perdomo et al. [40] studied the corrosion of API 5LB and X52 steels at both field level and laboratory scale when they are exposed to Furrial's crude oil from different wells in presence of H_2S and CO_2. The experiments were performed for different water cuts. The corrosion rates for both materials were almost the same with corrosion resistance of X52

steel being slightly greater. This higher resistance could be due to higher content of sulphur and manganese as compared to the API 5LB steel. Pitting on the materials was significant. Higher water cuts yielded higher corrosion and oil showed its natural inhibiting properties at low water cuts.

Ma et al. [41] studied the influence of H_2S on carbon steels using electrochemical impedance under varying conditions of pH, H_2S concentration and exposure time. By increasing the pH from 0.75 to 3.5, the charge transfer resistance was increased, which depicts the formation of inhibition sulphide film. When the specimen was exposed to higher exposure time (> 2hr) the probability of formation of sulphide film increased. H_2S augmented both the anodic and cathodic reactions. The sulphide films transforms from loose mackinawite film to firm and stable pyrite film with the passage of time.

Lee and Nesic **[**42**,**43] studied the effect of H_2S and CO_2 corrosion using impedance spectroscopy method. In Nyquist plots depressed semi-circles were found which suggested that the film formed on the surface was heterogeneous and rough and caused the non-uniform distribution of current density on the surface. Thin film of sulphide was rapidly formed on the surface and was reportedly classified as Mackinawite (FeS). Polarization resistance increased with time specifying the formation of film on the surface.

Brown and Nesic [44] highlighted the importance of scale forming on H_2S and CO_2 corrosion. The formation of mackinawite reduced the corrosion rate in all experiments. The precipitation values of iron carbonate and iron sulphide played a key role in

augmenting the corrosion values. The film composed of multi-layers in presence of carbon dioxide and hydrogen sulphide.

Fang et al. **[**45**]** studied the concentration effect of NaCl on corrosion. It was observed that the increasing the concentration of NaCl reduced the CO_2 corrosion rate as the salt slow down the anodic and cathodic reactions. Presence of high concentration of salt reduced the cathodic charge transfer reaction. Velocity didn't have any significant effect on corrosion at higher salinity concentrations.

Sun et al. [30] studied the kinetics of the scale formed in the presence of CO_2 and H_2S. The rate of precipitation of CO_2 was function of iron carbonate super saturation, solubility, temperature and surface area to volume ratio. For X65 steel using H_2S the corrosion rate increased initially but declined as the time proceed. The formation of Mackinawite was dominant and increased with H_2S concentration, but long exposures resulted in reduction in thickness. The precipitate of iron carbonate along with Mackinawite was only found for 0.1% H_2S and 50 ppm of Fe^{2+} concentrations. Corrosion rate was seen to be dependent upon the rate of scale precipitation.

Fang et al. [46] investigated the effect of elemental sulphur on corrosion. Elemental sulphur is usually formed by the contamination of hydrogen sulphide. Acidification reaction with water was observed at temperature higher than 80^oC. It was confirmed that the iron sulphide scale formed is mackinawite. The scale thickened as the time progressed. Localized corrosion was more pronounced.

Han et al. [47] conducted his study on the passive films that are formed in CO_2 environments on mild steel. Experiments were performed at 80^oC, 0.53 bar CO_2 pressure

and 1 wt.% NaCl. It took longer time approximately 55 hours for the passive film to be formed. As the passive film formed the corrosion potential increased dramatically. X-ray diffraction identified additional traces of Fe_3O_4 and magnetite along with major portion of $FeCO_3$.

Abelev et al. **[**48**,**49] performed experiments to test the effect of H_2S on iron in presence of CO_2 and 3 wt.% brine. At low H_2S concentrations (5 ppm) with CO_2 and temperature ranging from 25 – 55^oC it showed inhibitive properties. Corrosion rate augmented as the concentration of H_2S was increased. Higher corrosion rate were observed at elevated temperatures (~80^oC). In H_2S free, CO_2 saturated experiments at 85^oC XRD results revealed the presence of iron carbonate with traces of Fe_3O_4 and iron hydroxides.

Koteeswaran [15] in his master's thesis studied the effect of CO_2 and H_2S in oil pipelines. His experimentation was based on the testing of carbon steel at different pH and CO_2/H_2S concentrations. H_2S gas was generated using sodium sulphide. Higher corrosion rates were observed for the H_2S/CO_2 system than just H_2S alone. The protective film was formed at lower temperatures as FeS precipitates easier than $FeCO_3$. Corrosion rate of iron was increased by increasing the concentration of H_2S. Corrosion rate was observed to reduce with increase in pH. Passivation due to iron carbonate was diminished as the sample was introduced in H_2S solution. The dissolution of $FeCO_3$ might be due to under saturation of CO_2 in H_2S system.

Jingen et al. [50] studied the effect of H_2S to CO_2 ratio on the corrosion of N80 steel coupons. Corrosion rates were higher for CO_2 alone, but dwindled as the H_2S was purged. The corrosion rate increased as the ratio of pCO_2/pH_2S increased up to 100, and

then declined. From the EDS analysis, iron carbonate peaks were observed for CO_2 alone, and FeS peaks where the ratio of H_2S and CO_2 was changed. It was believed that the formation of FeS (mackinawite) film prevented the diffusion of ions and retards corrosion.

Wen-Fei et al. [51] tested the corrosion behaviour of 110S tube steel using high temperature and high pressure autoclave in presence of H_2S and CO_2. Under all test conditions different phases of iron sulphide were formed as corrosion products. All the corrosion processes were controlled by H_2S. The corrosion rate decreases up to 110^oC and further increase in temperature resulted in an increase in corrosion. It was believed that more adherent film was formed at 110^oC. Increase in CO_2 partial pressures transformed the compact fine grain into bulky one thus enhancing the corrosion rate.

Kappes et al. [33] studied the corrosion of carbon steel using thiosulphate solutions in acidified media along with brine. They generated H_2S gas from thiosulphate anions. It was revealed that the corrosion rate increased by increasing the thiosulphate content. Anodic and cathodic reactions were also augmented. H_2S was generated at the open circuit potential and thin iron sulphide was formed on all the samples. The cathodic reactions were enhanced in the presence of sulphide film. The H_2S evolution current rom thiosulphate was maximum for 0.01 M $S_2O_3^{2-}$ and decreased as the concentration was further increased. The reduction of $S_2O_3^{2-}$ to H_2S was greatly dependent upon pH. Corrosion rates were slightly higher for $S_2O_3^{2-}$ solutions as compared to H_2S saturated solutions.

Kappes et al. [27] explained the reaction paths that followed in the generation of H_2S from thiosulphate anion. They highlighted the kinetics of H_2S evolution to estimate the range of partial pressures of H_2S that can be simulated with thiosulphate solutions. It was concluded that H_2S was generated in thiosulphate solution when it becomes in contact with immersed steel. H_2S generation rate increased from 10^{-4} M to 10^{-2} M $S_2O_3^{2-}$, and then slightly decreased on further increase of thiosulphate molarity. By increasing the $S_2O_3^{2-}$ concentration from 10^{-4} to 10^{-3} M, the surface concentration of H_2S sharply increased. H_2S generation rate for all thiosulphate concentrations were above the sulphide content of film. Growing of iron sulphide film was faster in acid thiosulphate solutions. Maximum concentration of H_2S was found at the specimen surface.

Ning et al. [52] focused on the thermodynamic behaviour of mild steel corrosion under H_2S solutions. Mackinwite film was detected at 25^oC and pyrite at 60^oC. K_{sp} values increased initially due to changes in iron sulphide film. It was believed that the amorphous iron sulphide film changed to mackinawite. Kinetics of mackinawite were faster than other sulphide films, and can be found on short exposures. Pyrite was most likely found at higher pH and higher potentials.

Tanupabrungsun et al. [53] studied the mechanisms of CO_2 corrosion on mild steel using electrochemical and surface analysis techniques at temperatures between 80 to 200^oC. Higher corrosion rates were observed at pH 4 than at pH 6. For pH 6, the corrosion rate dwindled with time. Corrosion rate also retarded as the temperature was augmented from 80 to 200^oC. Dense crystals of $FeCO_3$ were formed at pH 6 which lowered the corrosion rate as compared to pH 4, where slight patches of crystals were formed. XRD results

revealed that at higher temperatures of more than 120^{o}C oxides of iron were also found along with iron carbonate.

Faichuk et al. [54] investigated the electrochemical properties of the sulphide films formed by thiosulphate solution on alloy 600. The passive film formed with 0.1 M $Na_2S_2O_3$ was composed of two layers with Cr rich inner layer and outer layer mixture of Ni and Fe. Corrosion resistance was dictated by the inner layer at all the potentials. The removal of $Cr(OH)_3$ resulted in reduced protection of inner layer and the porosity of outer layers was higher in all the cases.

Nazari et al. [55] investigated the effects of pH and temperature on the properties of corrosion product form on X70 steel by CO_2 corrosion. No carbonate film was detected at temperatures below 55^{o}C. As temperature increased to 60^{o}C, iron carbonate was found at all pH's. The increase in temperature resulted in an increased thickness of carbonate film and the most compacted film was observed at pH 6.5 and 75 ^{o}C. The formation of film was more dependent upon temperature than pH.

2.1.2 Rotating Cylinder

Tewari et al. [56] conducted a study on the sulphide films formed on carbon steel as it was exposed to the aqueous H_2S solutions. Erosion-corrosion environment was created with the help of rotating disk electrode. To avoid oxidization, Nitrogen was purged and then H_2S was introduced into the system. Experiments were performed up to 1.6 MPa and 120^{o}C. After each experiment the sulphides were descaled and weighed. Sulphide phase analyses were conducted using x-ray diffractometer and concentration of iron ions moved into solution using atomic absorption. It was observed that the rate of metal loss increased with the rotation speed but the amount of sulphide deposited on the sample

remained independent of the rotation speed. It was also confirmed that at high speeds less adherent film mackinawite was formed that can easily be peeled off. At low speed or stagnant conditions, tenacious pyrrhotite-pyrite film was formed which cannot be dissolved easily. If the surface was pre-conditioned with pyrrhotite-pyrite, no significant loss in weight was observed. Analyses also showed the dependence of hydrodynamic conditions on type of film formation.

Wikjord et al. [13] carried out a study to understand the deposition phenomenon of iron sulphide phases during Girdler Sulphide process. They conducted their research in a titanium autoclave which is resistant to corrosion and would not allow the passage of iron ions. Sample disk was dipped in autoclave mounted on a stirrer and rotated at 100 rpm. Autoclave was exposed to a pressure of 1.5 ± 0.1 MPa and three temperatures 308, 373, and 433^{o}K. It was observed that the iron phase changed from iron rich to sulphur rich phases. Temperature was directly proportional to the rate of sulphide phase transformation. The iron ions generated from the disk fell into the bulk solution, combined with SH^{-} ions and deposited on the titanium wall as FeS_2. H_2 was evolved from the overall reaction. The deposition phase of FeS_2 was pyrite at high temperatures and pyrrhotite at lower temperatures.

Neville et al. [57] experimentally investigated the erosion-corrosion behavior of three different steels naming carbon manganese steel, austenitic and duplex stainless steel. The erosion-corrosion rate was initially calculated using 100 m/s jet and then after some time silica particles were added to it. The addition of silica particles showed a sudden increase in the corrosion rate. Carbon manganese steel is more susceptible to erosion-corrosion, other two steels passive films have tendency to withstand. But with the addition of silica

particles, the passive film gets thinner. DC anodic potentiodynamic polarization was used to obtain the corrosion potential. It was also seen that impact angle have a complex response to corrosion rate.

Choi et al. [32] carried out experiments at laboratory level to investigate the complex effect of H_2S and CO_2 on corrosion of carbon steel. Experiments were carried out in a closed container containing carbon steel (AISI C1018) sample mounted on rotating disk electrode, platinum counter electrode, inlet and outlet for combined CO_2 and H_2S gases and Ag/AgCl reference electrode. To determine the acidity effects on the thin sulphide & carbonate film, tests were conducted at pH 3 and 4. The 1 wt. % NaCl electrolyte solution was deoxygenated by passing CO_2 for two hours before the samples were immersed. Experiments were conducted in three stages: initially the samples was exposed only to CO_2 (Stage 1) then after some time CO_2 and 100 ppm H_2S (Stage 2) and at last again to CO_2 (Stage 3). Electrochemical Impedance spectroscopy, Linear Polarization and Potentiodynamic tests were conducted at each stage corroborated by SEM scans. The results showed that at both pH 3 and 4, the corrosion rate decreased and potential increased with the addition of H_2S. This was also supported by the EIS and potentiodynamic scans. This decrease in corrosion rate was attributed to the formation of thin but tenacious iron sulphide film. At low concentrations, H_2S showed inhibition effect. From stage 2 to 3, the corrosion rate increased at pH 4 but it remained constant at pH 3. This unusual behaviour led to conduct another experiment at pH 3 altering the initial conditions and it was concluded that the initial exposure to CO_2 resulted in more anodic dissolution of iron thus forming firm film of iron sulphide film as compared to $CO_2 + H_2S$ initial exposure.

Arzola et al. [58] performed an electrochemical investigation of X70 steel in H_2S solution using electrochemical cell. NaCl in presence of H_2S reduced the steel impedance. Higher steel impedance was observed for H_2S alone. It is believed that a thin film of Mackinawite was formed. Corrosion rate dwindled with time as the concentration of H_2S was increased. For turbulent conditions, the corrosion rate declined when the rotor was stirred at 1000 rpm. Corrosion in stirred solution of H_2S was lower than the unstirred one.

Sun and Nesic [59] performed an experimental study and then propose a mechanistic model for H_2S corrosion. Mackinawite was mostly deposited on the steel surface. The retain ability of scale was dependent on both formation rate and removal rate of scale. Using H_2S, the corrosion rate increased with increase in velocity but as the time elapsed the corrosion rate declined significantly due to the formation of protective film. Corrosion rate was more pronounced at shorter exposure times. The erosion of sulphide film was observed in hydrodynamic experiments.

Tian and Cheng [60] studied the corrosion of X65 steel using RDE when it was exposed to oil and sand mixture. By increasing the rpm the corrosion potential moved towards noble direction and corrosion current slightly increased. Nquist plots showed an increase in charge transfer resistance as the rotational velocity increased. An increase in the cathodic current density and a decrease in anodic current density were observed with the inclusion of oil. Charge transfer resistance increased as the oil content was increased from 0 to 30 % oil. As oxygen is highly soluble in oil, the reduction reaction of oxygen was dominating and less solubility of iron ions inhibited the metal dissolution. Also the presence of sand particles accelerated the corrosion.

Tang et al. [61] carried the above mentioned study to see the combined effect of erosion and corrosion. X65 steel showed significant passive behaviour in static condition when oil-water emulsion stroked the electrode at 90^{o}. The anodic and cathodic current densities increased as the static conditions were changed to hydrodynamic (3 m/s). Metal loss was higher for sand-oil-water emulsion than oil-water alone. Maximum mass loss was observed for an impact angle of 45^{o}. Nyquist plots revealed that the polarization resistance dwindled as the concentration of sand was increased in oil-water emulsion.

Feyeri et al. [62] tested the corrosion of two different steels in three phase flow. They performed experiments in high speed jet flow. The results revealed that the impact of particles (Sand and water) eroded the siderite ($FeCO_3$) film. The film was thin at the point of impact and thickness increases as the distance increased from impact point. Loss of metal also augmented with an increase in velocity. Deeper attack was observed for normalised steel as compared to quenched and tempered steel. Hill like surface topography for ferritic-pearlitic materials and crater like shape for tempered martensite steel were observed. Martensite showed lower degradation rates as compared to ferritic pearlitic steels.

Zhang and Cheng **[**4**]** used rotating disk electrode technique to determine the corrosion of X65 steel in oil/water emulsion. Oxygen reduction was dominant in both oil containing and oil free solutions. The increase in rotational speed resulted in accelerated oxygen diffusion and thus cathodic reaction. Corrosion of steel dwindled in the presence of oily layer covering the steel surface. βc was slightly higher in oil-containing solutions. βa was reduced as the rotational speed was increased, similar trend was observed for oil-containing solutions. The potential moved toward positive direction. An increase in

corrosion current and a decrease in potential was found as the temperatures were elevated.

2.1.3 Flow Loop

Lotz and Postlethwaite [63] conducted their research on erosion-corrosion when fluid was allowed to flow through sudden expansion and contraction. Series of experiments were conducted on a slurry test loop consisting of heat exchanger, aeration tank, slurry pump, flow stratifier with and without silica sand. NaCl (3 wt. %) was allowed to flow through the flow loop and the solution was saturated with air, nitrogen and carbon dioxide. Weight loss and polarization resistance tests were performed and rate of mass loss was obtained along the length of test section. Much of the erosion-corrosion phenomenon was observed at the beginning of the constriction. In aerated conditions the oxygen mass transfer phenomenon was dominating due to the presence of rust film. Downward corrosion trend was observed in CO_2 saturated solution as compared to aerated one. The suspended particles were main attributers to the erosion of metal or film and it validated that corrosion rates are higher in presence of solids.

Zhou and Jepson [17] studied the dependence of corrosion rate on flow parameters in three phases; oil, water, and gas slug flow. It was observed that by increasing Froude number the bubbles appearing inside the pipe increased, thus their turbulence caused enhanced corrosion. Effect of oil on corrosion rate was similar upto 60 % of oil beyond that corrosion rate declined due to appearance of oil in continuous phase at the bottom. Erosion was mostly due to the impingement of the bubble particles. Pressure drop can be correlated to the corrosion rate in slug flow.

Jepson [64] studied the effect of flow characteristics on sweet corrosion in three phase horizontal pipes at high pressures. The importance of intermittent phases formed due to different fluids was highlighted because their properties were different from the native fluids thus behaved differently. Electrical resistance, linear polarization and metal coupons of 1018 carbon steel were used for corrosion measurements. For liquid flow, corrosion rate augmented with increase in partial pressures of carbon dioxide and velocity. Increase in temperature up to 60^{o}C showed the increase in corrosion for saltwater only, beyond that it declined due to formation of protective iron carbonate film. In case of oil only, the corrosion tended to increase with temperature. Slug flow had larger effect on corrosion in flow regimes pattern. Increased in Froude number resulted in increased turbulence and caused enhanced corrosion.

Vuppu et al. [65] conducted their research to determine the effect of temperature on corrosion rates in sweet corrosion and to determine the corrosion products formed under varying conditions. For full pipe horizontal flow at 80^{o}C, the corrosion rate became constant after around 24 hours. Majority of the work was compared with the de Waard and Milliams equation and shows good comprise. Corrosion rate increased with temperature in presence of CO_2, but after 60^{o}C it started to decline due to formation of carbonate film. For a fixed composition of salt water and oil, the corrosion rate increased 5 times upon doubling the temperature. At increased CO_2 partial pressure, higher corrosion rate along with cracks and no carbonate film was observed. The single phase correlations gave huge error when applied to multiphase flow at large diameters.

Jepson and Menezes [3] studied the corrosion in three phase horizontal flow by varying the viscosities of oil. Oil with viscosities ranging from 2 cp to 96 cp was under

consideration. It was observed that the increase in velocity increases corrosion and the increase in oil composition resulted in an increased corrosion rate up to 60% of oil, beyond 60 % oil there was negligible corrosion. For slug flow, increased Froude number showed increase in corrosion rate due to higher turbulence. Higher void fraction was observed at bottom at higher Froude number. Viscosity was inversely proportional to the amount of bubble entrainment.

Gopal et al. [66] studied the mechanisms that lead to enhanced corrosion in horizontal multiphase slug flows. Experiments were conducted on two different diameter pipes with ranging composition of oil/gas, and velocities. Slug flow was initiated with the introduction of CO_2. It was observed that the pulses of bubble formed when stroked the bottom of the pipe made a phenomenon similar to the cavitation process. They eroded the corrosion products and caused increased shear stresses. Direct relation of Froude number with corrosion rate was found.

Kang et al. [67] investigated the behaviour of corrosion when multiphase flow is allowed to flow in an inclined channel. They carried out their experiments using inclinable flow loops with brine, water, oil, and CO_2. It was observed that the slug flow dominates in inclined pipe thus the flow pattern is dependent on the inclination of pipe. Due to slug flow it had a considerable impact on corrosion inside. The higher velocity of liquid resulted in higher slug frequency but the opposite was in case of gas; increase in gas velocity reduced the slug frequency. Higher corrosion rate was observed for higher Froude numbers.

Jepson and Bhongale [68] conducted the parametric study on the corrosion rate due to multiphase slug flow in 10 cm 316 stainless steel pipe. They conducted experiments for different temperature, pressure and oil compositions. The corrosion rate was seen to increase with the increase in temperature and carbon dioxide partial pressure. No upper limit of corrosion rate was found as depicted in other literatures. For oil compositions between 0 to 40% the corrosion rate tend to decrease at lower rate but after wards a sudden sharp decrease and negligible at 80% oil.

Zhang et al. [69] developed a model to predict the sweet corrosion in multiphase (oil/water/gas) flow. The model was established incorporating all electrochemistry, reaction kinetics and mass transport effects. The established model was compared with the existing experimental data available at Ohio corrosion multiphase center for 2 cP oil. Good conformity of the model with experimental data was seen. For mass transfer in turbulent flow, it was observed that the turbulence effect has to be added to get good harmony of results.

Hernandez et al. [70] performed an experimental study using dynamic field tester to investigate H_2S and CO_2 corrosion induced by flow in crude oil wells. Different materials were placed in line of flow on two different pipe diameters connected to each other. It was found that material with higher chromium content showed higher corrosion resistance. Dominant effect of water cut on corrosion was observed, higher values of water lead to an increase in corrosion rates. Corrosion rate tend to decrease with increase in pipe diameter due to decrease in Reynolds number. The effect of H_2S was dominant at higher temperatures resulting in inhibiting corrosion. At temperatures ($> 60^oC$), formation

of iron carbonate was influential. The formation of film was dependent upon the partial pressures of both H_2S and CO_2.

Brown et al. [71,72] performed experiments on flow loop to study the effect of trace amounts of H_2S in multiphase flow. The corrosion rate was higher at 3 ppm of H_2S and retarded when increased to 15 ppm. This trend was not observed in single flow. Higher corrosion rates were observed in multiphase flow as compared to single flow. Characterisation results revealed that the production of thin film was responsible for the reduction in corrosion. The formation of film was also dependent upon temperature.

Habib et al. [73] performed simulations on the erosion and penetration rates of pipe protruded in sudden contraction. Erosion phenomenon became significant at velocities higher than 3 m/s. Higher corrosion rates were observed for velocity up to 8-10 m/s in protruding pipe. Erosion of protruding area was enhanced by the inclusion of particles. Erosion rate was inversely proportional to protruded pipe depth and thickness. Lower corrosion rate up to 40% were observed by increasing the hardness of material by 60%.

Brown et al. [74] performed series of flow loop experiments for a month at 60^oC, 7.7 bar partial pressure of CO_2, pH 6, 1wt.% NaCl and partial pressure of H_2S from 0.1 mbar to 1mbar. It was concluded that the galvanic couple between protective and non-protective areas on corrosion product film is not possible without surface film failure. The surface corrosion product film can be assumed to have lateral strength. Iron carbonate was observed to retard the corrosion rate in presence of trace amount of H_2S. Dissolution of iron carbonate was found in the presence of H_2S which was in some way helpful to

increase the thickness of iron sulphide film. Localised corrosion attack is possible by the breaking of iron sulphide film.

Nor et al. [75,76] determined the corrosion rate of API X65 carbon steel in high CO_2 environments using RCE and flow loops. Corrosion rate was significantly higher for 50^oC than for 25^oC at 10 bar and pH of 4. The increase in rpm resulted in increase in an corrosion rate but there was no significant difference at higher rpms. Corrosion rate increased slightly for all the rpms as the pH was decreased to 3. Iron carbide was seemed to be formed and it didn't provide any sufficient protection. Anodic reaction was flow insensitive.

2.2 University Research

Institute for corrosion and multiphase technology (ICMT) at Ohio University is one of the renowned corrosion research centres. They have H_2S multiphase corrosion flow loop, inclinable multiphase corrosion flow rig, wet gas corrosion flow loop and transparent multiphase corrosion flow loop. They are mainly focusing on H_2S and CO_2 corrosion in multiphase and single flow [77].

Erosion corrosion research center at university of Tulsa is mainly focusing on erosion corrosion testing using impingements test and flow loop. CO_2 corrosion is mainly under investigation [78].

Fontana research center at Ohio state university is mainly focusing on corrosion of different steel alloys and corrosion after different surface treatments. They don't have any large corrosion setup or multiphase flow loop [79].

Corrosion center at Curtin university is mainly focusing on top of the line corrosion (TLC), under deposit corrosion, sour service research and coatings research [80].

2.3 Research Motivation

The main motivation behind this research is that the above mentioned literature and the research institutes do not cater emulsion corrosion. The effect of thiosulphate has not also been studied in emulsion or multiphase flow. This research was carried out to address the issue of emulsion corrosion in the presence of thiosulphate. A novel emulsion flow loop was fabricated to mimic emulsion flow in vertical pipes. The advantage of flow loop is that it mimics the same flow conditions at research scale and help in finding better solution to the problem.

CHAPTER 3

EXPERIMENTAL APPARATUS

Erosion–corrosion phenomenon can be studied using three methods i-e. i) Rotating Cylinder Electrode (RCE) ii) Flow Loops and iii) Impingement tests. The current corrosion investigation was performed using rotating cylinder electrode and flow loop. Rotating cylinder electrode will be discussed in this chapter and flow loop in the next chapter. The corrosion behaviour is totally different in static and hydrodynamic conditions thus rotating cylinder electrode is a convenient method to study the corrosion under hydrodynamic conditions.

3.1 Rotating cylinder electrode

3.1.1 Experimental setup

As our experiments involves the formation of oil-water emulsion. The RCE setup was customized and fabricated in Research Institute, KFUPM workshop. As shown in Figure 3.1 the shaft was customized to hold two specimens i.e. one for electrochemical measurements and the other one for weight loss. The shaft was fabricated using SS 316 and then Teflon cover was press fitted on it. The electrochemical measurement sample (working sample) has the least clearance with the SS 316 shaft to ensure maximum conductivity and to avoid any loop hole for crevice corrosion. The internal diameter of weight loss sample was slightly greater than the working sample. Teflon tape was wrapped beneath the weight loss sample to completely insulate it from the SS 316 shaft. The conductivity of both the samples was measured using resistance meter. Electrochemical measurement sample showed zero resistance and for the weight loss

sample the resistance was in mega ohms. Weight loss sample was placed first followed by Teflon washer then working sample then again washer followed and were tightened by a Teflon screw cap.

The key element on the rotating shaft was the impeller. As we know oil and water are immiscible, the impeller is solely responsible for the formation of emulsion and to avoid oil-water separation. The impeller was made up of stiff wires curled around each other and was placed above the weight loss sample on the rotating shaft.

3.1.2 Procedure

The experiments were conducted in a corrosion cell as shown in Figure 3.2. To make corrosion cell top closed, the rotating shaft was mounted in a bearing which was then fixed in a hard Teflon cork. The ball bearing was placed to provide friction free environment to the shaft. A small hole was made in the hard Teflon cork for the placement of counter electrode. The counter electrode was made up of Hastelloy C276 and it was given circular shape to provide the uniform current distribution to the working electrode. Working sample shaft was passed through the center of circular counter electrode. Ag/AgCl was used as a reference electrode. The reference and counter electrodes were placed near to the rotating working sample to reduce the uncompensated resistance. The holes of glass cell were sealed using corks. Bubbler was placed in the cell for dearation and purging of CO_2. Gamry rotating motor was attached at the top of the shaft.

1 L of solution was used for each experiment and the impeller and samples were immersed in the solution. It was ensured that while the shaft is running the samples are

still wetted/immersed by the solution. The CO_2 was used for the deaeration purposes and to maintain the pH of 5. Temperature was maintained constant at 25°C.

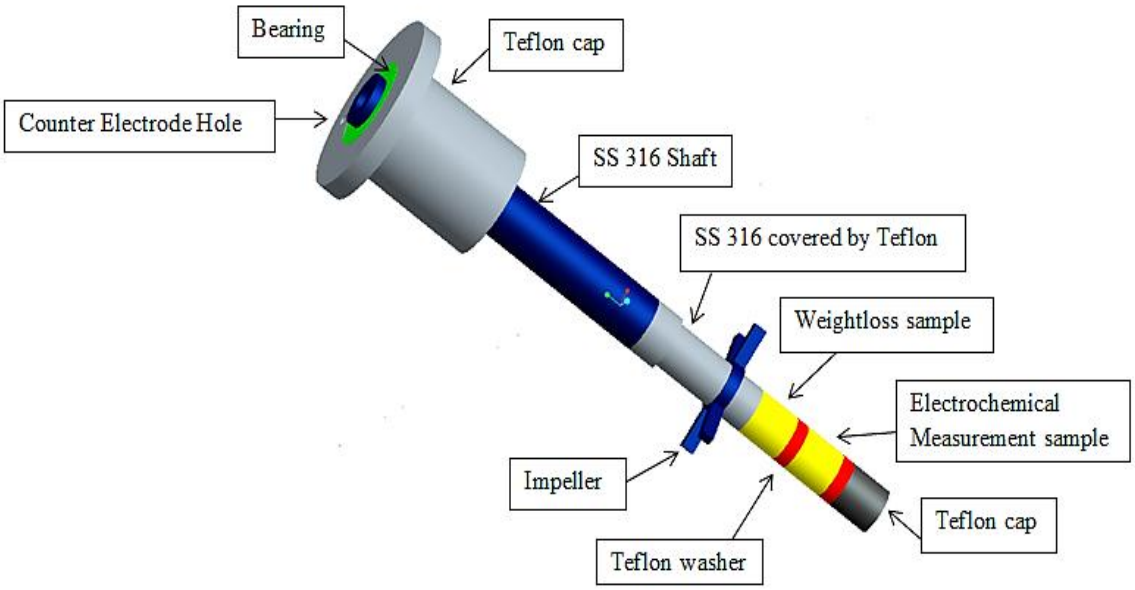

Figure 3.1 Rotating shaft with working samples and impeller.

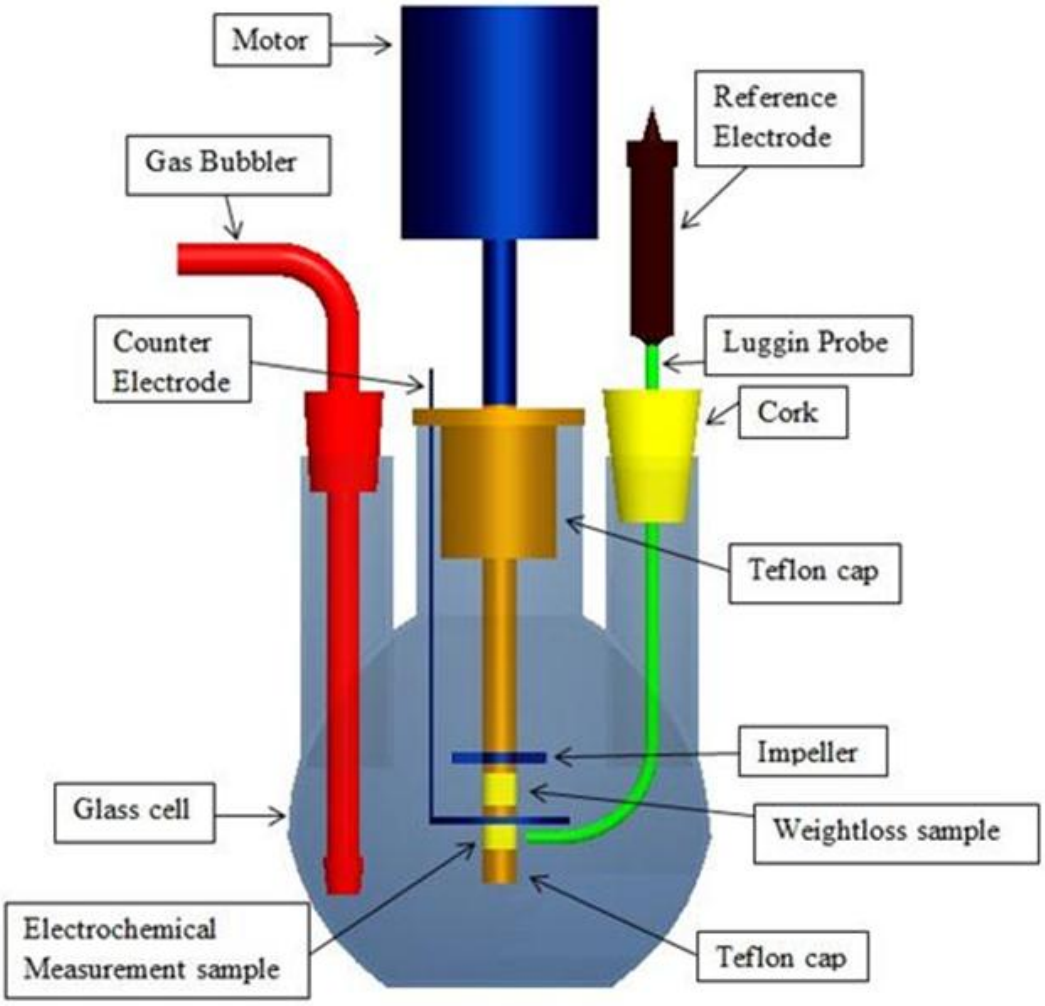

Figure 3.2 The experimental apparatus.

3.1.3 Data reduction

All electrochemical measurements were performed using AUTOLAB potentiostat 128N. Each experiment was lasted for almost 24 hours. Open circuit potential (OCP) was measured for the first two hours so that the potential of the system get stabilized, afterwards linear polarisation resistance (LPR) was measured after every 30 minutes. The potential was allowed to sweep from -15 to 15 mV against OCP at a scan rate of 0.167 mV/s. After 31-32 LPR readings, potentiodynamic polarization was performed with potential ranging from -75 to 75 mV against OCP at a scan rate of 0.167 mV/s.

The corrosion rate measured by weight loss was calculated using Equation 3.1:

$$CR = \frac{K \times W}{A \times t \times \rho} \tag{3.1}$$

Where K = 8.76 x 10^6 (mm m^{-1}) (h y^{-1}) is a unit conversion constant to convert the units of CR to mm y^{-1}, t is the time of exposure in hours, A is the exposed area of the electrode in m^2, W is the mass loss in kg, and ρ is the specimen density in kg m^{-3}.

Testing

Experimental tests were performed using Exxsol D80 oil and 0.01 M $Na_2S_2O_3$ solution. The chemical and physical properties of Exxsol D80 oil and D130 are shown in Table 3.1. The main aim of these experiments is to see the behaviour of two steel grades (X65 and SA-543) when exposed to emulsion in presence of harsh environments like H_2S and CO_2. $Na_2S_2O_3$ was used instead of toxic H_2S [26-27,33,67]. $Na_2S_2O_3$ concentration of 0.01 M was selected due to high H_2S generation rate at this concentration [11,27]. The two steel grades were tested in an emulsion solution of 30% oil mixed with 0.01 M

$Na_2S_2O_3$ at 25 ^oC and 1 m/s (1 m/s approximately corresponds to 1909 rpm according to a diameter of 10 mm). Also, the addition of NaCl, CO_2, and NaCl + CO_2 to the 0.01 M $Na_2S_2O_3$ solution was investigated. The solution was bubbled with CO_2 gas during the experiments, which involve CO_2. The pH of the solution was 5.

Table 3.1 Chemical and physical properties of Exxsol D80 and D130 oils.

	Exxsol D80	**Exxsol D130**
Colour	Transparent	Transparent
Initial Boiling Point	237 ^oC	279 ^oC
Flash Point	82 ^oC	140 ^oC
Density (15.6 ^oC)	0.795 g/ml	0.827 g/ml
Kinematic Viscosity (25 ^oC)	2.18 mm^2/s	6.89 mm^2/s
Aromatic Content	0.2 wt. %	1 wt. %

The steel grade which showed higher corrosion resistance was further investigated at various oil concentrations, velocities and temperatures in order to assure the maximum reliability for possible scaling up to a real industrial application.

3.2 Novel emulsion flow loop

3.2.1 Experimental setup

The experimental work was performed using a novel emulsion flow loop. The whole emulsion flow loop is made up of Hastelloy C-276 as shown in Figure 3.3. The witted parts of the emulsion flow loop are Hastelloy C-276 and PTFE (Teflon). These materials were chosen because of its high corrosion resistance to most corrosive environments. Hastelloy C–276 is a special alloy of high content nickel alloy. This alloy is very expensive and has high corrosion resistance to many corrosive environments. Teflon is a polymer material which has high corrosion resistance to almost all chemicals and can stand a temperature as high as 260^{o}C. The operating temperature and pressure should not exceed 180^{o}C and 20 bar respectively, since these are the safety limits for the weakest component of the loop (the flowmeter and the autoclave)

The main components of the flow loop are the mixing tank, autoclave, test sections of 4 different diameters, transparent pipe, and Hastelloy C-276 pumps. Two pumps are installed on the flow loop, in order to achieve higher flow rates. The flow was monitored using the magnetic flow-meters. Heaters are placed on the outlet wall of autoclave and mixing tank. For the formation of emulsion, special spiral static mixers are inserted below the entrance region of each test section. These spiral mixers help in the uniform formation of oil-water emulsion. The detailed description of flow loop components is mentioned below:

Figure 3.3 Emulsion flow loop.

Test Section: The test section is the most important part of the loop. The flow loop comprised of 4 test sections of 0.5'', 1'', 1.5'', and 2'' diameters. The test sections are shown in Figure 3.4 and Figure 3.5. The middle test section consists of both 1'' and 0.5'' diameter pipes. The outer most test sections are of 1.5'' and 2'' diameters as shown in Figure 3.5. 1.5'' and 2'' test sections are 1200 mm long with an option of electrode positioning at inlet, middle, and exit as shown in Figure 3.5. Similar electrode positioning is available for 1'' and 0.5'' pipes which are 800 mm and 400 mm long respectively as shown in Figure 3.6. The test sections can be used to study the effect of sudden expansion and contraction of flow on the corrosion behaviour of emulsion. The middle test section can be used to study the corrosion kinetics at high speed (> 6 m/s). The electrode placement at different positions along the pipe helps us to study the corrosion behaviour of developing and developed flow. The rest of the piping in the flow loop is 1''. Transparent pipe is installed to see the flow pattern and to ensure that uniform emulsion is formed. The transparent pipe section cannot be used at high pressures. The red electrodes are working electrodes and green ones are counter electrodes as shown in Figure 3.6.

Figure 3.4 Flow loop front view.

Figure 3.5 Flow loop test sections.

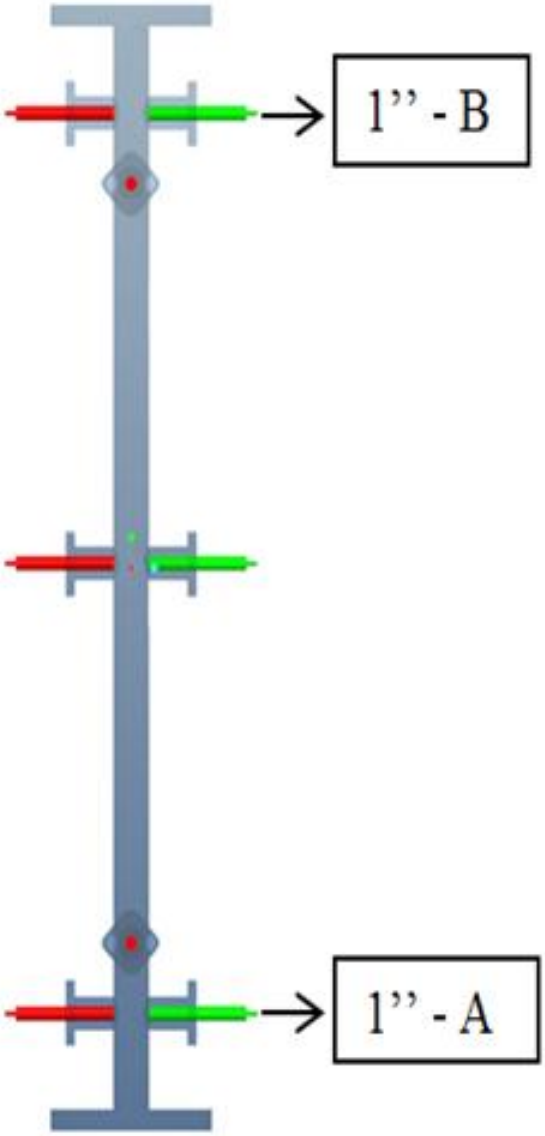

Figure 3.6 Electrodes positioning in test section.

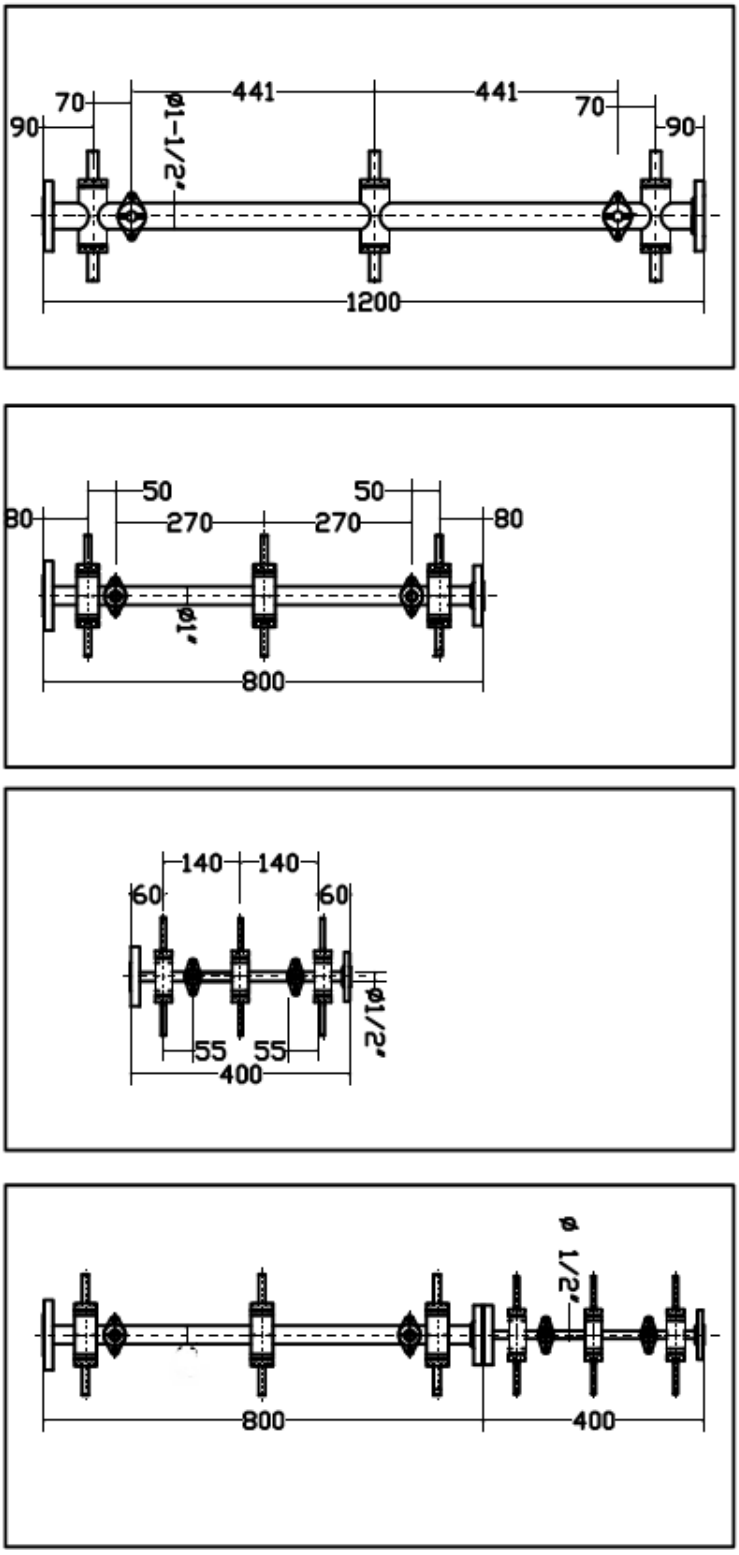

Figure 3.7 Test sections dimensions in mm.

Main Frame: The main frame was made up of stainless steel to hold the components of flow loop. Rollers were placed beneath the frame for easy movement of the loop.

Gas Cylinders: CO_2 gas cylinder was placed on the frame and nitrogen gas cylinder was attached to the back side of the frame. Special lock system was designed on the flow loop frame to firmly lock the cylinders in place.

Preparation tank: The preparation tank was made up of Hastelloy C-276 with diameter of 300 mm and 800 mm height. Preparation tank was fixed with mixer to help in the formation of emulsion. Solutions were initially poured into the preparation tank, and then transferred to the autoclave. The photograph of the preparation tank and mixer is shown in Figure 3.8.

Autoclave: The autoclave act as a reservoir for the solution. The autoclave was 300 mm in diameter and 650 mm in height, and it can bear up to the pressure of 20 bars. The photograph of the autoclave is shown in Figure 3.9. Injection of gases took place in autoclave. Gas inlet was provided at the bottom, for insertion of gases.

Heater: Heater jackets were placed on both the preparation tank and the autoclave. The heater was operated by the control panel. A thermocouple was placed inside the heater jacked as shown in Figure 3.9 which was directly touching the both of metal. The heater and the thermocouple were connected to a temperature controller in order to control the temperature of the experiment.

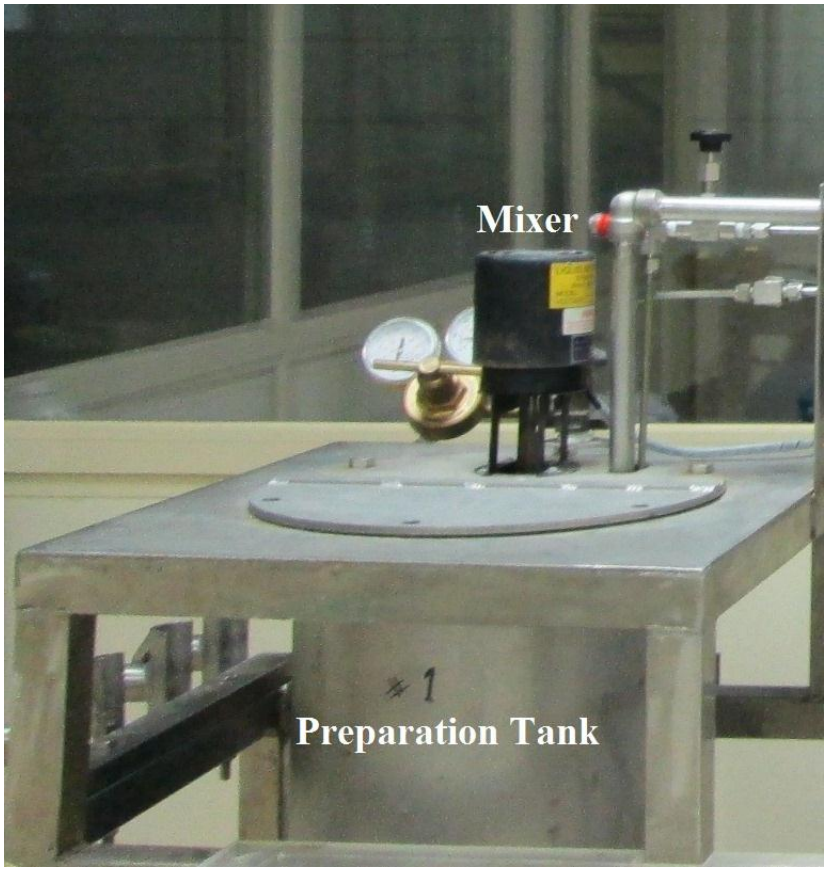

Figure 3.8 Preparation tank and mixer.

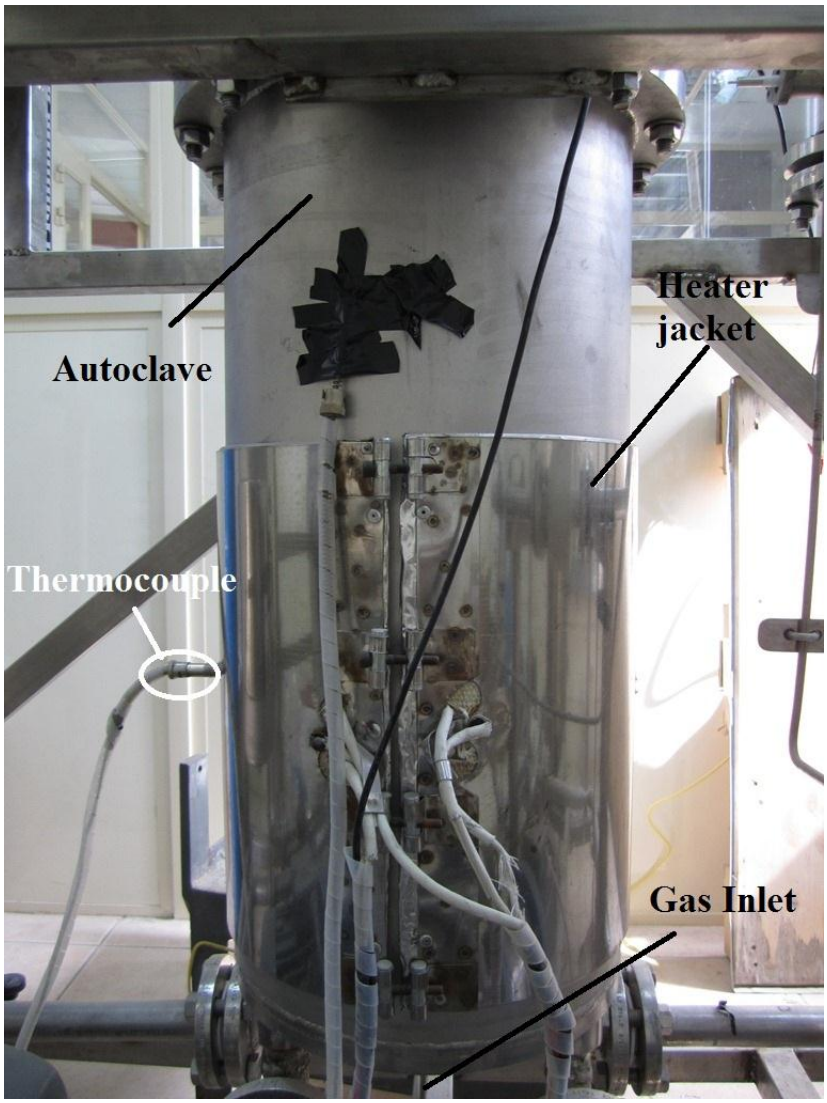

Figure 3.9 Autoclave.

Pumps: Two gear pumps were used in this flow loop, transfer pump and circulating pump, as shown in Figure 3.10. The transfer gear pump is used to transfer solution from preparation tank to the autoclave, and the circulating pump is used to circulate the solution in the flow loop. The two pumps can be run at a time for high velocity flows. The specifications of the pumps are mentioned in Table 3.2.

Chemical dosing pumps: Two dosing pumps were installed on the flow loop as shown in Figure 3.11 to maintain adjust the required pH. One for dozing hydrochloric acid (HCl) and one for dozing sodium hydroxide (NaOH) solution in order to adjust/control the pH to the required value.

pH probe: pH probe was installed to continuously monitor the pH of the emulsion. When the emulsion is flowing in the test sections, the emulsion rises from a thin tube to the pH chamber and falls back into the autoclave from the top of the pH chamber as shown in Figure 3.12.

Control panel: Control panel as shown in Figure 3.14 contains all the switches of flow loop, pumps panel, heater and pH meter were all installed on the control panel. Control panel was placed in a separate operating room.

Flow-meters: There were three magnetic flow meters to determine the velocity of the solution, one for each test section line as shown in Figure 3.15. The magnetic flow meter has a wafer style flow tube lined with perfluoroalkoxy (PFA). The flow meter measurement range is 0–12 m/s. It can stand a maximum temperature of 180^{o}C, and a maximum pressure of 3.5 MPa. Flow-meter specifications are mentioned in Table 3.3.

Table 3.2 Pumps specification.

	Transfer Gear Pump	**Circulating Gear Pump**
Liquiflo Gear Pump	H7FH1PEEU000004	H9RH1PEEU000004
Hastelloy / Peek	Magnet Coupling	Magnet Coupling
Housing	Hastelloy C	Hastelloy C
Shaft	Hastelloy C	Hastelloy C
Tooth wheel 1	Hastelloy C	Hastelloy C
Tooth wheel 2	Teflon	Teflon
Bearing	Teflon	Teflon
Suction size	3/4" NPT	1" NPT
Discharge size	3/4" NPT	1" NPT
Capacity	35 L/min	50 L/min
Pressure	6 bar	6 bar
System Pressure	15.5 bar	16 bar
Temperature	-40 to +260°C	-40 to +260°C
Viscosity	10 cP	100 cP
Voltage	230/400V, 60 Hz	230/400V, 60 Hz
Power	1.5kW / 1750 U/min	1.5kW / 1750 U/min
Protection	Class IP55	Class IP55

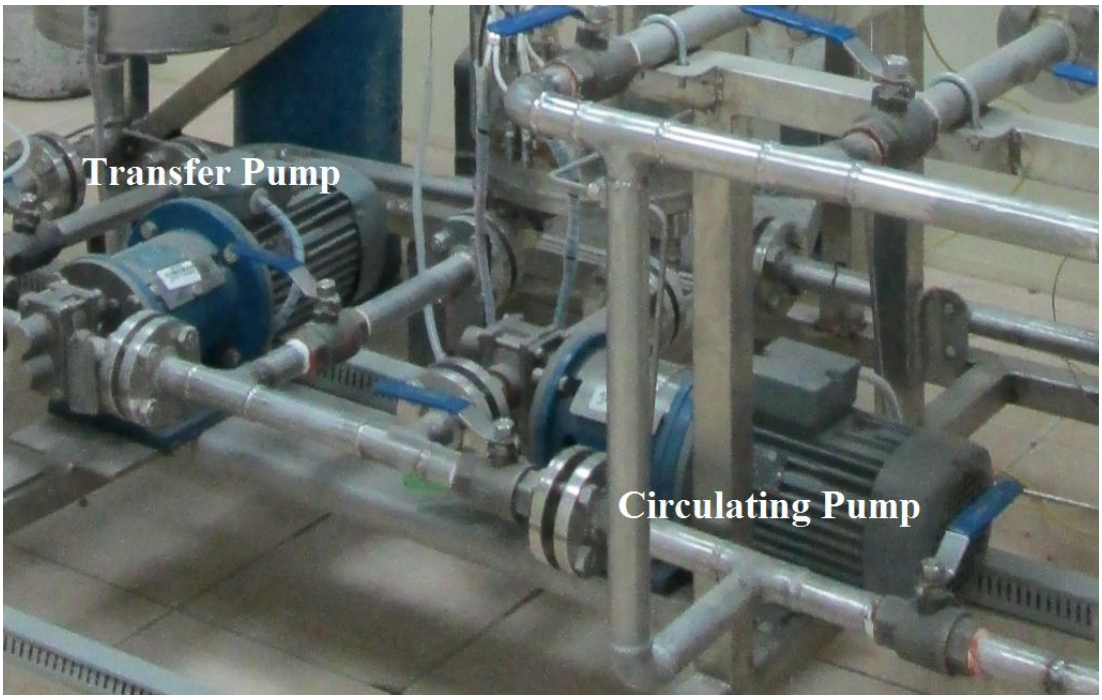

Figure 3.10 Pumps.

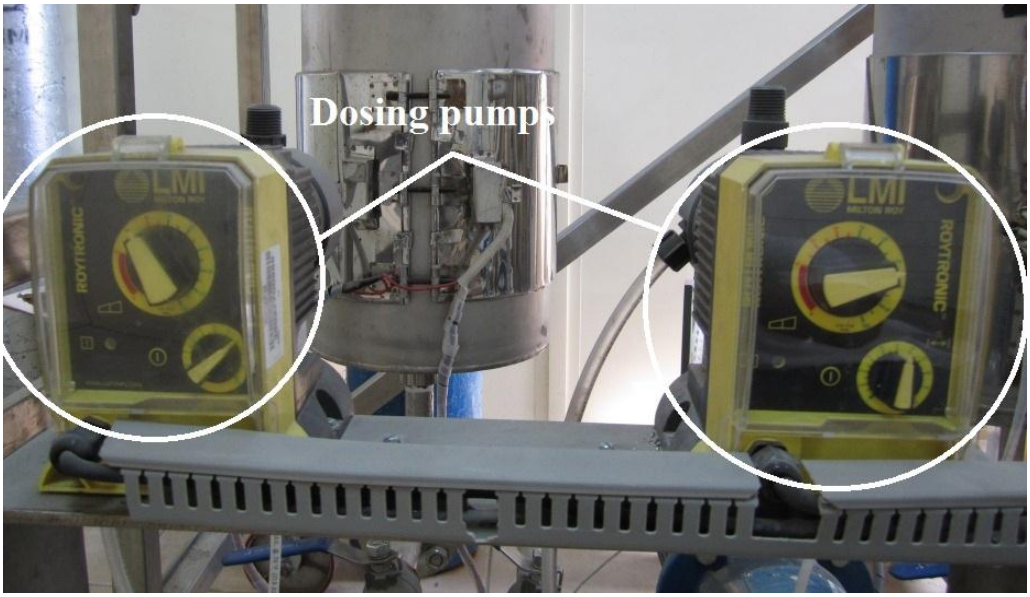

Figure 3.11 Dosing Pumps.

Figure 3.12 pH chamber.

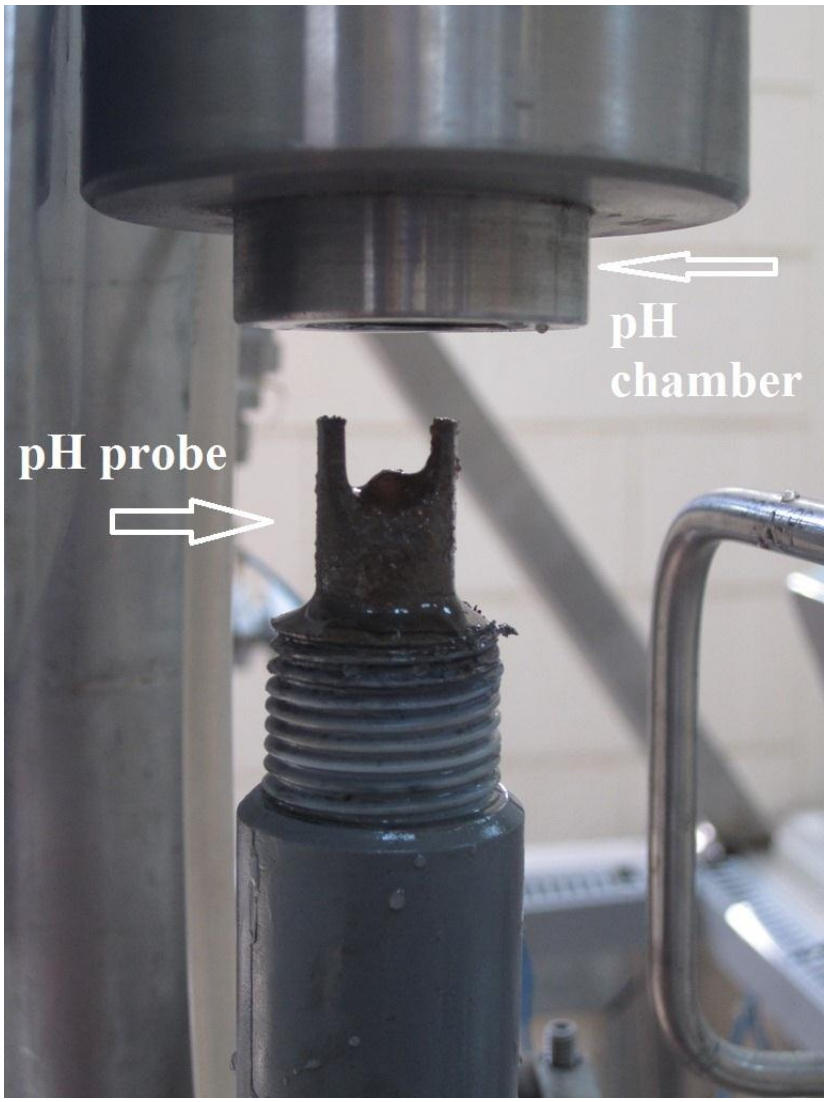

Figure 3.13 pH probe.

Figure 3.14 Control panel.

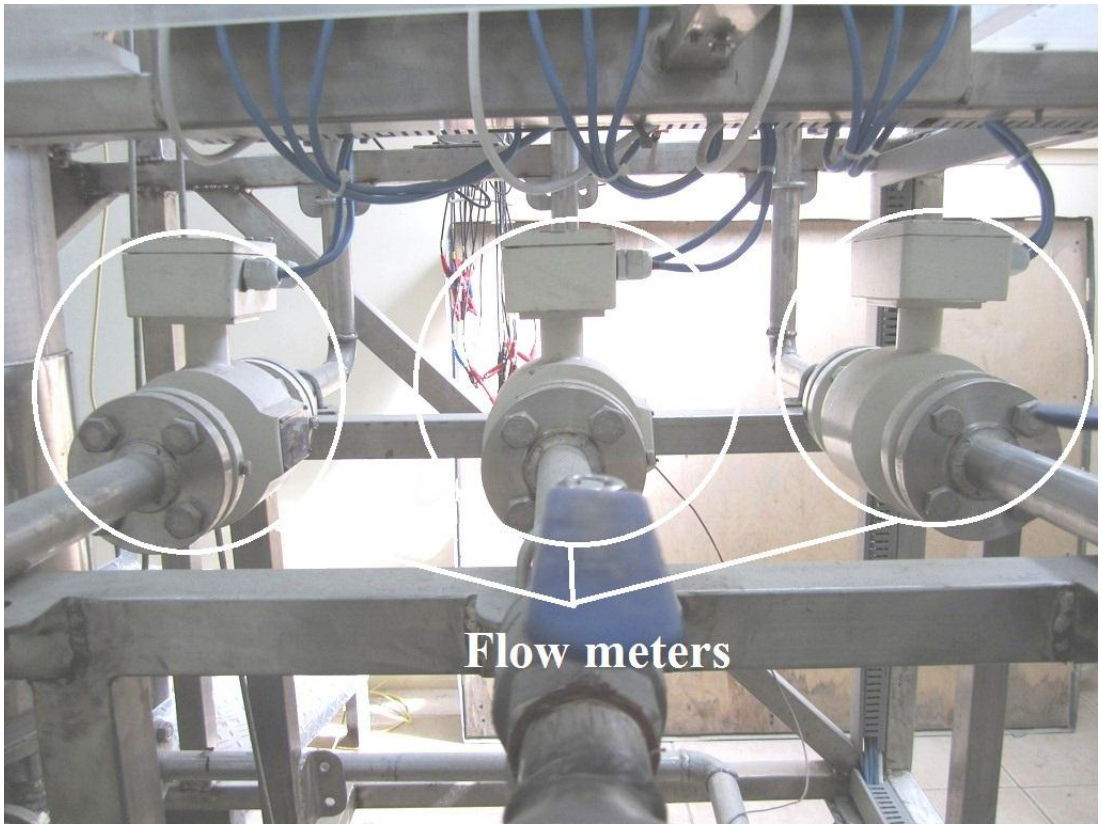

Figure 3.15 Flow meters.

Table 3.3 Flow-meter specification.

Model	MGG/C-25041212EAA-1
Serial no:	1012026
$K_1/K_2/K_3/K_4$	K~0.948
Meter size	25 mm
Accuracy	0.50%
Damping time constant	0 - 100 s
Frequency output	1 - 5000 Hz
Pressure	2 MPa
Lining material	PTFE
Electrode material	Hastelloy C
Max. temperature	180^{o}C
Ambient humidity	5 - 100 % RH

Specimen holder: This is to hold the sample/specimen (working electrodes) in its place to be part of the pipe. The detailes of the sample/specimen holder is shown in Figure 3.16 and Figure 3.17. For each specimen/working electrode, there is a counter electrode of the same size and geometry placed diametrically opposite to the working electrodes in order to ensure a symmetrical current distribution during electrochemical polarization measurements. For each test section; two electrodes are inserted in the sudden expansion disturbed flow region, one in the stabilized flow region, and two electrodes are inserted in the sudden contraction disturbed flow region. The working electrodes are made from the material to be tested, which are SA-543 and X65 steels in this work. The counter electrodes are made from SS 316, because this material has a high corrosion resistance to many chemicals. The working and counter electrodes are enclosed in Teflon sleeves to avoid contact with the test section body as illustrated in Figure 3.16 and Figure 3.17.

Static mixer: This is spiral obstacles placed in the pipe in order to keep mixing the solution components (oil and water) as it passes through it.

Side glass bypass: This part of the loop is a transparent pipe made from glass which is used to monitor the emulsion flow as shown in Figure 3.4. This section is in parallel with a Hastelloy pipe and can be isolated from the main loop by two ball valves. If the experiment is performed at a pressure and temperature which the side glass can't stand, the side glass section is isolated from the loop by closing the two valves and the flow will pass through the Hastelloy pipe

Potentiostat: A potentiostat as shown in Figure 3.18 AUTOLAB 128N for AC and DC electrochemical measurement is used to monitor the corrosion rate on line. The

potentiostat is equipped with a 28 channel multiplexer and can be used to log sequentially and continuously the corrosion rate of all working electrodes according to a prescribed program. The multiplexer is shown in Figure 3.19.

H_2S detection system: This is for safety issue, it is used to detect if there is any leak of H_2S gas, and the detector is connected with an alarm system.

Reference electrode: There is only one external Ag/AgCl reference electrode attached to the reference electrode chamber as shown in Figure 3.20. In all of the experiments a simple Ag rod (2 mm diameter and 45 mm long) coated by AgCl was used which was prepared by anodically polarizing the Ag rod in a saturated KCl solution at room temperature. A current density of 10 mA/cm^2 was used for three minutes in order to coat the rod with a durable AgCl layer. In the experiments, the reference electrode was continuously wetted by the solution which was extracted from the loop. The IR drop resulting from varying distance between the reference electrode and the working electrodes was measured to be very small due to the high conductivity of the solution.

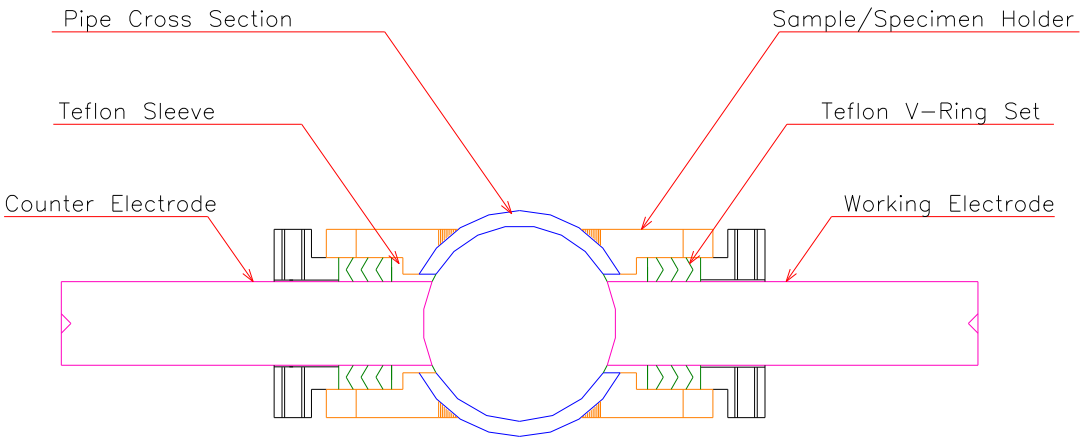

Figure 3.16 A detailed drawing of the sample/specimen holder.

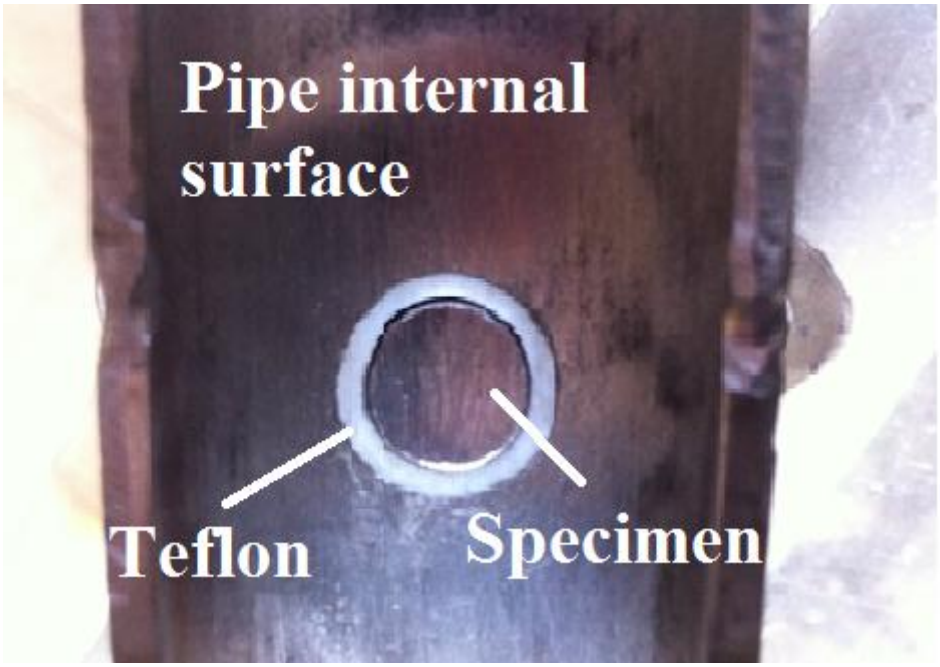

Figure 3.17 The electrode surface through a cross section of a test section.

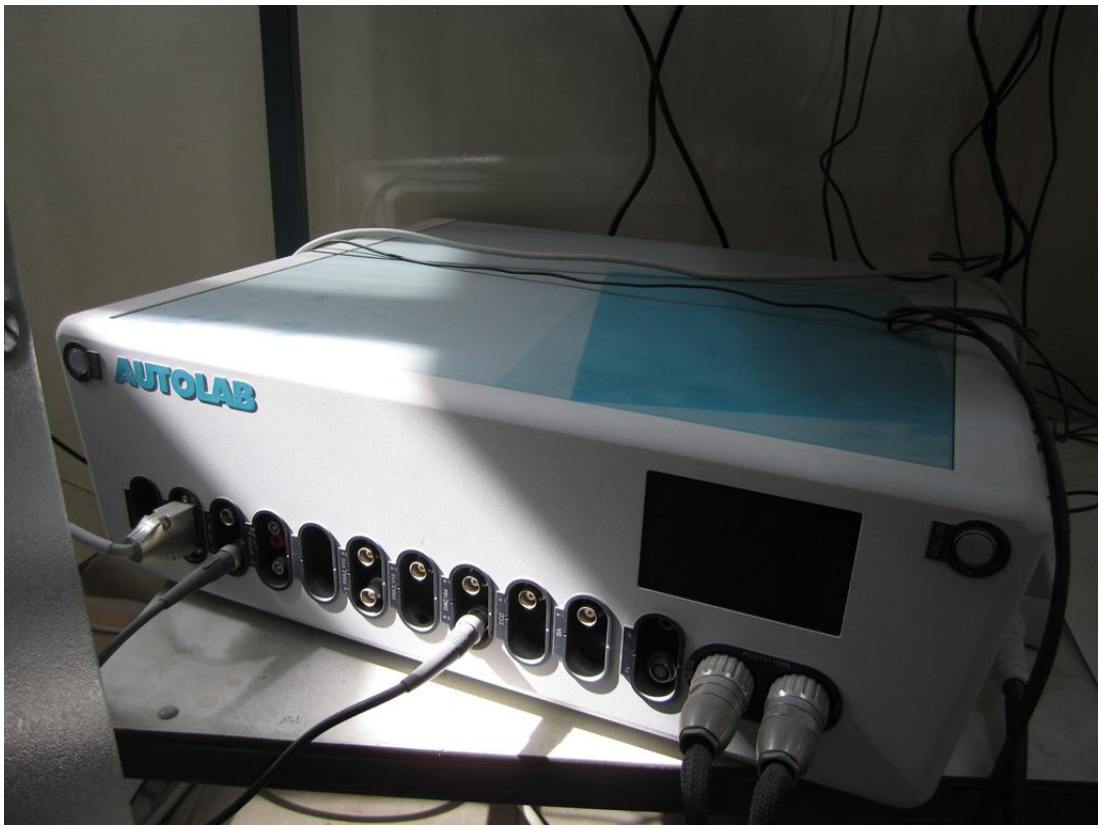

Figure 3.18 Potentiostat.

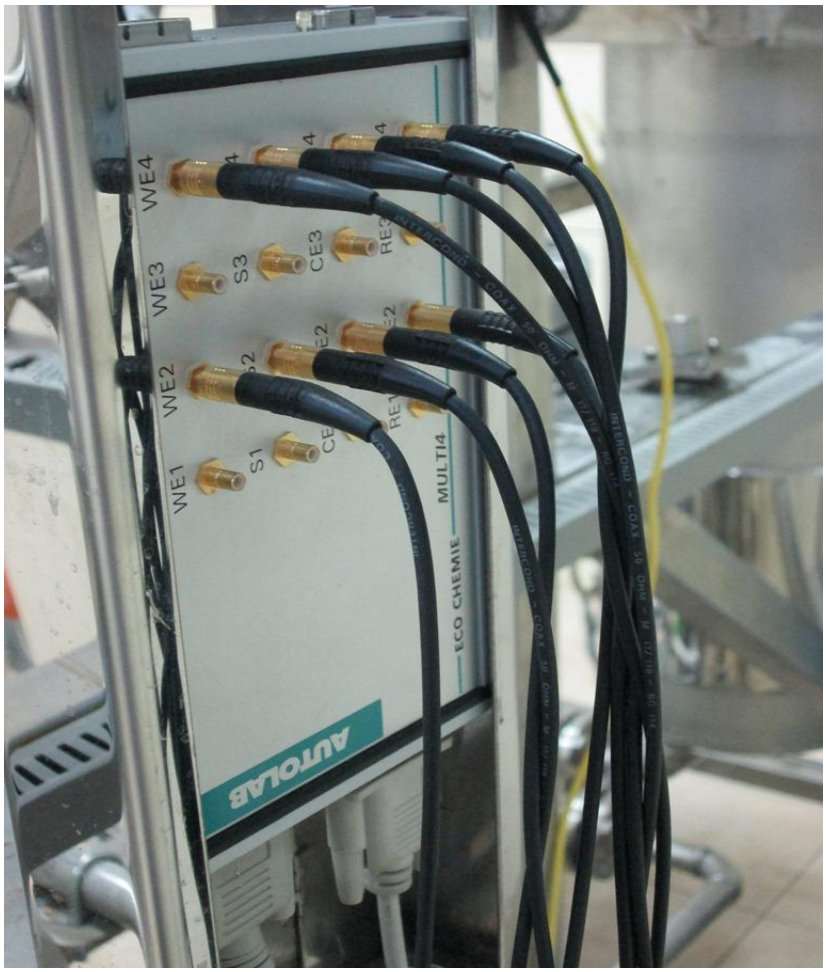

Figure 3.19 Multiplexer.

Figure 3.20 Reference chamber.

3.2.2 Procedure

10 L of emulsion was produced by pouring 3 L of oil and 7 L of 0.01 M $Na_2S_2O_3$ solution in the preparation tank as shown in Figure 3.21 and Figure 3.22. As oil and $Na_2S_2O_3$ solution is immiscible, mixer was used to assist in the formation of emulsion. Pump 1 (transfer pump) was started with valves V1, V4, and V5 opened and V2, V3, and V6 closed to transfer the emulsion to autoclave as shown by arrow direction in Figure 3.23. Once the mixing tank was emptied, the mixing tank valve V1 was closed and V2 opened to allow the emulsion to move in a horizontal loop comprising of spiral mixers as shown in Figure 3.24. During horizontal circulating flow the test sections valve V7, V8, V9, V10, V11, V12, were closed. The pump 2 was also started to increase the agitation process. The pumps suck the emulsion and after passing through spiral mixers move back into the autoclave. The heater was switched on to set the desired temperature. The purpose of moving the emulsion in horizontal loop was to set the desired pH and temperature before allowing the emulsion into the test sections.

In the mean while the autoclave was purged with high purity N_2 to deaerate the emulsion. Deaeration is important to avoid the oxidation of sulphide to yield sulphur [11,33]. The excess pressure was released using the relief valve. After N_2 purging, CO_2 was inserted to set the pH to 5. pH was continuously monitored via pH controller, as the pH came to 5.1 the CO_2 cylinder was closed. It was closed at 5.1 because the pH tends to drop further as the emulsion was allowed to pass through the test sections. The excess pressure was released using the safety valve V16. The pH deviation for all the experiments was 5 ± 0.2. The pH increased along the course of experiment usually after 24 hours. Along with pH, the pressure also increased upto 0.05 bar. This phenomenon

was also observed by Kappes et al. [**7**], as the system is closed the H_2S generated inside the system increase the pressure inside the system.

Once the desired pH and temperature was attained, valve V5 was closed and the desired test section valve was opened to allow the emulsion to flow in a closed loop as shown by red lines in Figure 3.25. The flow falls back into the autoclave via valves V15 and V16. At the entrance of each test section, flow-meter was installed for the determination of flow velocity. This process allows hitting the fresh working electrodes directly with and emulsion flow at the required temperature. The pump speed was adjusted to maintain a flow speed of 1 ± 0.01 m/s. The flow was turbulent in all the experiments. The turbulence of flow was estimated using Reynolds number. The emulsion was continuously monitored via transparent pipe by closing valves V13 and V14. The emulsion seemed to be milky from the transparent pipe as shown in Figure 3.26. Each experiment normally took about 26 hours. Once the experiment was finished the pumps were switched off and the solution fell back into the autoclave. The H_2S exhaust system was on during the whole experiment to remove any gases in case of leakage. The drainage valve V6 was opened to empty the autoclave. The system was than initially flushed with tap water at high and low speeds. Tap water was slightly heated as it helps to reduce the oil viscosity and ease its removal. Afterwards, the tap water was flushed away and the loop was flushed with distilled water. The electrodes were placed before the start of each experiment. SS316 was used as a counter electrode and Ag/AgCl as a reference electrode.

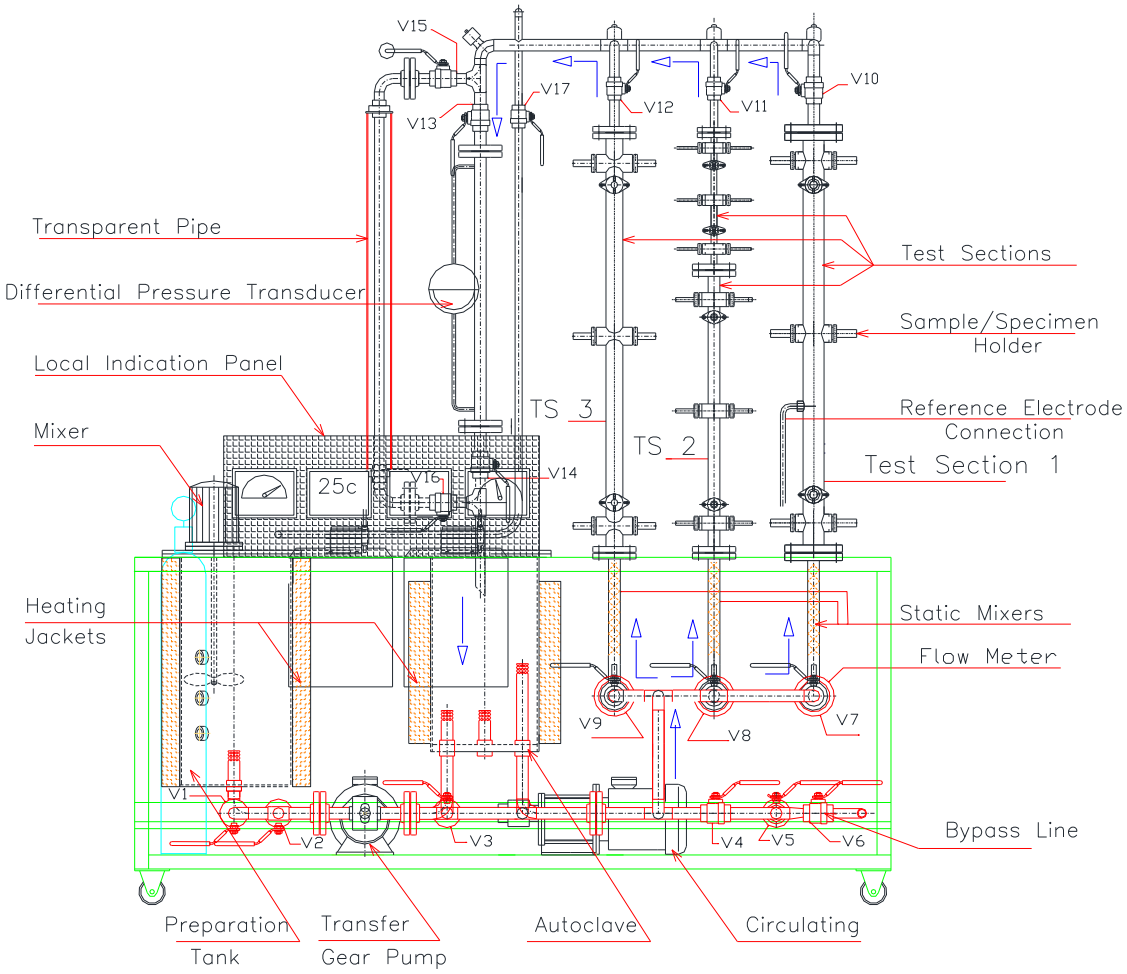

Figure 3.21 A diagram illustrating the direction the flow (front view).

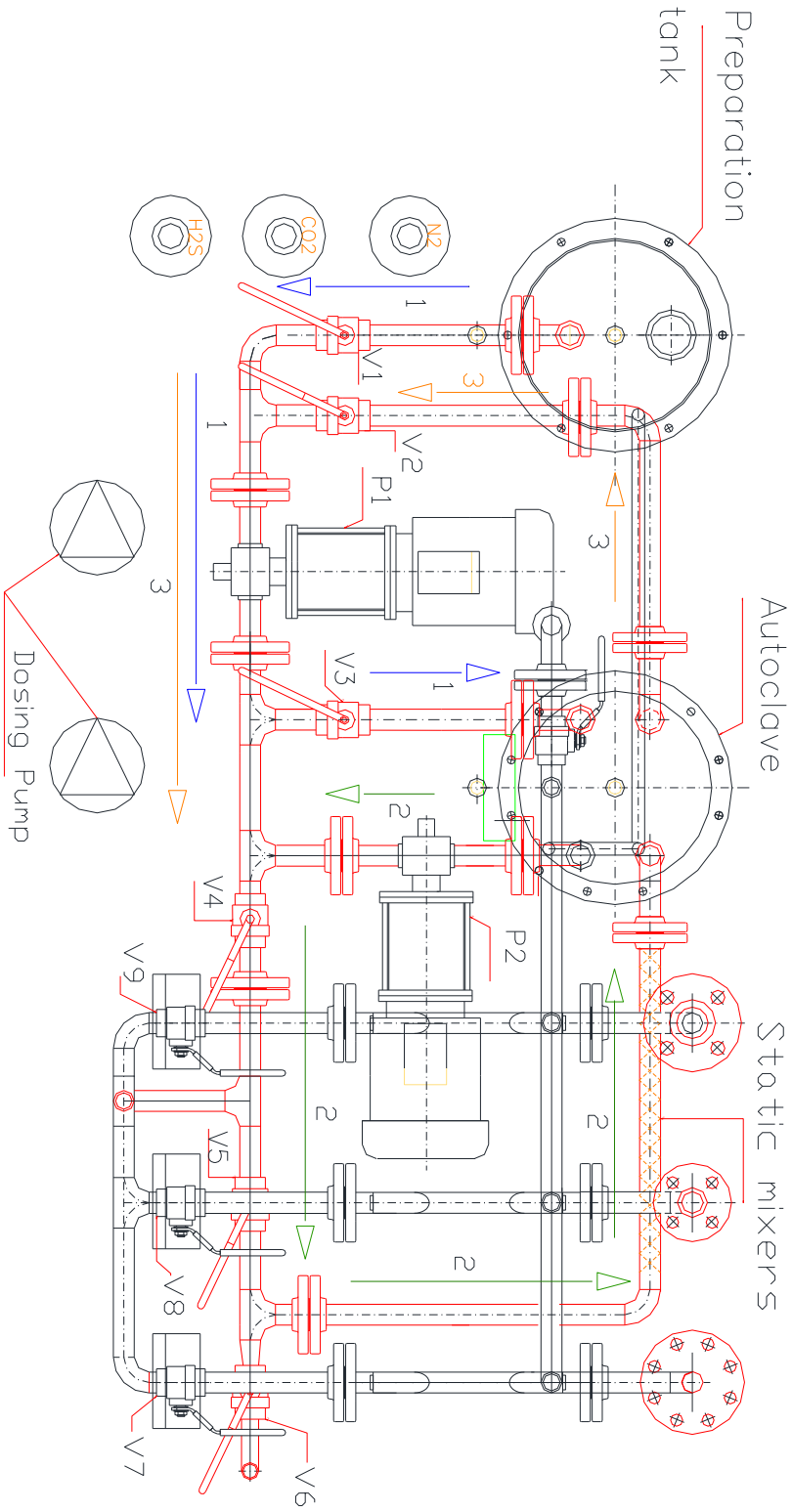

Figure 3.22 A diagram illustrating the direction the flow (top view).

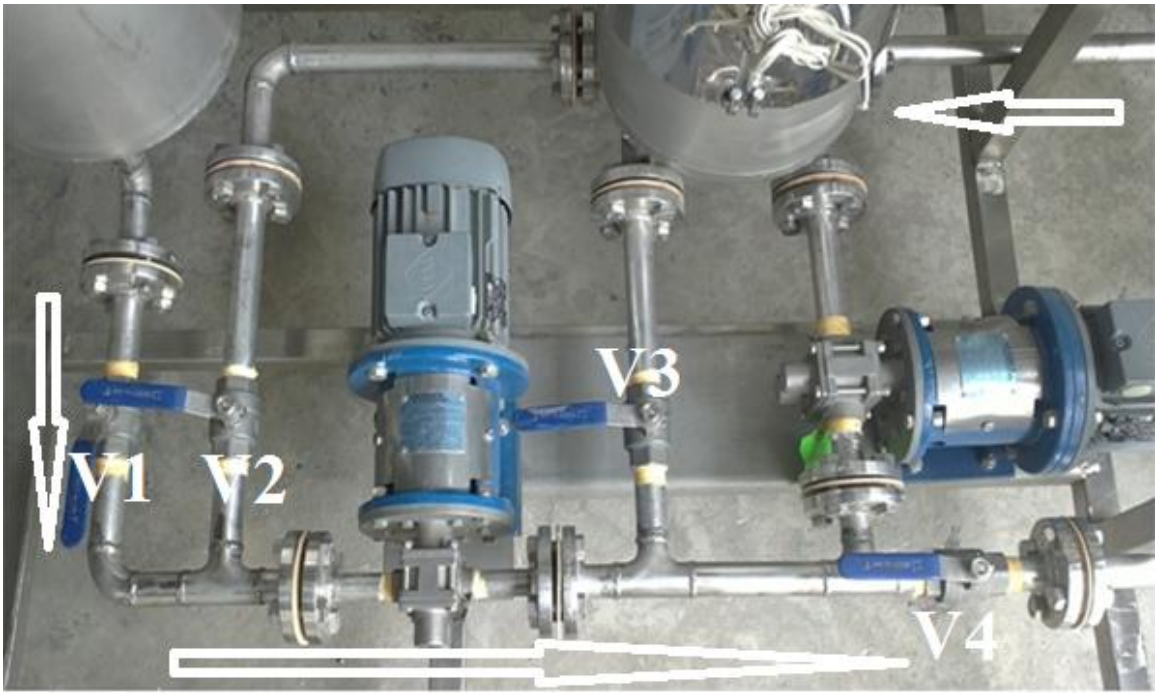

Figure 3.23 A photograph illustrating the direction the flow (top view).

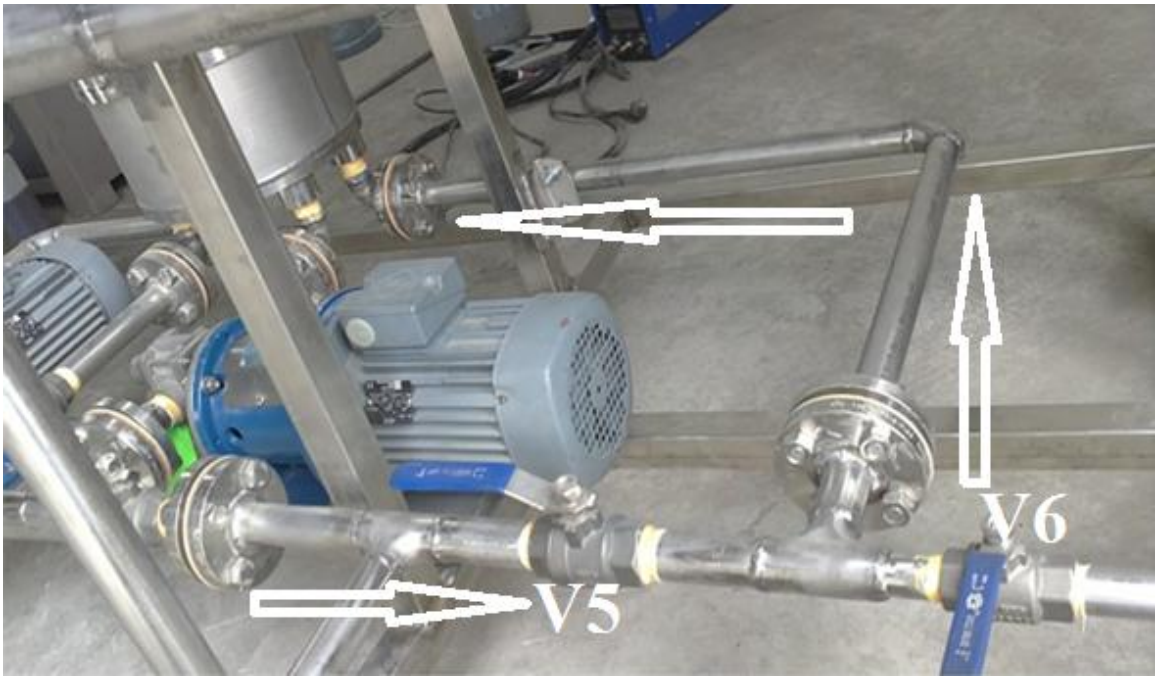

Figure 3.24 A photograph illustrating the direction the flow in the primary circulating loop.

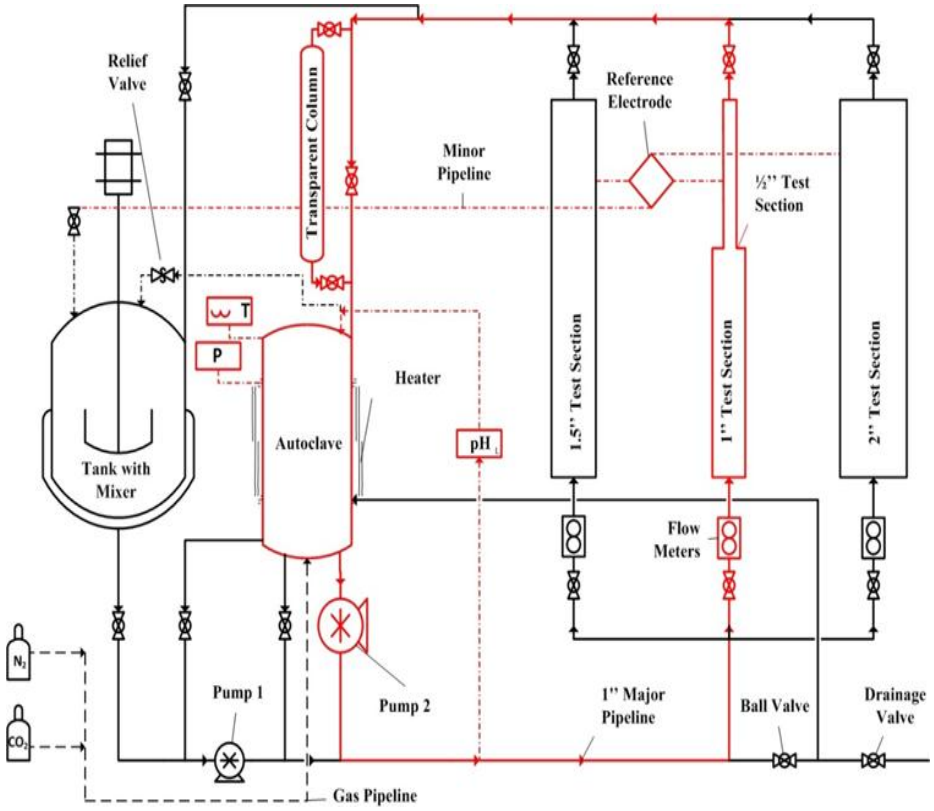

Figure 3.25 Piping and instrumentation diagram (PID) of emulsion flow loop.

Figure 3.26 Milky emulsion in transparent pipe.

3.2.3 Data reduction

Two multiplexer channels were used, one channel was connected to 1''- A (inlet of 1'' pipe) and the second channel was connected to 1''- B (outlet of 1'' pipe) as mentioned in Figure 3.6. The rest of the holes for electrode positioning were closed with SS316 rods. Each experiment lasted for about 26 hours. For the initial 24 hours, linear polarization resistance (LPR) was performed after every 30 minutes. The program was set in such a way that it first scanned the open circuit potential (OCP) of 1'' – A for 120 seconds, then its LPR then after 5 seconds wait it repeated the similar procedure for 1'' – B. Once both electrodes were scanned, the potentiostat waited for 30 minutes to start another loop. The potential was swept from -15 mV to +15 mV against OCP at a scan rate of 0.167 mV/s.

Once the 24 hours elapsed from the start of experiment, potentiodynamic polarization was performed with a scan range of -250 mV to +250 mV against OCP with a scan rate of 0.167 mV/s. Each electrode took almost one hour for potentiodynamic polarization. Once the measurements were completed the potentiostat was switched off. The corrosion rate was calculated by taking the time average of polarization resistance and inserting them into the equations 3.2 & 3.3. The slopes were taken from Tafel plots.

$$j_{corr} = \frac{\beta_a \times \beta_c \times 1000}{2.3 \times R_p \times (\beta_a + \beta_c) \times A} \tag{3.2}$$

$$\text{Corrosion Rate (mm/yr)} = 0.00327 \times j_{corr} \times \frac{\text{Eq. Wt.}}{\rho} \tag{3.3}$$

Where 0.00327 is a constant factor used for unit conversion, j_{corr} is the current density in $\mu A/cm^2$, βa and βc are Tafel slopes in mV/decade, R_p is the average polarization

resistance in Ω, A is the area of exposed surface in cm^2, ρ is the density of material which is taken as 7.83 g/cm^3 and Eq. Wt. of both steels is taken as 56.

Solutions and experimental setup

The solutions of 0.01 M $Na_2S_2O_3$ were prepared using 17.36 g of $Na_2S_2O_3.5H_2O$ in 7L of distilled water. Fresh solution was prepared before the start of each experiment. Exxsol D80 oil was used along with $Na_2S_2O_3$ to form oil-in-water emulsion. The initial experiment was performed to test the better steel grade in 70 % 0.01 M $Na_2S_2O_3$ and 30 % Oil emulsion. Another test was also conducted with same emulsion concentration but with inclusion of CO_2. The molarity of $Na_2S_2O_3$ was selected to be 0.01 M due to its higher rate of H_2S generation **[**15**]**. The experiments were conducted at 1 m/s, 25°C and pH 5 (in CO_2 case).

The steel grade which showed higher corrosion resistance was further investigated at various velocities and temperatures in order to assure the maximum reliability for possible scaling up to a real industrial application.

3.3 Test material

Two steel grades (X65 and SA-543) were tested. The as receives chemical composition of the metals is shown in Table 3.4.

The microstructure of the two metals is shown in Figure 3.27 and Figure 3.28. The surfaces were etched using 2% nital (2 mL nitric acid + 98 mL ethyl alcohol), then some ethanol was dropped on the surface and dried. The microstructure of SA-543 steel is tempered martensite with probably some bainite and the microstructure of X65 steel is pearlite (dark) in ferritic matrix (bright).

Table 3.4 Chemical Composition of SA-543 and X65 steels.

Steel	C	P	Mn	Si	S	Cu	Ni	Cr	Mo	Fe
SA-543	0.11	0.003	0.35	0.25	0.001	0.01	3.27	1.66	0.58	Balance
X65	0.091	0.0075	1.31	0.249	0.0044	0.0274	0.0177	0.0117	Trace	Balance

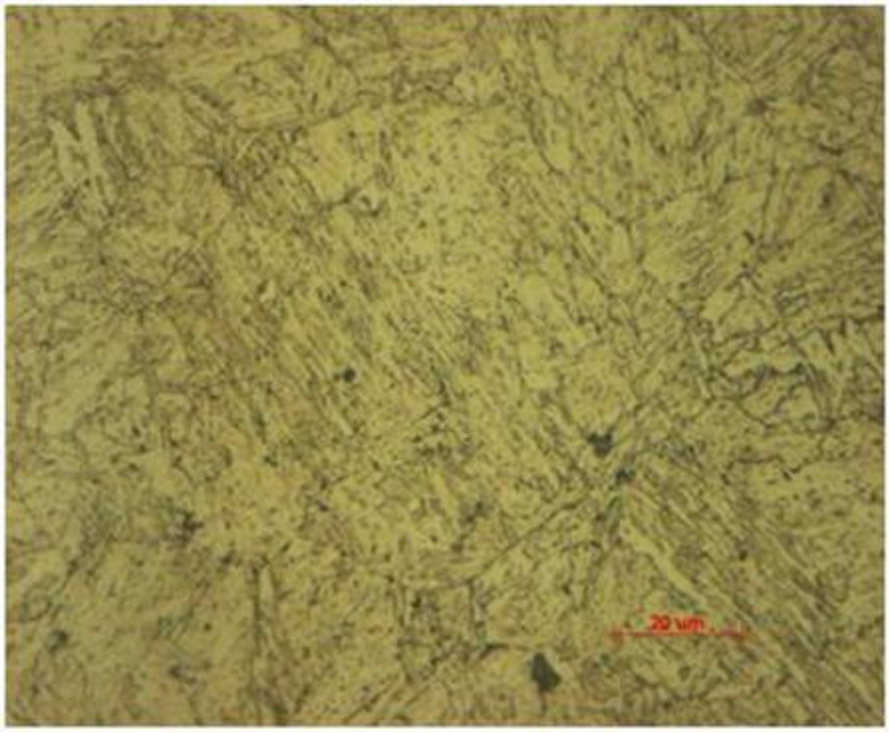

Figure 3.27 The microstructure of SA-543 steel.

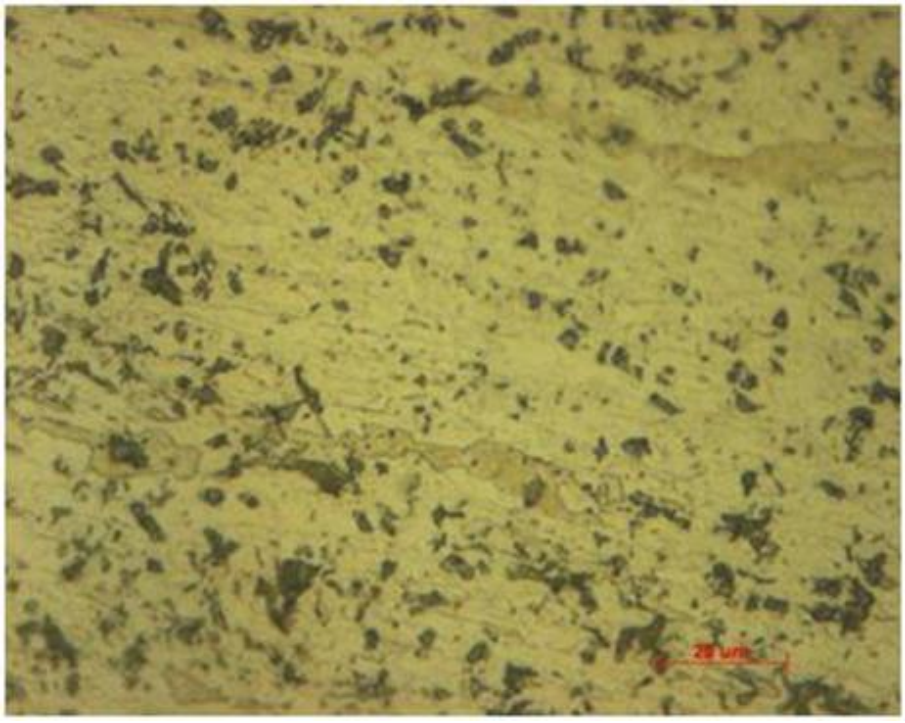

Figure 3.28 The microstructure of X-65 steel.

3.3.1 Test area of RCE

X65 and SA-543 steels were fabricated into hollow cylinders with 1 cm in both diameter and length and exposing the area of 3.14 cm^2. The surface of the testing materials was polished using silicon carbide paper of 1200 mesh.

3.3.2 Test area for flow loop

Each steel grade (X65 and SA-543 steels) was fabricated in a cylindrical shape with diameter of 10 mm and length of 100 mm. The front face of each electrode was curvatured according to the curvature of pipe as shown in Figure 3.17. This was done to ensure that there are no perturbations in the flow due to offset of electrodes. Figure shows the electrode surface through a cross section of a test section. The working and counter electrodes are enclosed in Teflon sleeves to avoid contact with the test section body as illustrated in Figure 3.16 and Figure 3.17. Teflon was chosen because of its excellent corrosion resistance to almost all chemicals. Also, it can withstand temperatures as high as 310^oC. The exposed areas of electrode for different test sections are shown in Table 3.5. The area of curvature was calculated using trigonometry as shown in Figure 3.30. Electrodes surface was polished using silicon carbide paper of 600 mesh. Special polishing mounting was made to maintain the curvature during the polishing as shown in Figure 3.29.

Figure 3.29 Sample mounting.

Table 3.5 Exposed area of test electrodes in different test sections.

Diameter (in)	Exposed Area (cm^2)
0.5	1.1513
1	1.028
1.5	1.0118

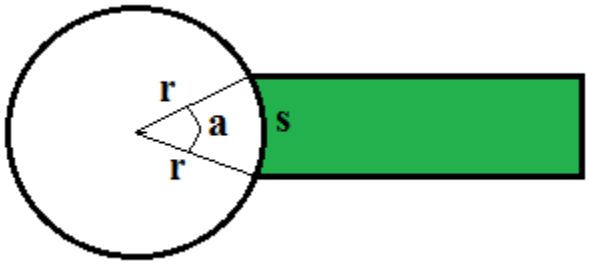

Figure 3.30 Diagram to calculate exposed electrode area.

We know the diameter of electrode and the diameter of test section. By using the cosine formula as shown in Equation 3.4 we can estimate the angle 'a'. Then by using Equation 3.5 we can estimate the curvature length, and area of exposed surface can be calculated using Equation 3.6.

$$d = 2r^2 - 2r^2\cos(a) \tag{3.4}$$

$$s = r \times a \tag{3.5}$$

$$A = s \times d \tag{3.6}$$

CHAPTER 4

RESULTS AND DISSCUSSIONS

4.1 Rotating cylinder electrode

4.1.1 Effect of $Na_2S_2O_3$, CO_2 and NaCl

Potentiodynamic polarization measurements

Figure 4.1 shows the potentiodynamic polarization curves of X65 and SA-543 steels in 0.01M $Na_2S_2O_3$ solution with 30% Oil at 25^oC and 1909 rpm (1 m/s for 10 mm cylinder). It is evident from the potentiodynamic polarization curves that SA-543 steel is more corrosion resistant than X65 steel since it has lower corrosion current values and more noble corrosion potentials as compared to X65 steel as shown in Table 4.1. The corrosion potentials and corrosion currents were calculated using Tafel extrapolation. Tafel extrapolation was performed using intersection of anodic slope of Tafel and E_{corr}. The higher corrosion resistance of SA-543 steel can be attributed to its composition as it contains 3.27 % Ni, 1.66 % Cr and 0.98 % Mo as shown in Table 3.4. On the other hand X65 contains very minute percentages of these elements. When CO_2 was added into the system (pH 5), the corrosion potential of both steels moved to noble direction. In the presence of CO_2 there was an additional reduction reaction of carbonate anion which is dominating at pH 5 [81]. The formation of iron carbonate which is more stable and adherent than mackinawite reduces the dissolution of iron in the emulsion thus reducing its corrosion [4].

The presence of NaCl with $S_2O_3^{2-}$ increases the corrosion current and shifted the E_{corr} to more negative potential. Chloride ions heavily affected the corrosion current of both

steels. The effect of NaCl, was slightly reduced when CO_2 was injected. The presence of CO_2 with $S_2O_3^{2-}$ and NaCl reduced the corrosion current as compared to $S_2O_3^{2-}$ and NaCl. The chloride ions are responsible for the dissolution of carbonate films so the effect of CO_2 was not much more significant in NaCl solution as compared to without NaCl solution.

Table 4.1 Tafel extrapolation data.

		0.01 M $Na_2S_2O_3$	0.01 M $Na_2S_2O_3$ + CO_2	0.01 M $Na_2S_2O_3$ + NaCl	0.01 M $Na_2S_2O_3$ + NaCl + CO_2
SA-543	Ecorr (V)	-0.213	-0.176	-0.279	-0.298
	Icorr (µA)	66.9	39.6	185.2	130
X65	Ecorr (V)	-0.344	-0.302	-0.364	-0.345
	Icorr (µA)	121.4	88.4	325.3	142.5

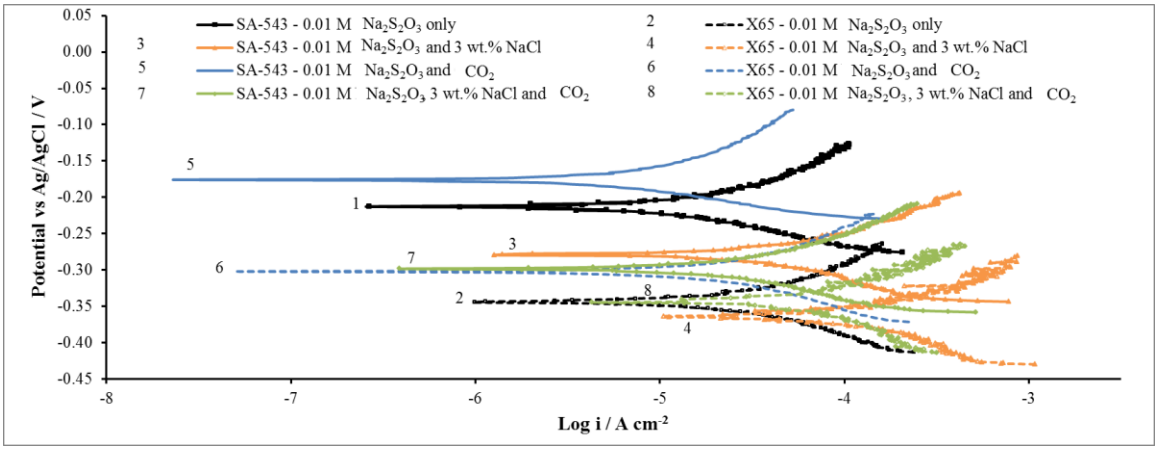

Figure 4.1 The potentiodynamic polarization curves of SA-543 and X65 steels in 0.01 M $Na_2S_2O_3$ solution with 30% oil at 1 m/s, and 25^{o}C after 24 hours.

Variation of polarization resistance with time

Figure 4.2 shows the variation of polarization resistance (R_p) with time. The R_p of SA-543 steel was higher than X65 steel for the same solution (by comparing 1&2, 3&4, 5&6 and 7&8 in Figure 4.2). By comparing 2 & 4, 1 & 3 it was found that the effect of addition of NaCl to the $Na_2S_2O_3$ solution was similar for both steels. There was a significant decrease in Rp with the presence of Cl^-. The effect of CO_2 with $Na_2S_2O_3$ was compared using 1 & 5 for SA-543 steel and 2 & 6 for X65 steel. The addition of CO_2 increased the R_p of SA-543 steel; but no significant change was observed in R_p of X65 steel. In case of SA-543 steel, the presence of CO_2 with $S_2O_3^{2-}$ has much more inhibition effect as compared to $S_2O_3^{2-}$ alone. It is possible that a protective film is formed on the samples as mackinawite (FeS) film, in the presence of $S_2O_3^{2-}$ or H_2S solutions [28,30,33,82]. With the passage of time the protective film formed in presence of CO_2 becomes more tenacious resulting in higher R_P for SA-543 steel.

The effect of CO_2 in presence of NaCl and $Na_2S_2O_3$ was compared in 3 & 7 for SA-543 steel and 4 & 8 for X65 steel. The behaviour was similar for both the steels. There was no significant change in R_p with addition of CO_2.

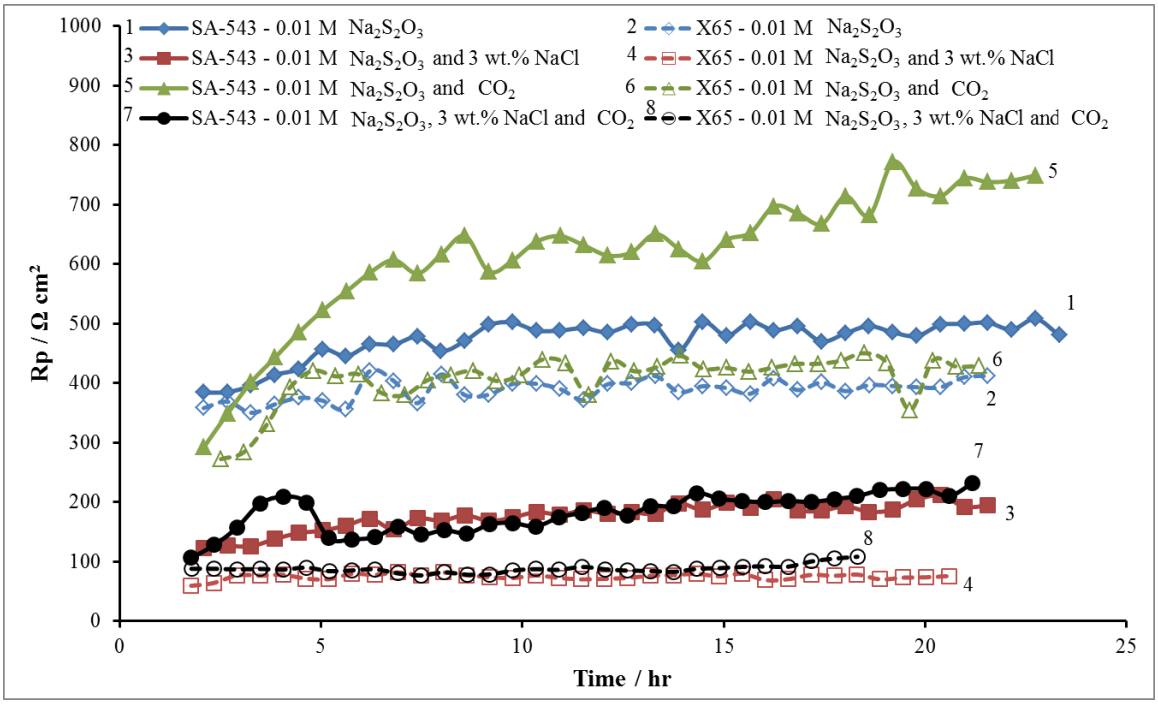

Figure 4.2 Polarization resistance of SA-543 and X65 steels with time in 0.01 M $Na_2S_2O_3$ solution with 30% oil at 1 m/s, and 25^{o}C.

Weight loss measurement

Figure 4.3 shows the weight loss comparison of X65 and SA-543 steels in different emulsion conditions. Weight loss measurements corroborate the electrochemical measurement of Figure 4.2 as discussed above. With the introduction of CO_2 to $Na_2S_2O_3$ the corrosion rate declined for both the steels. Higher corrosion rates were observed in both steels with presence of NaCl and $Na_2S_3O_3$. There was a slight decrease in corrosion rate with the presence of CO_2 in ($Na_2S_2O_3$+NaCl) as compared to $Na_2S_2O_3$+NaCl alone.

The results of the LPR, potentiodynamic polarization, and weight loss techniques showed that SA-543 steel is more corrosion resistant than X65 steel. Therefore, the corrosion behaviour of SA-543 steel was further investigated at various oil percentages, velocities and temperatures. The detailed flow chart of experiments is shown in Table 4.2.

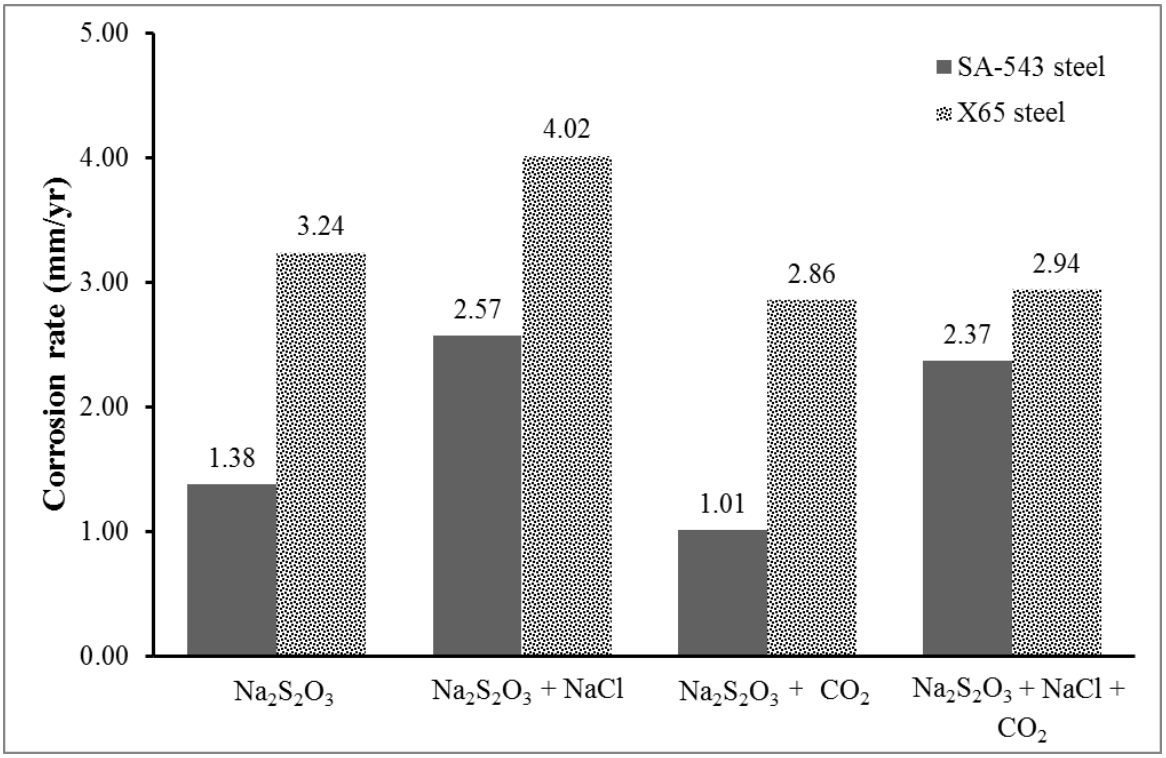

Figure 4.3 Corrosion rate measurement of SA-543 and X65 steels using the weight loss method in 0.01 M $Na_2S_2O_3$ solution with 30 % oil at 25^{o}C and 1 m/s.

Table 4.2 Experimental series chart.

Test Parameters	Variable Parameters	Fixed Parameters
Oil Concentration (% v)	10	1 m/s, 25 ^{o}C
	20	
	30	
Velocity (m/s)	0.75	30 % Oil, 25 ^{o}C
	1	
	1.5	
Temperature (^{o}C)	25	30 % Oil, 1 m/s
	50	

4.1.2 Emulsion at different oil percentages

These experiments were performed to test the effect of oil percentage on corrosion. All experiments were conducted using SA-543 steel in 0.01 M $Na_2S_2O_3$ at 25^{o}C, 1 m/s, and three oil percentages of 10, 20 and 30 %. The stability of emulsion depends upon the oil content at constant rotating speed [83]. Thus, a minimum of 10 % D80 oil was used; below that emulsion was not enough to wet the sample. The corrosion potential moved to a noble direction and corrosion current increased with an increase in oil percentage as shown in Table 4.3.

The increase in oil percentage augmented the formation of oily phase layer on the steel surface which inhibits the steel dissolution [27,28]. Zhang and Cheng [4] indicated that the reaction activation energy was increased by the presence of the adsorbed oily phase, which inhibits the corrosion of steel.

Figure 4.5 shows the R_p (determined by LPR method) as a function of time. The R_p increased with time for the first eight hours for the 30 % Oil and then remained constant with some fluctuations. The Rp of 20 % and 10 % oil remained nearly constant during whole experiment.

Huet et.al. [67,81] found that there is a significant fluctuation in the resistance of the electrolyte and the corrosion of the steel with the change in the composition of oil/water close to the electrode surface. The presence of a layer of oily phase covering the surface of the steel decreased the corrosion of the steel, and hence, the corrosion behavior of the steel could be significantly affected by destabilization of the emulsion. There is no significant difference in R_p at 20 % oil and 10 % oil, the reason being that the emulsion formed at these two concentrations has almost similar emulsion properties.

Table 4.3 Tafel extrapolation for different oil percentages

		30 % Oil	20 % Oil	10 % Oil
SA-543	Ecorr (V)	-0.213	-0.260	-0.279
	Icorr (µA)	66.9	109	120.6

Figure 4.6 compares the corrosion rate of SA-543 steel by weight loss method at different oil concentrations. From weight loss method it is also evident that there is not much corrosion difference (around 1%) between 10 and 20% oil composition, and then there is a slight drop at 30% oil with a percentage change of 18%.

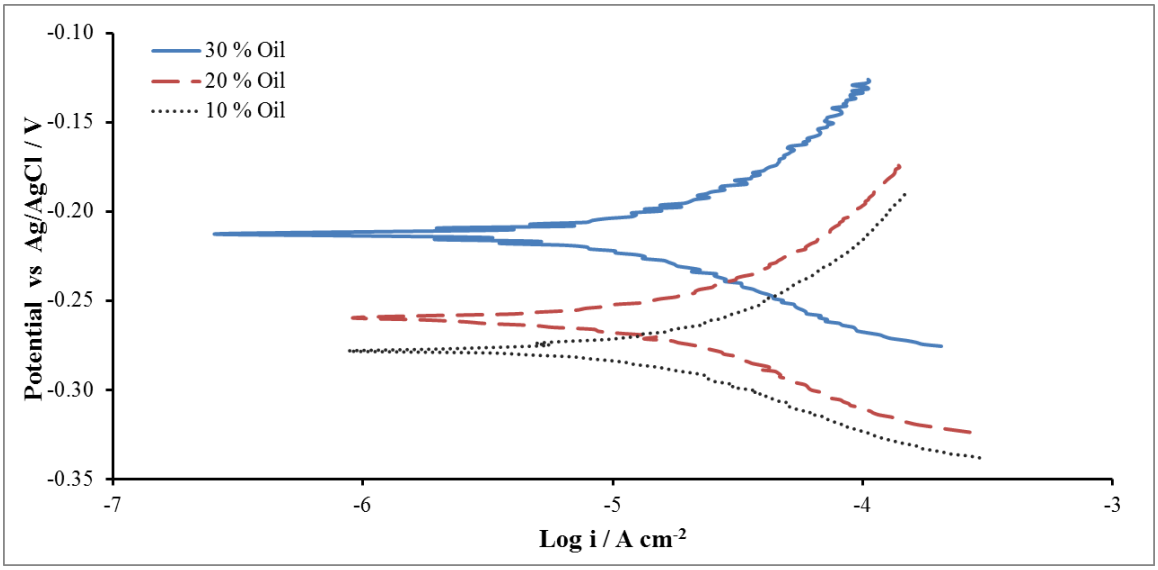

Figure 4.4 The potentiodynamic polarization curves of SA-543 steel in different oil percentages with 0.01 M $Na_2S_2O_3$ solution at 25^{o}C and 1 m/s.

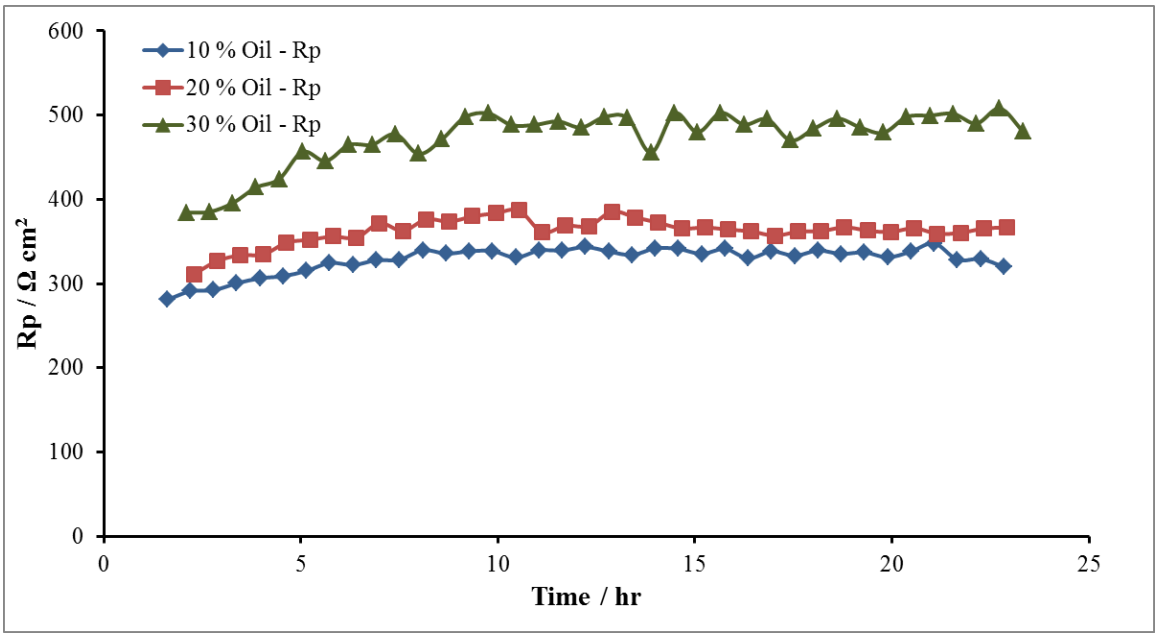

Figure 4.5 Polarization resistance of SA-543 steel with time in 0.01 M $Na_2S_2O_3$ solution with 30% oil at different oil percentages.

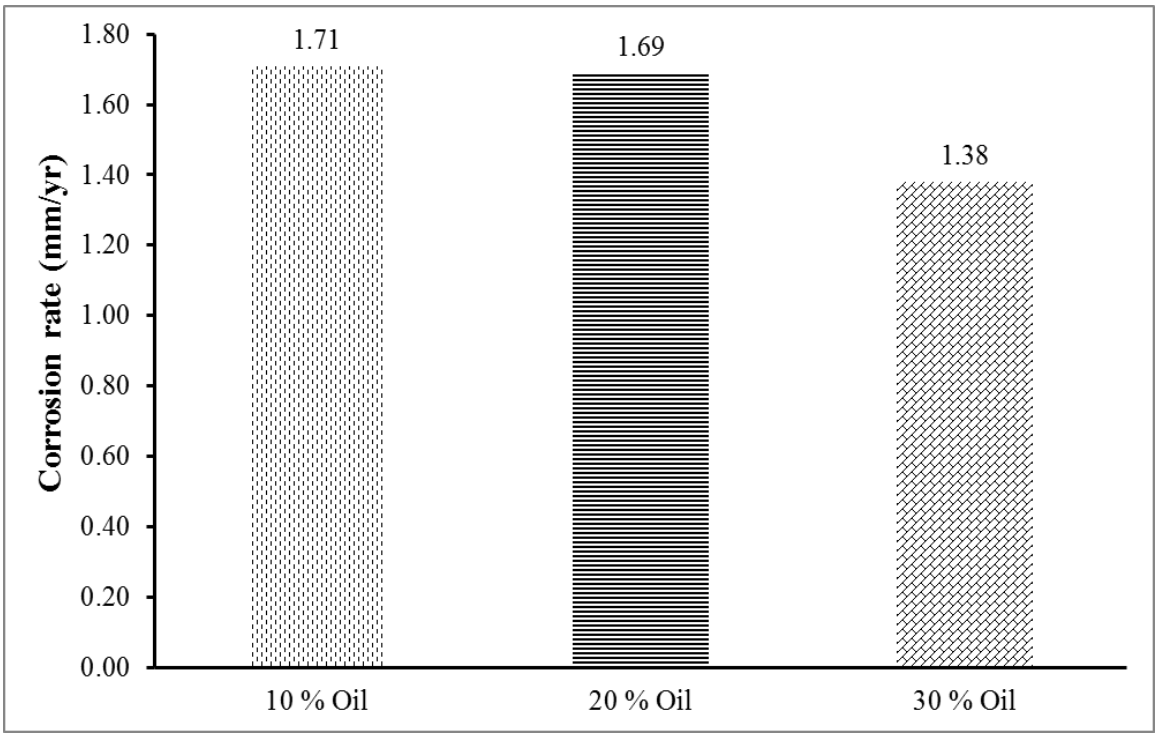

Figure 4.6 Corrosion rate measurement of SA-543 steel at different oil concentrations using the weight loss method.

4.1.3 Effect of Velocities

The experiments were performed on SA-543 with 30% Oil and 70% 0.01 M $Na_2S_2O_3$ at 25^oC with three different velocities of 0.75, 1, and 1.5 m/s. The corrosion current decreased and the E_{corr} shifted to a more positive potential when the velocity was increased as shown in Table 4.4. There was a slight difference in the corrosion current of 0.75 and 1 m/s as compared to 1 and 1.5 m/s velocities, due to velocity difference. This is attributed to the accelerated diffusion of reduction species towards the steel surface for reduction reaction, which enhances the formation of a protective film on the steel surface [4]. With the increase in velocity there will be more protective scale which hinders the dissolution of iron ions into the emulsion thus lowering corrosion current [32].

Figure 4.8 shows that there were no significant variations in R_p with increasing the velocity. There was a noticeable increase in R_p of 1.5 m/s in the later stages of experiment which can be related to the formation of adherent surface film. The result of a study by Tian and Cheng [60] showed that the diffusion and reduction of anions on the electrode surface was accelerated by the fluid flowing.

The corrosion rate obtained using weight loss method indicates that the corrosion rate decreased by increasing the velocity as shown in Figure 4.9. Weight loss corrosion rate of 1 and 1.5 m/s was not significant as compared to weight loss of 0.75 and 1 m/s.

Table 4.4 Tafel extrapolation for different velocities.

		0.75 m/s	1 m/s	1.5 m/s
SA-543	Ecorr (V)	-0.247	-0.213	-0.139
	Icorr (µA)	71.4	66.9	55.4

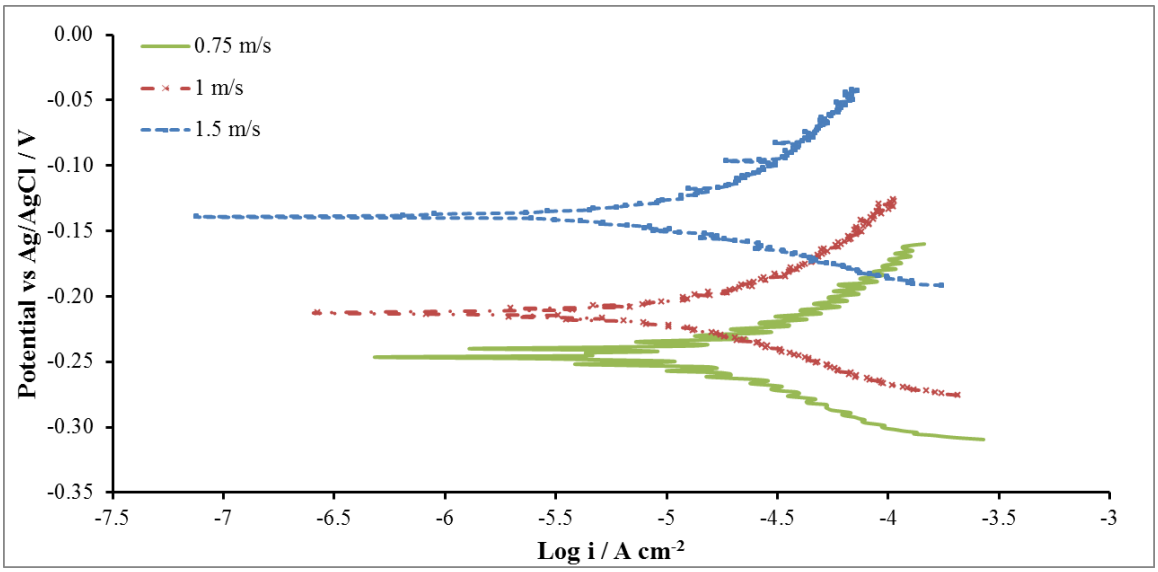

Figure 4.7 The potentiodynamic polarization curves of SA-543 steel in 0.01 M $Na_2S_2O_3$ solution with 30% oil at 25°C and different velocities.

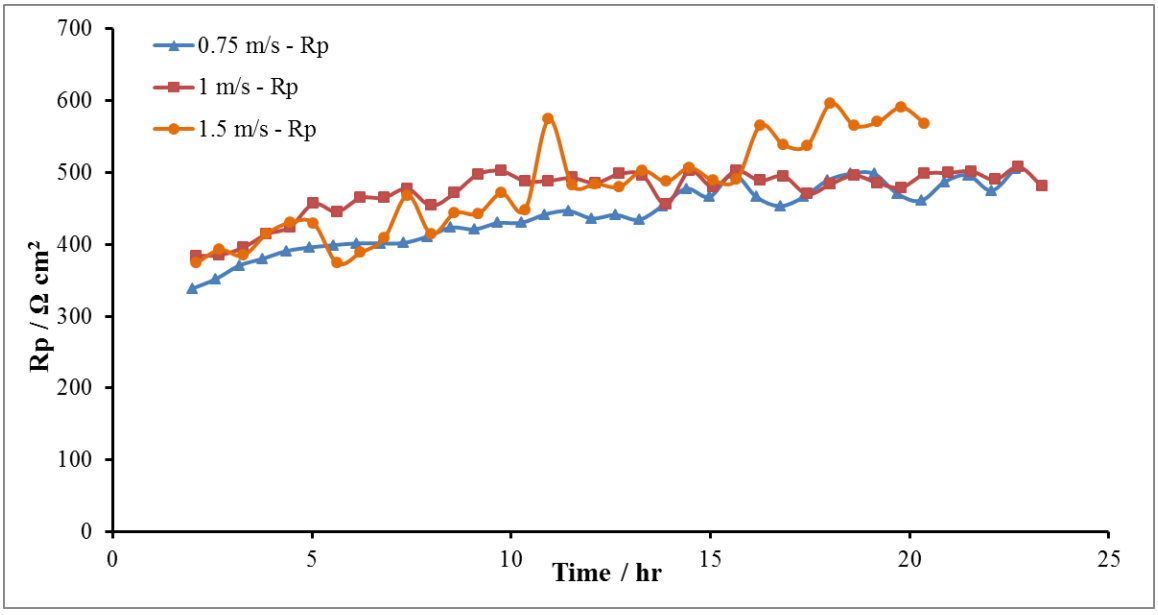

Figure 4.8 R_P of SA-543 steel with time in 0.01 M $Na_2S_2O_3$ solution with 30% oil at 25°C and different velocities.

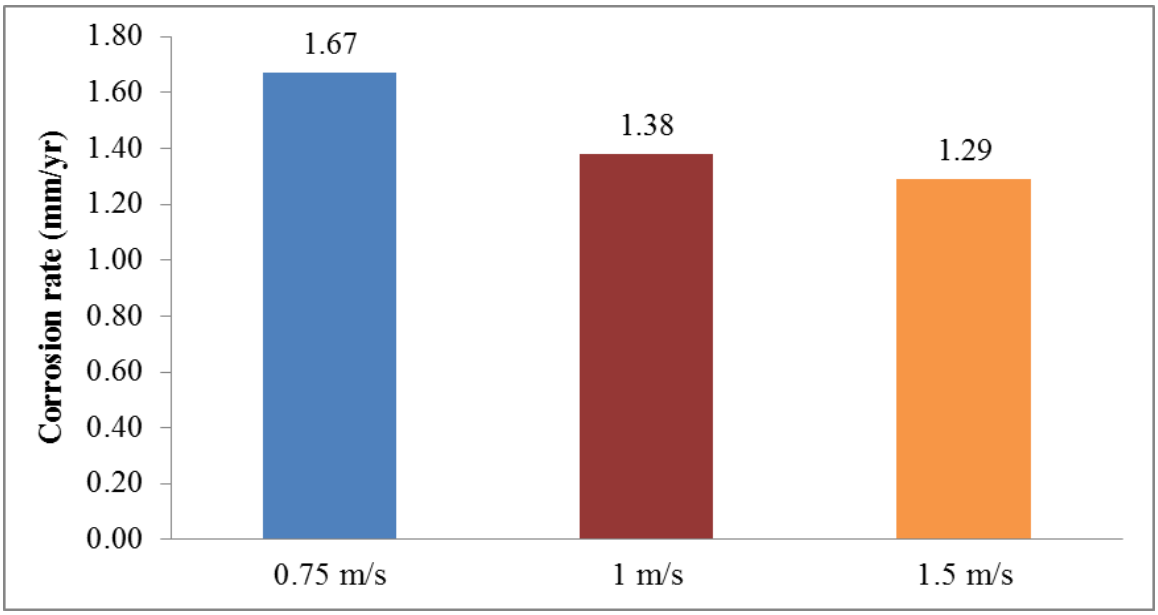

Figure 4.9 Corrosion rate measurement of SA-543 steel at different velocities using the weight loss method.

4.1.4 Effect of Temperature

These experiments were performed at two different temperatures of 25 and 50^{o}C. The corrosion rate increased with temperature, since the temperature changes the kinetics parameter of a chemical reaction [84]. Figure 4.10 and Table 4.5 shows that at higher temperatures the E_{corr} moved to a noble direction and there is a slight increase in corrosion current. The increase in temperature generally enhances the various interfacial reactions. Actually, there is a competence effect of the temperature on the corrosion of the steel via the effects of interfacial reactions and corrosion scale [4]. In the present study, the corrosion of the steel was slightly increased with increase in temperature. The increase in temperature also leads to the increase in the anodic and cathodic rate of reactions.

Figure 4.11 also shows that there were no significant variations in R_p with raising the temperature. There was a noticeable increase in R_P at 50^{o}C in the later stages of experiment which can be related to the formation of a protective surface film. Weight loss measurements in Figure 4.12 show that metal removal rate increased at elevated temperatures, but there was a contradiction between R_p and weight loss results.

Table 4.5 Tafel extrapolation for different temperatures.

		25 ^{o}C	50 ^{o}C
SA-543	Ecorr (V)	-0.213	-0.088
	Icorr (µA)	66.9	73.1

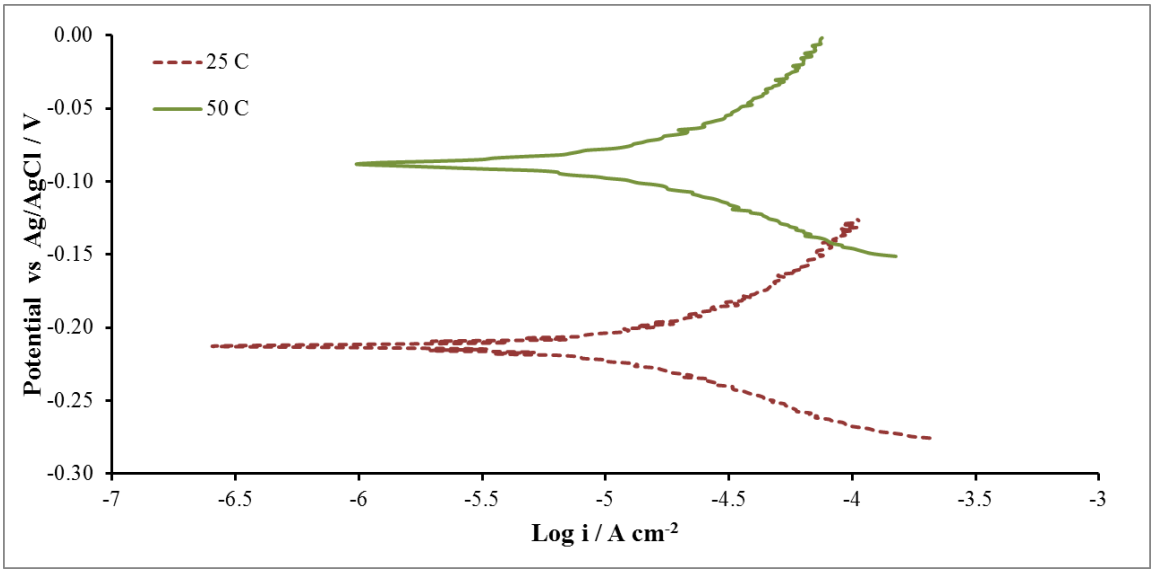

Figure 4.10 The potentiodynamic polarization curves of SA-543 steel in 0.01 M $Na_2S_2O_3$ solution with 30% oil at 1 m/s and different temperatures.

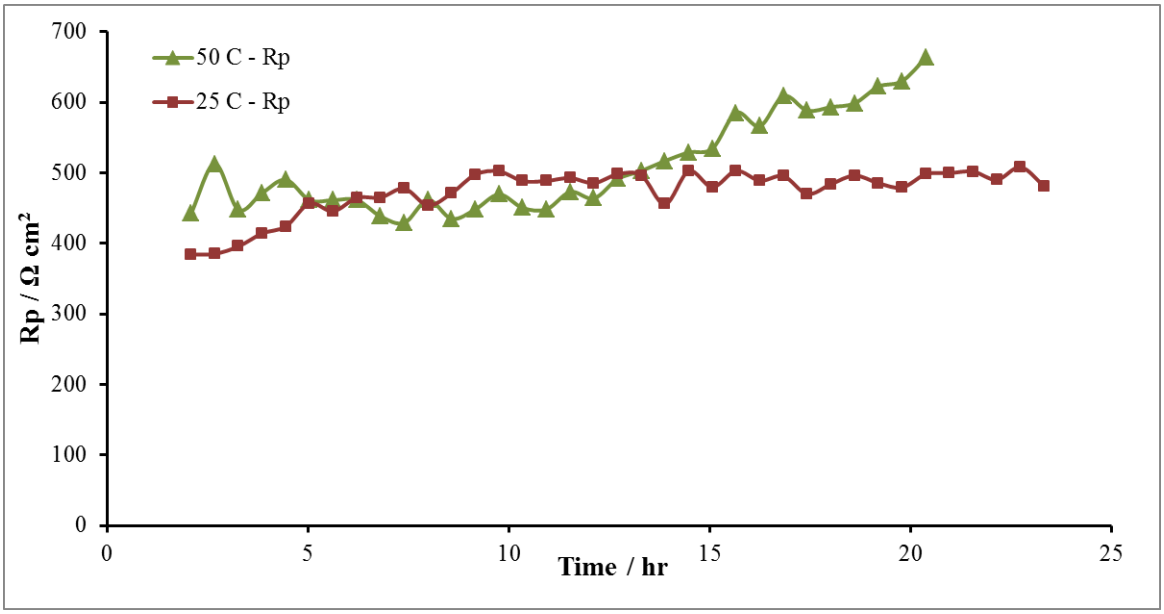

Figure 4.11 R_P of SA-543 steel with time in 0.01 M $Na_2S_2O_3$ solution with 30% oil at 1 m/s and different temperatures.

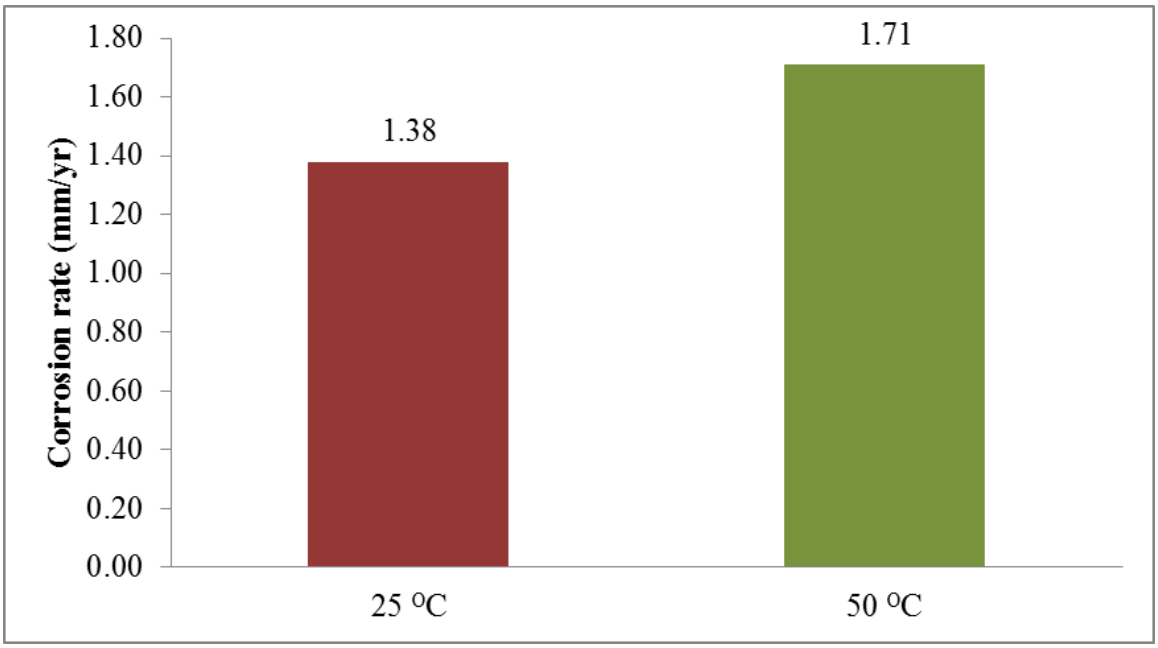

Figure 4.12 Corrosion rate measurement of SA-543 steel at 1 m/s and different temperatures using the weight loss method.

4.2 Flow loop

4.2.1 Effect of CO_2 emulsion corrosion

The experiments were initiated by testing SA-543 and X65 steels in 70% 0.01 M $Na_2S_2O_3$ and 30 % Oil emulsion. The pH of the emulsion was around 7 – 7.2. It was observed in Figure 4.13 that SA-543 steel was more corrosion resistant than X65 steel. The corrosion current (I_{corr}) of SA-543 steel was less than the X65 steel and corrosion potential (E_{corr}) was also more noble in both solutions as shown in Table 4.6. The high corrosion resistance of SA-543 can be attributed to its composition as it contains 3.27 % Ni, 1.66 % Cr and 0.98 % Mo as shown in Table 3.4. On the other hand X65 steel contains only traces of these elements. Also the different microstructural phases in X65 steel lead to the separation of anodic and cathodic sites that affect directly the rate of metal dissolution [85].

With the inclusion of CO_2, the pH was maintained at 5 ± 0.1. The polarisation curves moved in the noble direction. I_{corr} dwindled and E_{corr} became noble. SA-543 steel showed more corrosion resistance properties than X65 steel in the presence of CO_2. As the system was deareated, means the oxygen concentration was minute. So, the only reduction reactions were thiosulphate anion reduction and carbonate/bicarbonate anion reduction. The reduction of carbonate anion is dominating at pH 5 [81].

Table 4.6 Tafel extrapolation for $Na_2S_2O_3$ and CO_2

		0.01 M $Na_2S_2O_3$	0.01 M $Na_2S_2O_3$ + CO_2
SA-543	Ecorr (V)	-0.216	-0.115
	Icorr (µA)	71.7	40.3
X65	Ecorr (V)	-0.270	-0.192
	Icorr (µA)	249.5	135.3

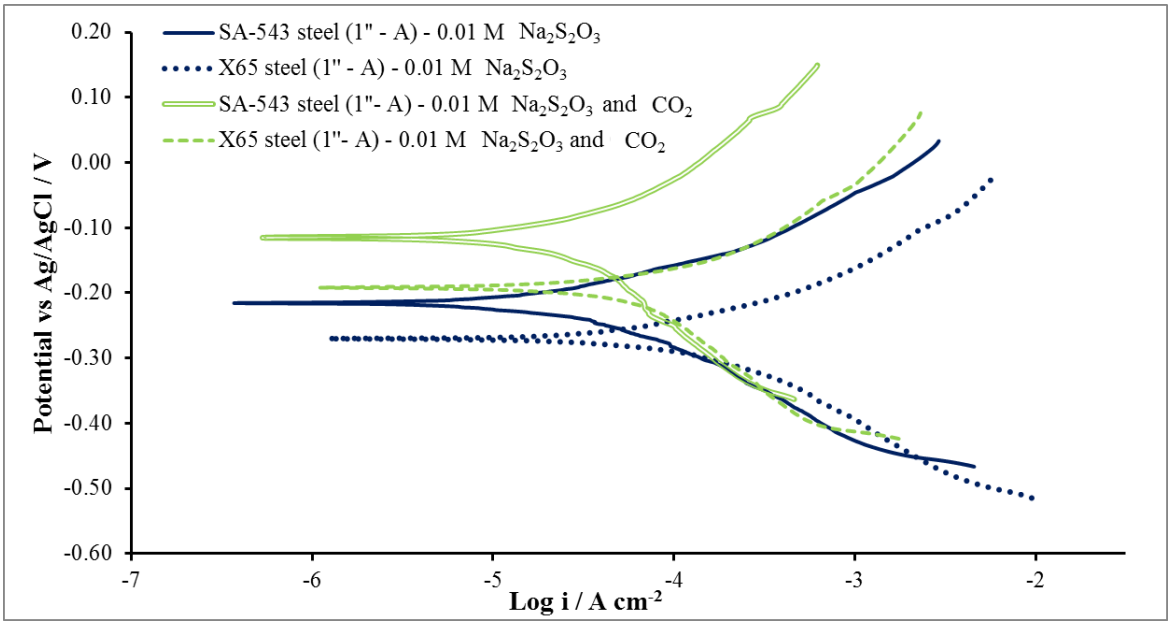

Figure 4.13 The potentiodynamic polarization curves of SA-543 and X65 steels in 0.01 M $Na_2S_2O_3$ solution with 30% oil at 1 m/s and 25^{o}C.

As depicted by curves 3 & 4 in Figure 4.14, the polarization resistance (R_p) value for both steels slightly increased with time in presence of CO_2, with SA-543 steel showing higher R_p than X65 steel. And for the case of $Na_2S_2O_3$ alone, the R_p remained almost constant. As mentioned earlier the reduction of thiosulphate anion produces elemental sulphur and H_2S. The reaction of H_2S with steel form a layer of iron sulphide (FeS). At initial stages, the Mackinawite is formed. It present in all H_2S and thiosulphate solutions [30,33,86,87]. The sulphide films provide good ground for the reduction reaction **[**11**,**42]. The reduction reaction of CO_2 forms iron carbonate precipitate on the steel surface. FeS precipitates much easier than $FeCO_3$. Both iron carbonate and mackinawite are formed under low H_2S concentration and high Fe^{+2} concentrations [15]. This iron carbonate along with mackinawite immensely reduces the iron dissolution.

Figure 4.15 portray the corrosion rates of both the steels. SA-543 steel proved to be the reliable corrosion resistant material as compared to X65 steel. Its corrosion rate is lower in both cases i.e. with CO_2 and without CO_2.

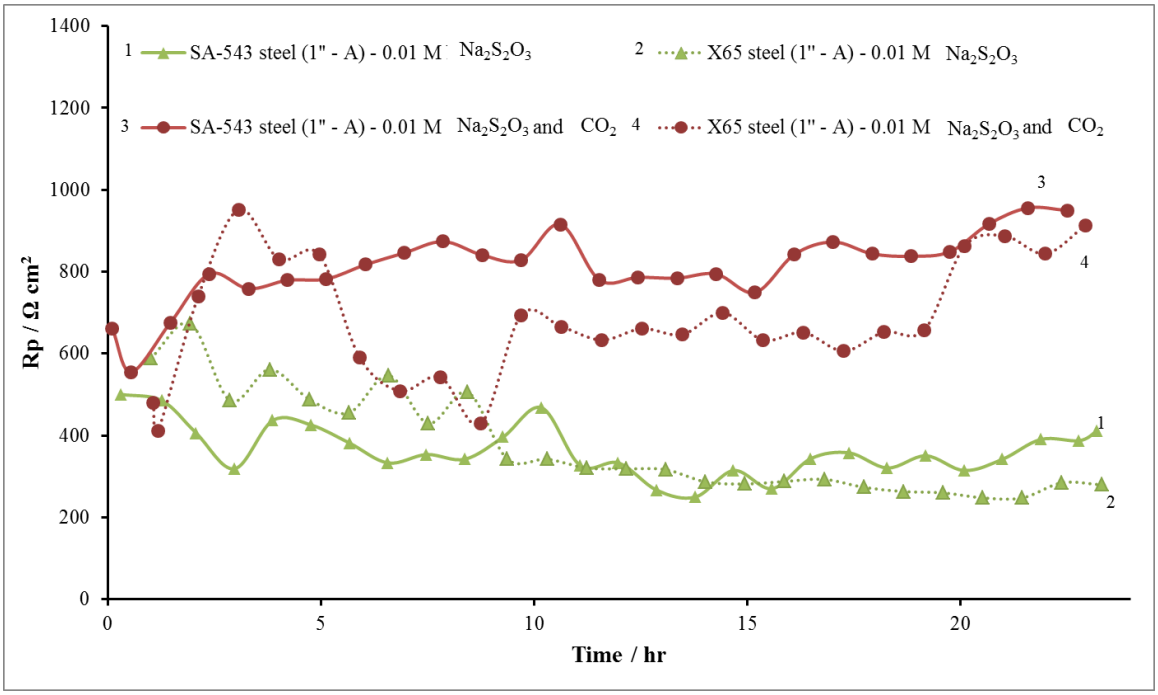

Figure 4.14 R_p of SA-543 and X65 steels with time in 0.01 M $Na_2S_2O_3$ solution with 30% oil at 1 m/s and 25°C.

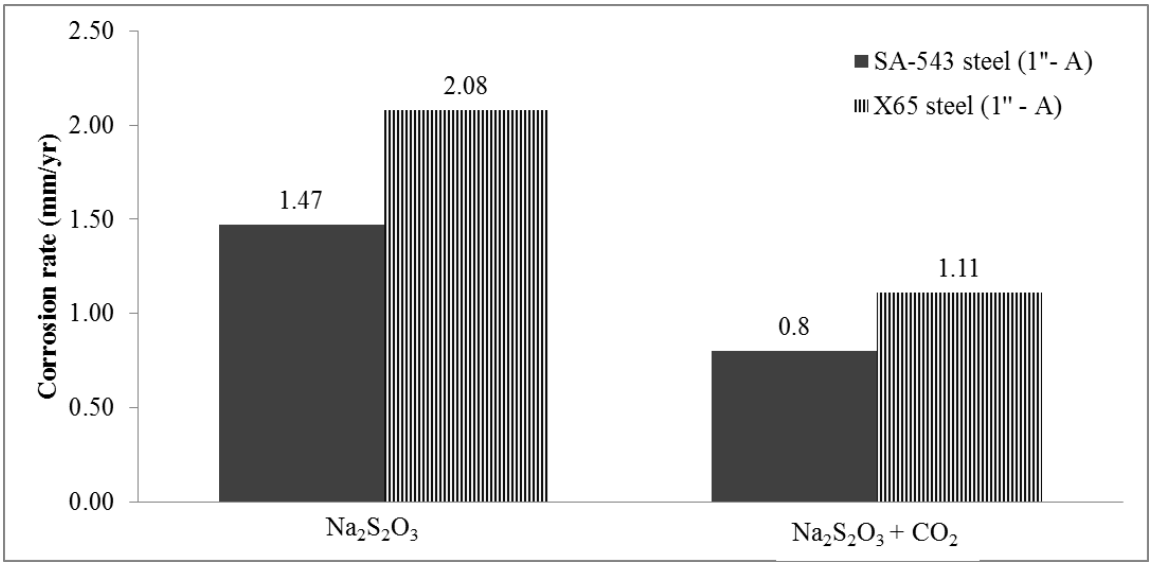

Figure 4.15 Corrosion rate measurement of SA-543 and X65 steels in 0.01 M $Na_2S_2O_3$ solution with 30 % oil at 25°C and 1 m/s.

4.2.2 Emulsion at different oil percentages

Experiments were performed to test the corrosion behaviour of SA-543 steel at different oil percentages of emulsions. The experiments were performed at 25 ± 1 °C, and pH of 5. The experiments were performed for 10, 20 and 30% of oil with 0.01 M $Na_2S_2O_3$ and CO_2. The polarization curves in Figure 4.16 and corrosion current values in Table 4.7 depicts that the corrosion rate dwindles as the oil percentage increases. The corrosion rate was higher for 10 % of oil and lowest for 30 % of oil. With the increase in oil percentage, the conductivity of emulsion also declined.

Figure 4.17 shows the trend of R_p with time. There were many fluctuations in R_p with time that might be because of the sticking of oily phase to steel surface and its removal by the flow. The corrosion current decreased as the concentration of oily phase increased. This is due to the formation of oily phase layer on the steel surface which inhibits the steel dissolution [27,87]. The presence of oily layer adsorbed on the surface increase the activation energy of the reaction thus reducing the corrosion **[**4**]**.

Table 4.7 Tafel extrapolation for different oil percentages

		1" - A		
		30 % Oil	20 % Oil	10 % Oil
SA-543	Ecorr (V)	-0.115	-0.127	-0.143
	Icorr (µA)	40.3	51	70.5

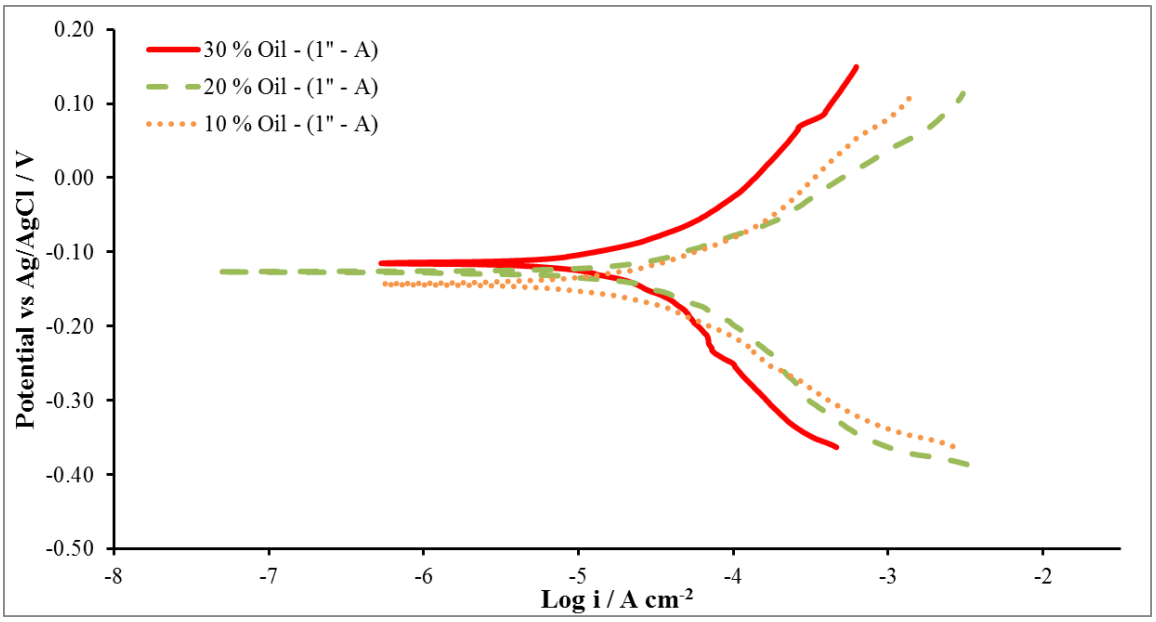

Figure 4.16 The potentiodynamic polarization curves of SA-543 steel in different oil percentages with 0.01 M $Na_2S_2O_3$ + CO_2 solution at 25^{o}C and 1 m/s.

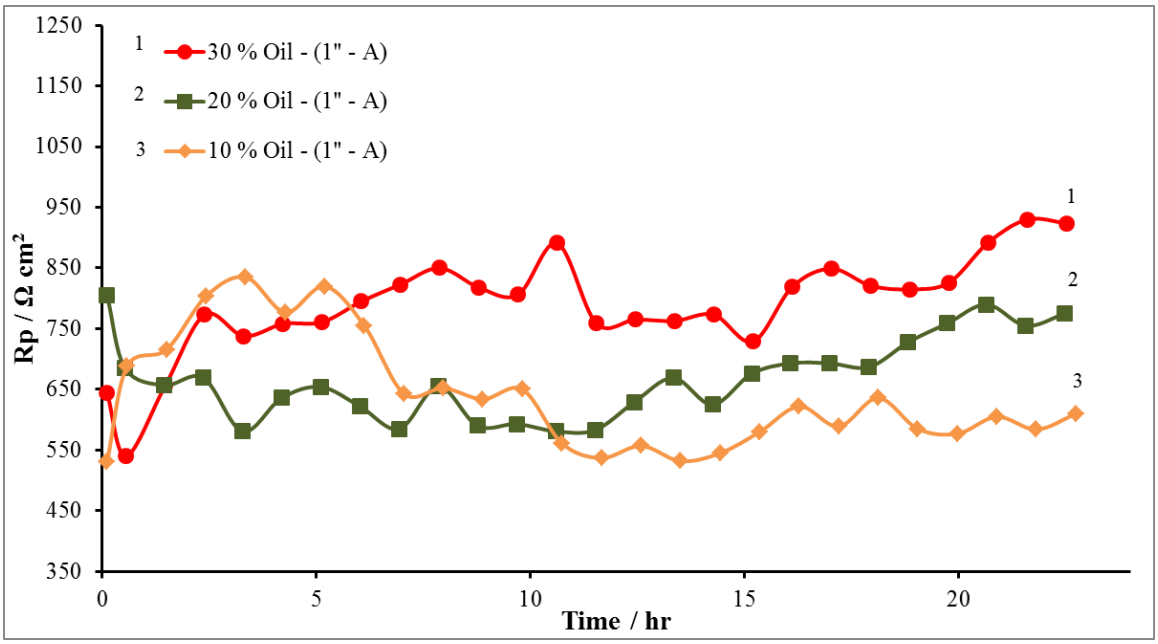

Figure 4.17 R_p of SA-543 steel with time in 0.01 M $Na_2 S_2O_3$ + CO_2 solution at different oil percentages.

Corrosion rate as shown in Figure 4.18 supports the description explained above. The difference between corrosion rates of 10% oil and 20% oil is not that significant because the emulsion formed at these two percentages has almost similar emulsion properties.

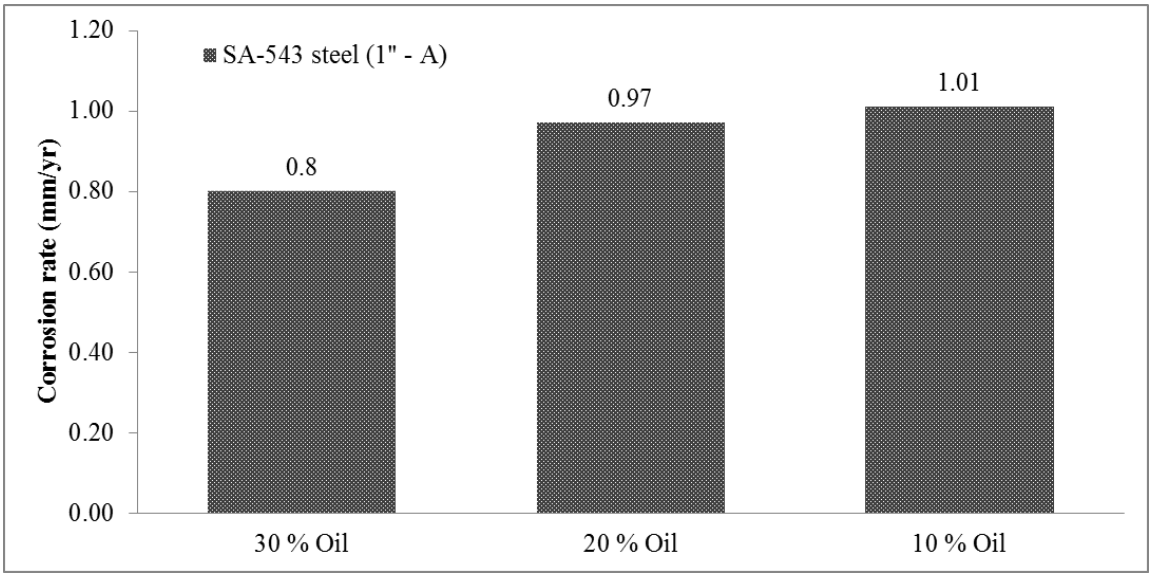

Figure 4.18 Corrosion rate measurement of SA-543 and X65 steels at different oil percentages.

4.2.3 Effect of velocity on corrosion

The experiments for different velocities were performed on SA-543 steel in 30 % Oil emulsion with CO_2. The Figure 4.19 and Table 4.8 show that the corrosion current dwindles and the corrosion potential moves to noble direction as we augment the velocity. The difference of corrosion potential was more noticeable in 1.5 m/s as compared to 0.5 m/s and 1 m/s. The increase in speed results an increase in reduction reaction at the steel surface, thus forming sulphide film at higher rate **[**4**,**60**]**. The thick sulphide film formed at higher velocity is adherent which hinders the dissolution of iron ions into the emulsion thus inhibiting the corrosion current **[**32**]**. Protective iron carbonate layer cannot be removed by mechanical forces exerted by flow alone **[**18**]**.

Figure 4.20 shows the variation of polarization resistance with time. The polarization resistance increased with time for 1.5 m/s but remained almost constant for 1 and 0.5 m/s. Polarization resistance was higher at higher velocities. The R_p for 1.5 m/s and 1 m/s was almost the same for the first 10 hours, then it is believed that the formation of a tenacious sulphide film increased the corrosion resistance at high speed.

The corrosion rate as shown in Figure 4.21 depicts a significant difference in corrosion rates of 0.5 m/s and 1.5 m/s. The corrosion rate is almost double as we reduce the velocity from 1.5 m/s to 0.5 m/s.

Table 4.8 Tafel extrapolation for different velocities.

		1" - A		
		0.5 m/s	1 m/s	1.5 m/s
SA-543	Ecorr (V)	-0.136	-0.115	-0.053
	Icorr (µA)	49.9	40.3	11.9

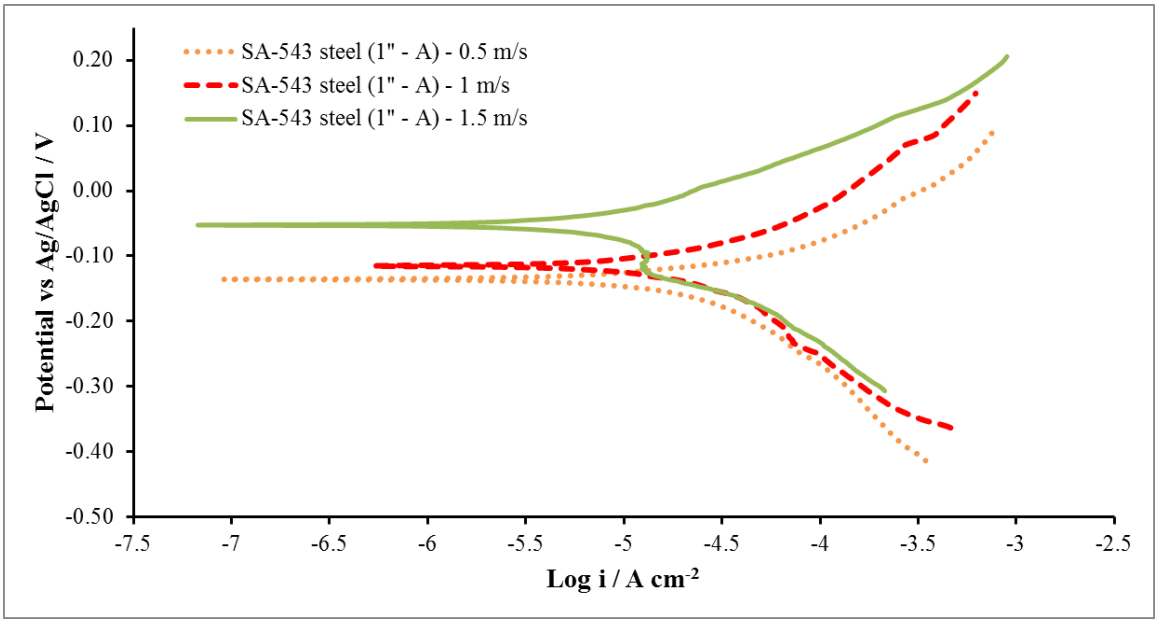

Figure 4.19 The potentiodynamic polarization curves of SA-543 steel in 0.01 M $Na_2S_2O_3$ + CO_2 solution with 30% oil at 25°C and different velocities.

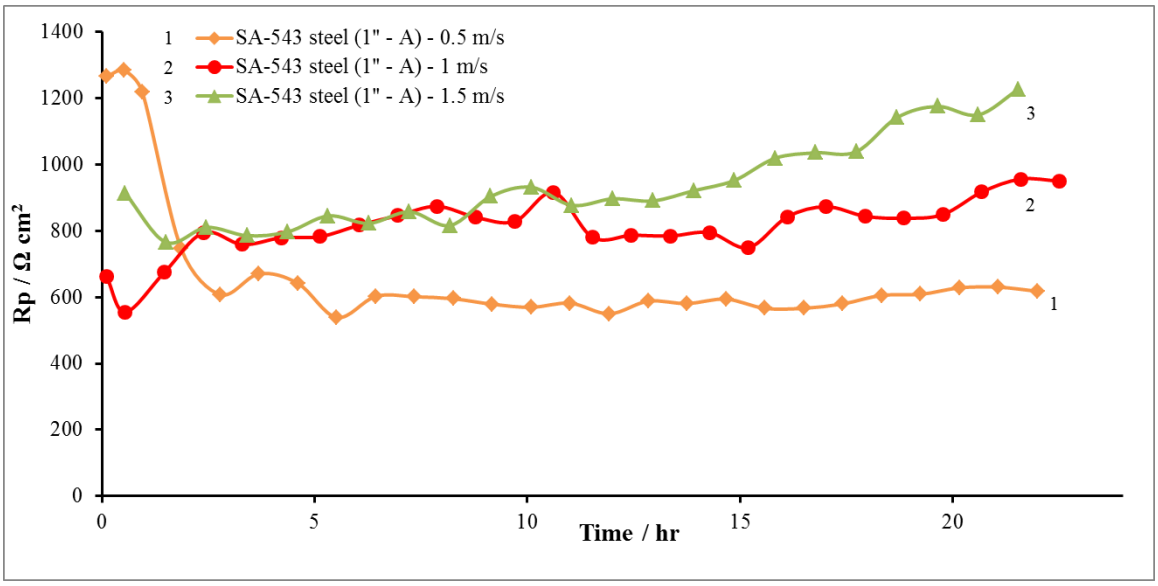

Figure 4.20 R_P of SA-543 steel with time in 0.01 M $Na_2S_2O_3$ + CO_2 solution with 30% oil at 25°C and different velocities.

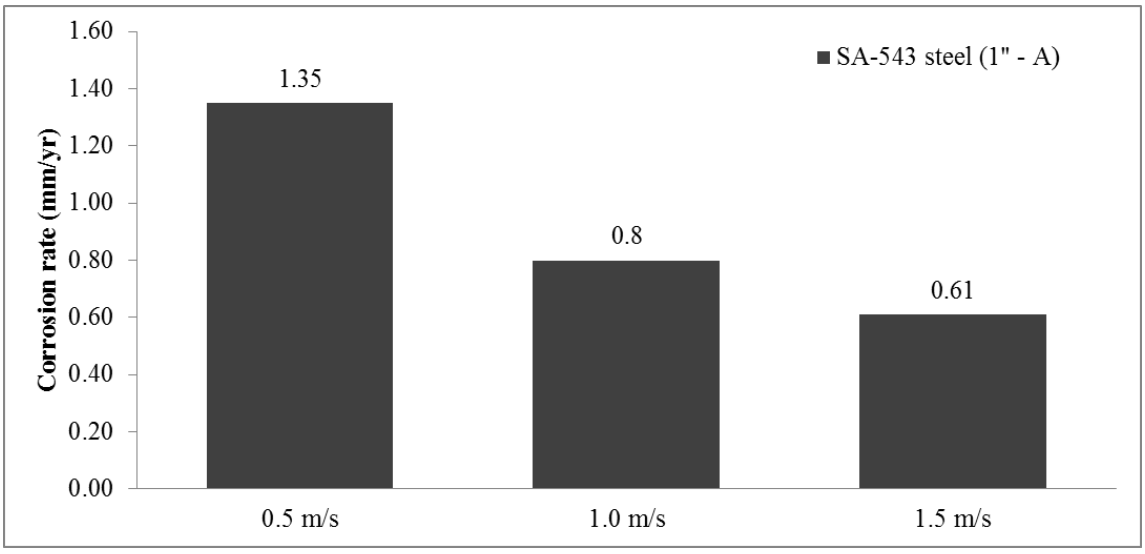

Figure 4.21 Corrosion rate measurement of SA-543 steel at different velocities.

4.2.4 Effect of temperature on corrosion

SA-543 was tested at 25 °C and 50 °C with 30 % oil emulsion and CO_2 at pH of 5 and 1 m/s. The results were contrary to the belief that corrosion increases with temperature. The corrosion rate increases with temperature, since the temperature changes the kinetics parameter of a chemical reaction [84]. In our case, with an increase in temperature the corrosion current slightly dwindled from and the corrosion potential moved towards the noble side as shown in Figure 4.22 and Table 4.9.

Figure 4.23 shows that the R_p for the 50 °C was initially less than 25 °C suggesting that the corrosion increases with temperature, but an increase in R_p at later stages suggests that some tenacious film has been formed on the surface. The formation of that protective film took some time to become firm and inhibit corrosion at later stages of the experiment. The increase in temperature enhances the kinetics of reaction and various interfacial reactions. The kinetics of reduction of thiosulphate and carbonate anion will speed up at higher temperature. At high temperatures pyrite (firm iron sulphide film) is usually forming [31,60]. It is adherent, and inhibits iron dissolution significantly. The precipitation of iron carbonate film also increased significantly with temperature **[**15**]**.

Table 4.9 Tafel extrapolation for different temperatures.

		1" - A	
		25 °C	50 °C
SA-543	Ecorr (V)	-0.115	-0.031
	Icorr (µA)	40.3	17

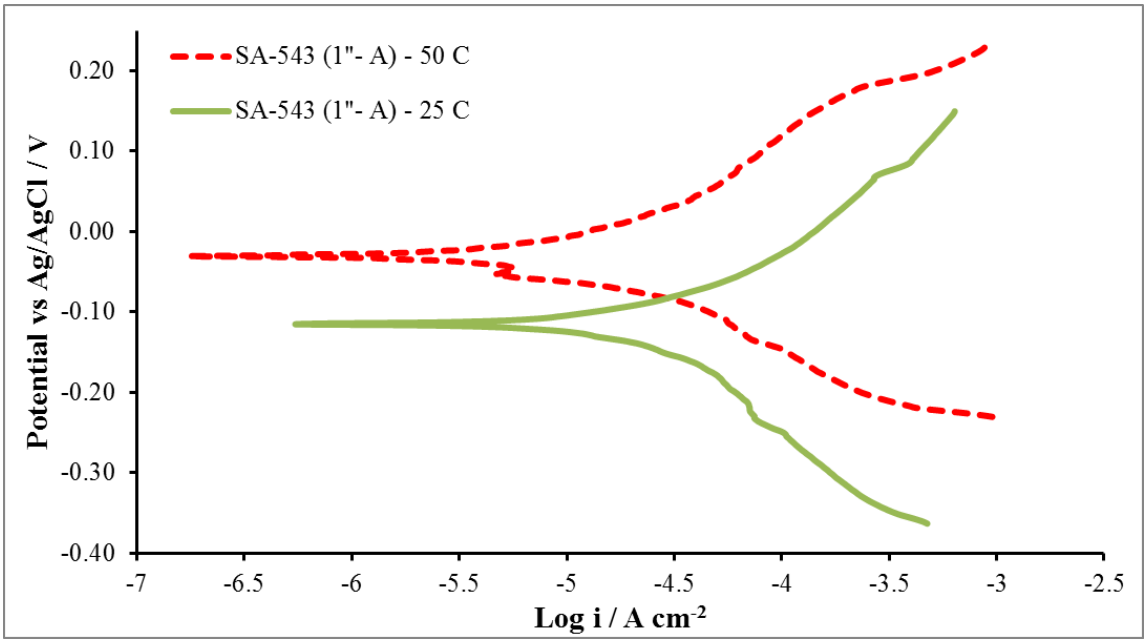

Figure 4.22 The potentiodynamic polarization curves of SA-543 steel in 0.01 M $Na_2S_2O_3$ + CO_2 solution with 30% oil at 1 m/s and different temperatures.

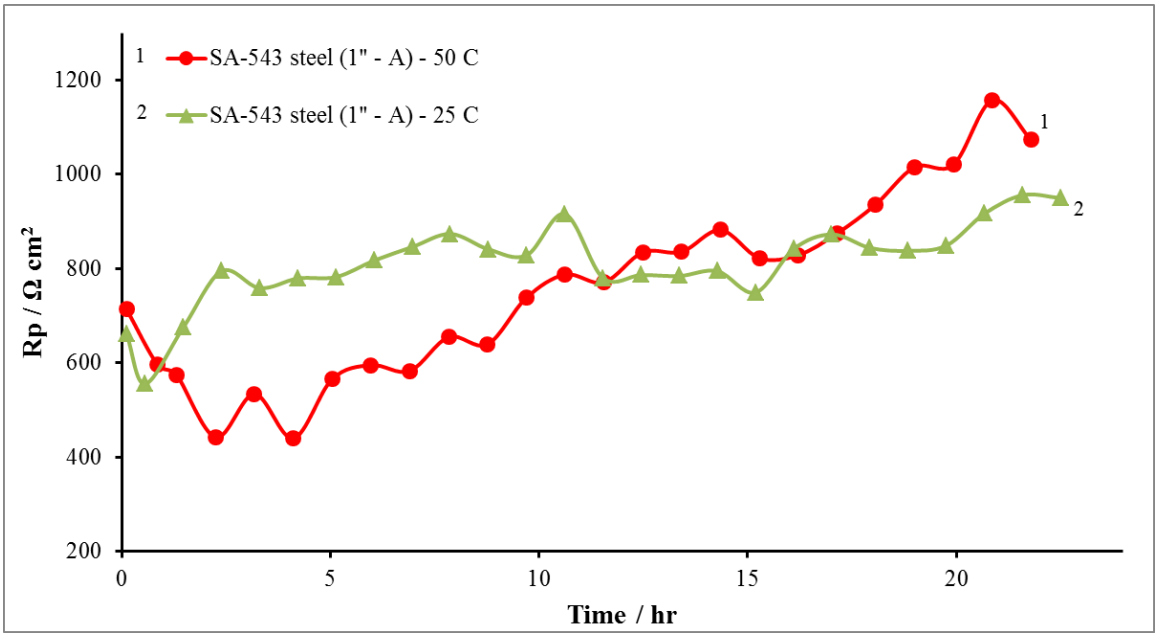

Figure 4.23 R_P of SA-543 steel with time in 0.01 M $Na_2S_2O_3$ + CO_2 solution with 30% oil at 1 m/s and different temperatures.

Figure 4.24 shows the numerical values of the corrosion rate at two different temperatures. The results support the explanation as mentioned above.

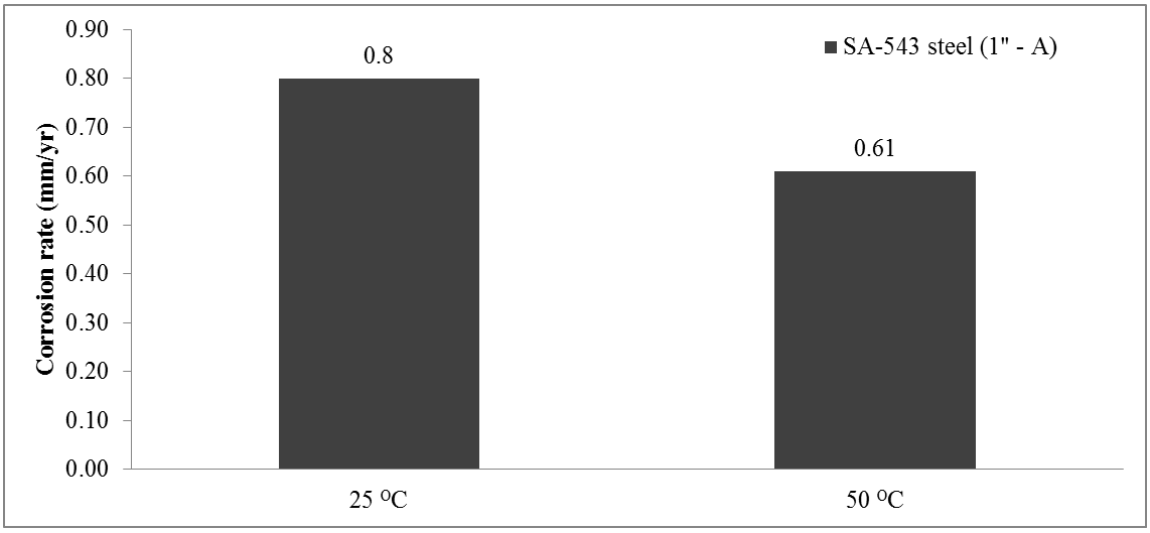

Figure 4.24 Corrosion rate measurement of SA-543 steel at 1 m/s and different temperatures.

4.2.5 Corrosion behaviour along the pipe length with D80 oil

Experiments were performed with emulsion containing 30% D80 oil and using middle test section. The inlet and exit electrodes of 1'' pipe and inlet and middle electrode of 0.5'' pipe were used. As the middle test section comprises of 1'' and 0.5'' pipes, the flow in the 1'' pipe was maintained at 1 ± .02 m/s and at 0.5'' pipe it augmented to 4 m/s according to continuity equation. It was observed that the corrosion current (I_{corr}) at 1'' inlet (1'' – A) was higher than the 1'' exit (1'' – B) as shown in Table 4.10. But the corrosion potential of (1'' – A) was more positive than (1'' – B). Reduction in pipe area resulted in an increase of velocity. The corrosion current at middle of 0.5'' pipe (0.5'' – B) was higher than at the inlet (0.5'' – A). The R_p for 30 % Oil D80 oil slightly increased with time for 1''- A and 1''-B electrodes.

The removal of film at (1''- A) and the high corrosion current as compared to (1'' – B) can be attributed to the turbulence and swirl of emulsion entering into the test section as just before the start of 1'' test section where there are spiral mixers for the formation of emulsion. The edges of gaskets between the flanges also induce perturbations into the flow. The flow is undeveloped and has high turbulent kinetic energy as compared to downstream electrode. The results were surprising when the corrosion rate of (0.5''- A) was less than the (0.5'' – B). The flow pattern was confirmed using a simulation software, it showed that as the flow move through the contraction area, the positioning of the (0.5'' – A) lies in the vena contracta region and the flow strikes the wall just ahead of the (0.5'' – A) electrode as shown in Figure 4.25, that's why corrosion at (0.5'' – B) was higher than (0.5'' – A).

Table 4.10 Tafel extrapolation along the pipe length.

		1" - A	1" - B	0.5" - A	0.5" - B
SA-543	Ecorr (V)	-0.115	-0.140	-0.098	-0.054
	Icorr (µA)	40.3	39.4	24.7	41.5

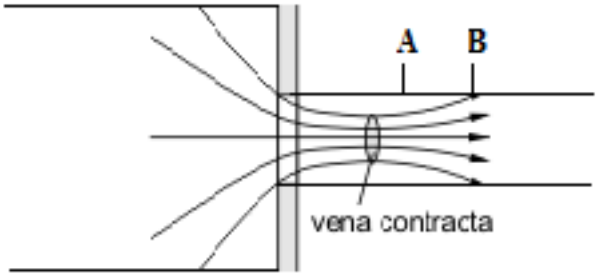

Figure 4.25 Vena contracta demonstration.

When a flow moves from larger area to smaller area the flow converges as it reaches the entrance of smaller area because the fluid streamlines cannot abruptly change direction. This contraction of flow will be maximum at a point known as vena contracta and it will be slightly downstream of the orifice. After vena contracta point flow starts to diverge. The flow again strikes the wall at point B. So, point B will experience higher corrosion as compared to point A. Working electrode (0.5''- A) was placed at point A. That's why it experienced less corrosion.

At high speed like 4 m/s and due to converging effect, the surface shear stress increases due to the boundary layer developed by reattached flow **[**34**]**.

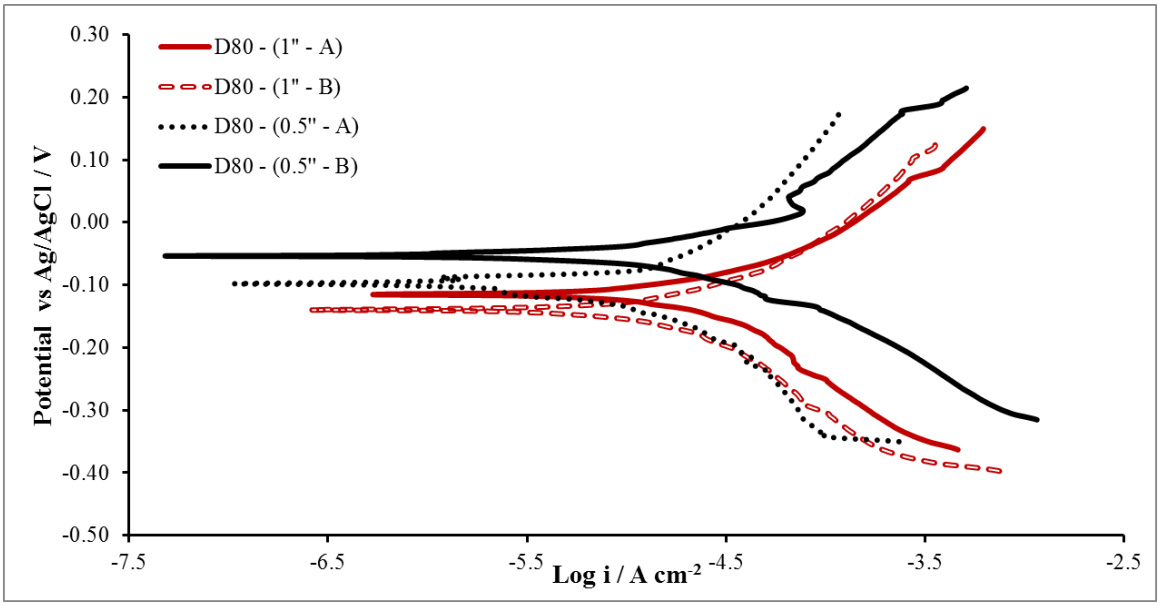

Figure 4.26 The potentiodynamic polarization curve for Exxsol D80 oil at 30% Oil and 70 % 0.01 M $Na_2S_2O_3$.

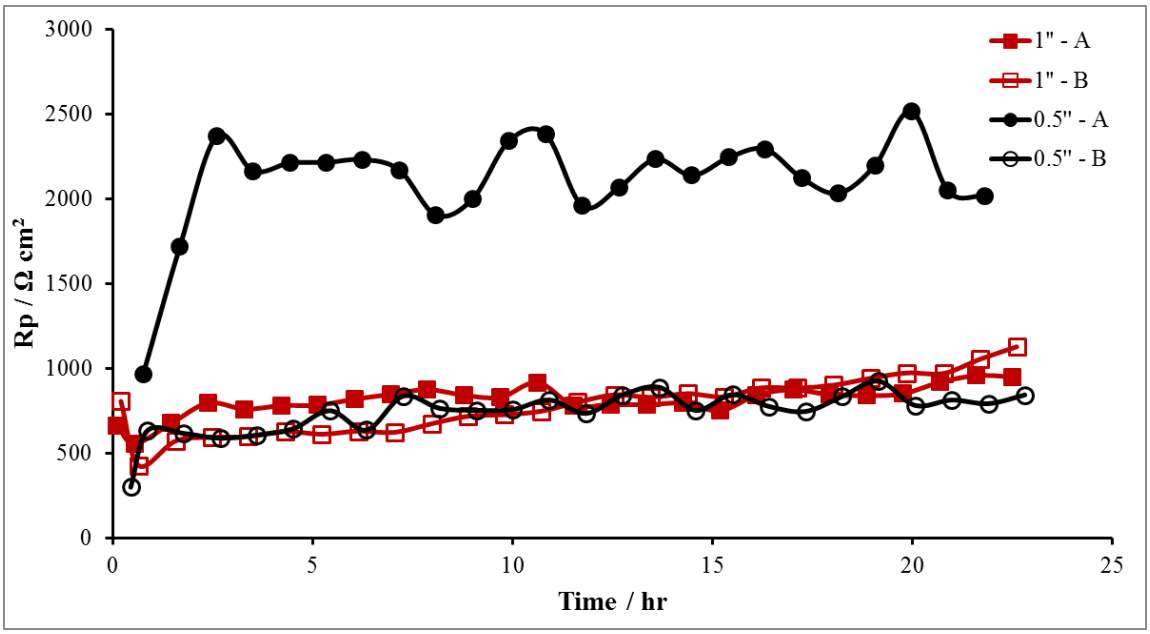

Figure 4.27 Corrosion rate trend for Exxsol D80 oil at 30% Oil and 70% 0.01 M $Na_2S_2O_3$.

Figure 4.28 shows the corrosion rate values at different electrodes positions. The corrosion rate decreased along the way and increased at the middle of 0.5'' pipe. The corrosion rate was higher in 0.5'' pipe than 1'' pipe except at the entrance of 0.5'' pipe.

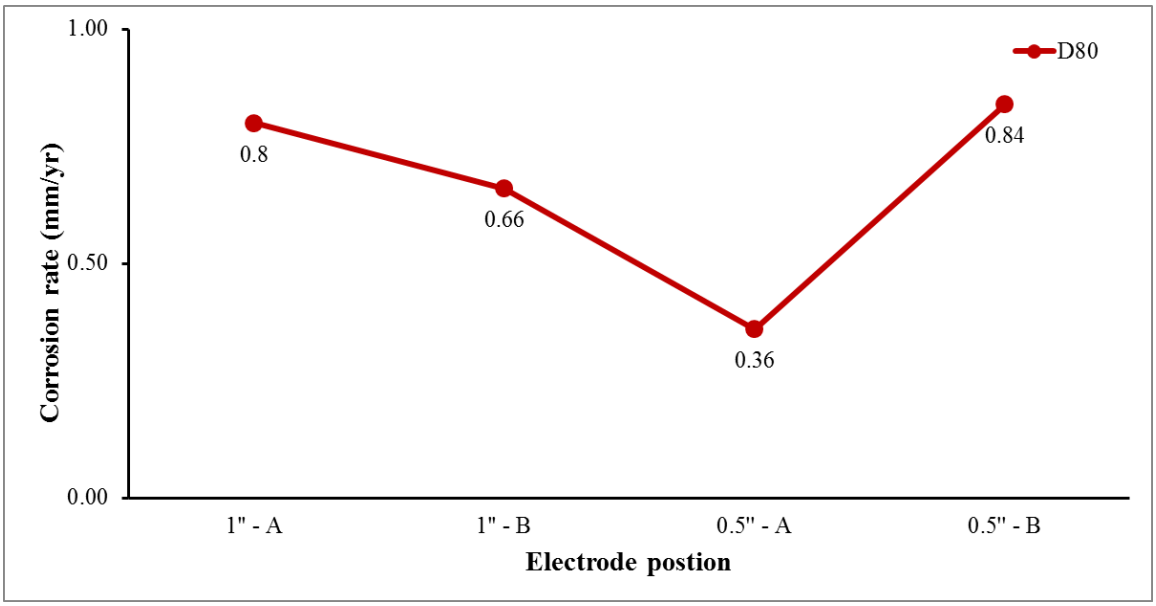

Figure 4.28 Corrosion rate of D80 oil at different electrode positions.

4.2.6 Effect of oil viscosity on corrosion

Two oils with different viscosity were examined. As the pumping power of crude oil extraction pump is dependent on the oil viscosity. Experiments were performed using Exxsol D130 oil with kinematic viscosity of 6.89 mm^2/s, other properties of D130 are listed in Table 3.1. Emulsion was produced using 30 % D130 oil and was allowed to flow in middle test section. The results showed in Figure 4.29 and Table 4.11 depicts that the I_{corr} of (1'' – A) was higher for D130 oil as compared to D80 oil. Similar results were obtained for the rest of the electrodes. Corrosion rates were higher for the high viscous oil. The βa and βc were higher for (1''- A) and (1''- B) electrodes with D130 oil as compared to D80 oil. As viscosity and shear stress are directly proportional, by increasing the viscosity the shear stress increases. Higher shear stress reduces the chances of formation of protective film or retard the film growth **[**37**]**. Thus the film form on the test electrode will be loosen and can easily be eroded making it more susceptible to corrode.

Table 4.11 Tafel extrapolation for different oils.

		D80		D130	
		1" - A	1" - B	1" - A	1" - B
SA-543	Ecorr (V)	-0.115	-0.140	-0.119	-0.127
	Icorr (µA)	40.3	39.4	46.1	44

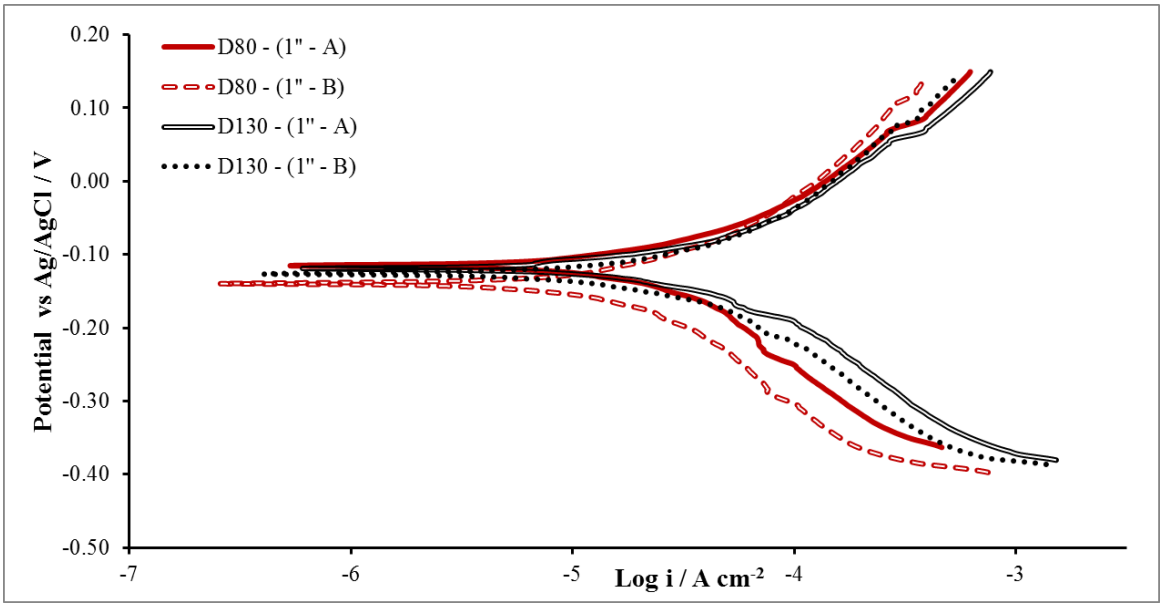

Figure 4.29 The potentiodynamic polarization curve for Exxsol D80 and D130 oils at 30% Oil and 70% 0.01 M $Na_2S_2O_3$.

Figure 4.30 shows the variation of R_p with D130 and D80 oil. The R_p of D130 oil is lesser than D80 oil. The R_p of D80 oil slightly increased with time, but the R_p of D130 oil remained almost constant. Corrosion rate of D130 oil depicted in Figure 4.31 matched the trend of D80 oil. The difference in corrosion rate of (1'' – A) and (1'' – B) electrode was higher for D130 oil.

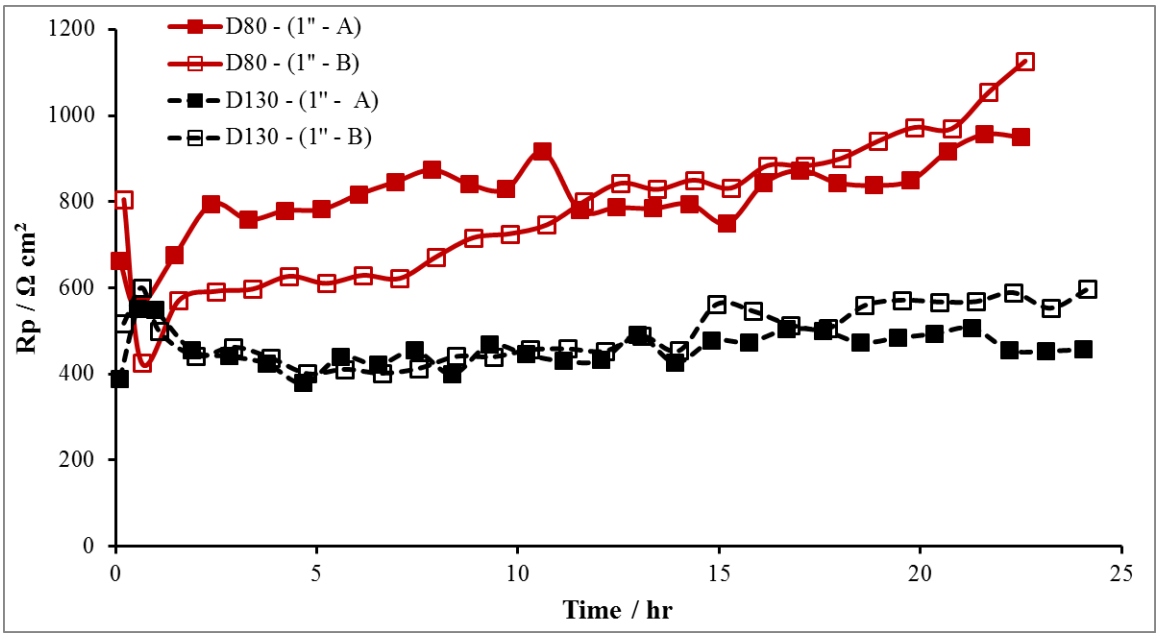

Figure 4.30 Corrosion rate trend for Exxsol D80 and D130 oils at 30% Oil and 70% 0.01 M $Na_2S_2O_3$.

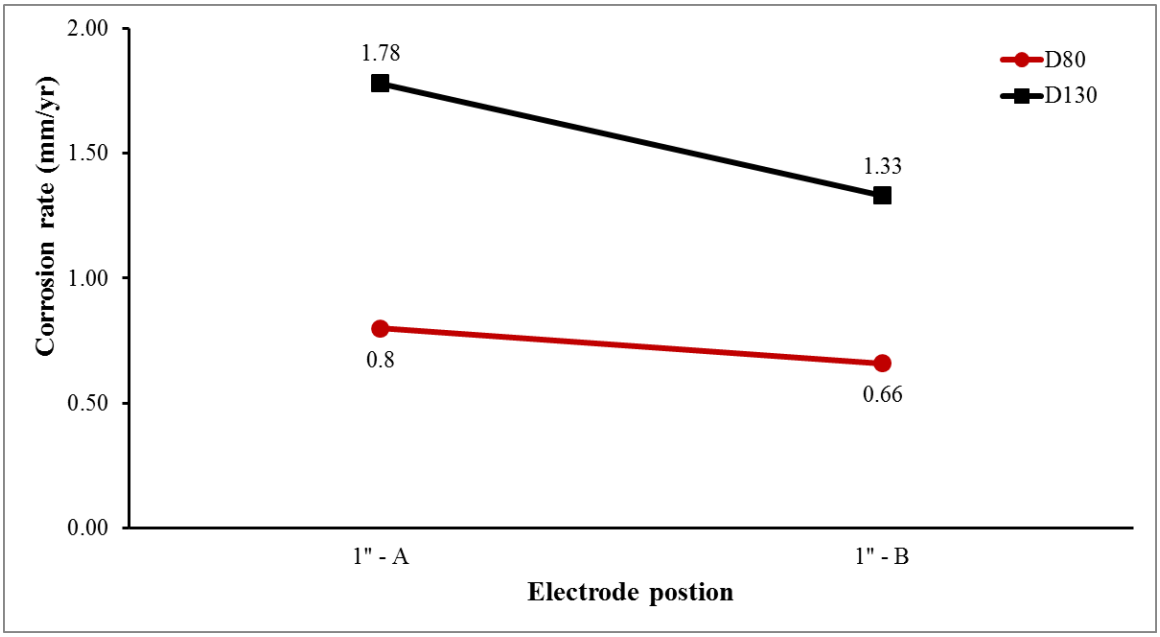

Figure 4.31 Corrosion rate of D80 and D130 oils at different electrode positions.

CHAPTER 5

CONCLUSIONS AND RECOMMENDATIONS

5.1 Conclusions

An experimental study was performed using the rotating cylinder electrode and flow loop to test the corrosion of SA-543 and X65 steels when they are exposed to oil-in-water emulsion containing $Na_2S_2O_3$ and CO_2.

5.1.1 Rotating Cylinder Electrode

- The corrosion resistance of SA-543 steel is better than X65 steel. Improved corrosion resistance of SA-543 steel can be attributed to the higher Cr, Mo and Ni contents.
- The addition of CO_2 to a solution containing $S_2O_3^{2-}$ increased the R_P of SA-543 steel due to the formation of more stable and firm iron carbonate ion film, while the addition of NaCl reduced the R_P. The presence of NaCl with CO_2 and $S_2O_3^{2-}$ reduced the R_P indicating that Cl^- is more effective than CO_2.
- R_P was increased with increasing oil concentration due to the inertness of oil and the formation of oily phase layer on the steel surface which inhibits the steel dissolution.
- The increase in the velocity raised the R_P due to the acceleration of diffusion species towards the steel surface for reduction reaction.
- SA-543 steel is a promising material to be used for fabrication oil and gas pipelines sine it has higher R_P and strength than X65 steel.

5.1.2 Flow Loop

- SA-543 steel showed higher corrosion resistance properties than X65 steel due to its higher Cr, Ni and Mo content.
- The reduction of thiosulphate anion forms a layer of sulphide film on the steel and it was present in all the experiments.
- The tenacity of film is dependent upon temperature. At high temperatures firm film formed which inhibited corrosion significantly.
- The presence of CO_2 along with $Na_2S_2O_3$ corroborates in corrosion reduction due to the precipitation of carbonate film on the steel surface.
- The presence of oily phase and its inertness reduces the corrosion current. The corrosion rate increased by decreasing the oily phase.
- The kinetics of reduction reaction increases as the velocity was increased; this speed up the growth of thick sulphide film and inhibited the corrosion.
- The corrosion rate was higher at the inlet electrode due to higher turbulent kinetic energy.
- The corrosion rate increased by increasing the viscosity of oil. This was attributed to the fact that the shear stresses are directly proportional to the viscosity. Higher shear stresses also hinder the formation of stable film on the test electrodes.

5.2 Recommendation

The following recommendations are made in order to extend the scope of the area of research.

- Perform the characterization of the films formed on the test electrodes to better understand the inhibition phenomenon.
- Perform corrosion experiments using inlet, middle and exit electrodes.
- Perform experiments using 2'' test section.
- Replace the metal test section with transparent test section, to observe the flow pattern and relating the corrosion behaviour to emulsion flow pattern.

REFERENCES

[1] E. Gileadi, *Electrode Kinetics for Chemists, Chemical Engineers and Material Scientists*. New York, USA: VCH publishers, 1993.

[2] H.Q. Becerra, C. Retamoso, and D.D. Macdonald, "The corrosion of carbon steel in oil-in-water emulsions under controlled hydrodynamic conditions", *Corrosion Science*, vol. 42, pp. 561 - 575, 2000.

[3] W.P. Jepson, and R. Menezes, "The effects of oil viscosity on sweet corrosion in multiphase oil, water/gas horizontal pipelines", *The NACE international annual conference and Corrosion show*, 1995.

[4] G.A. Zhang, and Y.F. Cheng, "Electrochemical corrosion of X65 pipe steel in oil/water emulsion", *Corrosion Science*, vol. 51, pp. 901-909, 2009.

[5] R.A. Mac Kay, and N.S. Dixit, "Micro emulsions as photogalvanic cell-fluids-the surfactant thionine iron (II) system", *Journal of physical chemistry*, vol. 86, p. 4593, 1982.

[6] M.G. Fontana, *Corrosion Engineering*, 3rd ed.: McGraw Hill, 1986.

[7] C. Retamoso, "Electrochemical processes in emulsions", Bucaramanga, Colombia, Final Report, ICP Project 1993.

[8] D.Y. Pena, Industrial University of Santander, Bucaramanga, Colombia, MSc. Thesis 1994.

[9] F. Echeverria, Industrial University of Santander, Bucaramanga, Colombia, MSc. Thesis 1995.

[10] (2014, February) Wikipedia. [Online]. http://en.wikipedia.org/wiki/Hydrogen_sulfide

[11] Mariano Alberto Kappes, "Evaluation of thiosulphate as a substitute for hydrogen sulphide in sour corrosion fatigue studies", The Ohio State University, Ohio, PhD Dissertation 2011.

[12] B.J. Berkowitz, and F.H. Heubaum, "The role of hydrogen in sulfide stress cracking of low alloy steels", *Corrosion*, vol. 40, no. 5, pp. 240 - 245, 1984.

[13] A.G. Wikjord, T.E. Rummery, F.E. Doern, and D.G. Owen, "Corrosion and deposition during the exposure of carbon steel to hydrogen sulphide water

solutions", *Corrosion Science*, vol. 20, pp. 651-671, 1980.

[14] M. Gomez-Duran, and D.D Macdonald, "Stress corrosion cracking of sensitized Type 304 stainless steel in thiosulfate solution: I. Fate of the coupling current", *Corrosion Science*, vol. 45, no. 7, pp. 1455 - 1471, 2003.

[15] M. Koteeswaran, "CO_2 and H_2S corrosion in pipelines", University of Stavanger, MS Thesis 2010.

[16] Y. Chen, and W.P. Jepson, "EIS measurement for corrosion monitoring under multiphase flow conditions", *Electrochimica Acta*, vol. 44, no. 24, pp. 4453-4464, 1999.

[17] X. Zhou, and W.P. Jepson, "Corrosion in three phase oil/water/gas slug flow in horizontal pipes", Corrosion in multiphase systems center, Ohio, 1994.

[18] Y. Yang, B. Brown, and S. Nesic, "Study of Protective Iron Carbonate Layer Dissolution in a CO_2 Corrosion Environment", *NACE Corrosion Conference and Expo*, Salt Lake City, 2012.

[19] H.M. Ezuber, "Influence of temperature and thiosulfate on the corrosion behavior of steel in chloride solutions saturated in CO_2", *Materials and Design*, vol. 30, pp. 3420 - 3427, 2009.

[20] S. Nesic, J. Postlethwaite, and S. Olsen, "An Electrochemical Model for Prediction of Corrosion of Mild Steel in Aqueous Carbon Dioxide Solutions", *Corrosion Science*, vol. 52, no. 4, pp. 280 - 294, 1996.

[21] H. Takabe, and M. Ueda, "The formation behaviour of corrosion protective films of low Cr bearing steels in CO_2 environments", *NACE Corrosion Conference and Expo*, Houston, 2001.

[22] S. Nesic, and L. Lunde, "Carbondioxide corrosion of carbon steel in two-phase flow", *Corrosion*, vol. 50, no. 9, pp. 717 - 727, 1994.

[23] D.A. Lopez, T. Perez, and S.N. Simison, "The influence of microstructure and chemical composition of carbon and low alloy steel in CO_2 corrosion", *Materials and Design*, vol. 24, pp. 561 - 575, 2003.

[24] Q. Zhichao, X. Chunming, C. Zeliang, Z. Zhihong, and Z. Chun, "Major corrosion factors in the CO_2 and H_2S coexistent environment and the relative anti-corrosion method:Taking Tazhong I gas field, Tarim Basin", *Petroleum exploration and*

development, vol. 39, no. 2, pp. 256 - 260, 2012.

[25] D.A. Lopez, W.H. Schreiner, S.R. Sanchez, and S.N. Simison, "The influence of carbon steel microstructure and on corrosion layers: An XPS and SEM characterization", *Applied Surface Science*, vol. 207, pp. 69 - 85, 2003.

[26] S. Tsujikawa, T. Yamada, A. Miyasaka, M. Ueda, and S. Ando, "Alternative for evaluating sour gas resistance of Low Alloy Steels and Corrosion Resistant Alloys", *Corrosion*, vol. 34, no. 5, pp. 409-419, 1993.

[27] M. Kappes, G.S. Frankel, N. Sridhar, and R.M. Carranza, "Reaction paths of thiosulphate during corrosion of carbon steel in acidified brines", *Journal of Electrochemical Society*, vol. 4, no. 159, pp. C195-C204, 2012.

[28] M. Mullet, B. Sophie, A. Mustapha, G.J. Marie, and E.J. Jacques, "Surface chemistry and structural properties of mackinawite prepared by reaction of sulphide ions with metallic iron", *Geochimica et Cosmochimica Acta*, vol. 66, no. 5, pp. 829 - 836, 2002.

[29] D.W. Shoesmith, P. Taylor, M.G. Bailey, and D.G. Owen, "The Formation of Ferrous Monosulfide Polymorphs during the Corrosion of Iron by Aqueous Hydrogen Sulfide at 21°C", *Journal of Electrochemical Society*, vol. 127, no. 5, pp. 1007 - 1015, 1980.

[30] W. Sun, S. Nesic, and S. Papavinasam, "Kinetics of iron sulphide and mixed iron sulphide/carbonate scale precipitation in CO_2/H_2S corrosion", in *Corrosion Conference*, New Orleans, 2006.

[31] M. Singer, J. Khamis, and S. Nesic, "Experimental study of sour top of the line corrosion using a novel experimental setup", *Corrosion*, vol. 69, no. 6, p. 624, 2013.

[32] Y.S. Choi, S. Nesic, and S. Ling, "Effect of H_2S on the CO_2 corrosion of carbon steel in acidic solutions", *Electrochimica Acta*, vol. 56, pp. 1752 - 1760, 2011.

[33] M. Kappes, G S. Frankel, N. Sridhar, and R M. Carranza, "Corrosion behaviour of Carbon steel in acidified, thiosulphate containing brines", *Corrosion*, vol. 10, no. 68, p. 872, 2012.

[34] W.H. Ahmed, M.M. Bello, M. Nakla, and A. Sarkhi, "Flow and mass transfer downstream of an orifice under flow accelerated corrosion conditions", *Nuclear Engineering and Design*, vol. 252, pp. 52 - 67, 2012.

[35] W.H. Ahmed, "Evaluation of the proximity effect on flow-accelerated corrosion", *Annals of Nuclear Energy*, vol. 37, pp. 598 - 605, 2010.

[36] M. El-Gammal, W.H. Ahmed, and C.Y. Ching, "Investigation of wall mass transfer characteristics downstream of an orifice", *Nuclear Engineering and Design*, vol. 242, pp. 353 - 360, 2012.

[37] D. Zheng, D. Che, and Y. Liu, "Experimental investigation on gas–liquid two-phase slug flow enhanced carbon dioxide corrosion in vertical upward pipeline", *Corrosion Science*, vol. 50, pp. 3005 - 3020, 2008.

[38] X.H. Zhao, Y. Han, Z.Q. Bai, and B. Wei, "The experiment research of corrosion behaviour about Ni-based alloys in simulant solution containing H_2S/CO_2", *Electrochimica Acta*, vol. 56, pp. 7725 - 7731, 2011.

[39] R. Hamzah, D.J. Stephenson, and J.E. Strutt, "Erosion of material used in petroleum production", *Wear*, vol. 186-187, pp. 493-496, 1995.

[40] J. Perdomo, J.J. Gonzalez, A. Viloria, H. Veer, and Y. Abreu, "Corrosion of API 5L B and X52 in crude oil/water/gas mixtures", *Materials Performance*, no. 39, p. 76, 2000.

[41] H. Ma, X. Cheng, G. Li, S. Chen, and Z. Quan, "The influence of hydrogen sulphide on corrosion of iron under different conditions", *Corrosion Science*, vol. 42, pp. 1669 - 1683, 2000.

[42] K.L.J. Lee, and S. Nesic, "EIS investigation of CO_2/H_2S corrosion", *Corrosion Conference*, Houston, 2004.

[43] K.L.J. Lee, and S. Nesic, "The effect of trace amount of H_2S on CO_2 corrosion investigated by using the EIS technique", *Corrosion Conference* , Houston, 2005.

[44] B. Brown, and S. Nesic, "CO_2/H_2S corrosion under scale forming conditions", *Corrosion Conference*, Houston, 2005.

[45] H. Fang, S. Nesic, B. Brown, and S. Wang, "General CO_2 corrosion in high salinity brines", *Corrosion NACE expo*, 2006.

[46] H. Fang, D. Young, and S. Nesic, "Corrosion of mild steel in the presence of elemental sulphur", in *NACE Corrosion Conference and Expo*, 2008.

[47] J. Han, D. Young, and S. Nesic, "Characterization of the passive film on mild steel

in CO_2 environments", in *17th International Corrosion Congress*, 2009.

[48] E. Abelev, J. Sellberg, T.A. Ramanarayanan, and S.L. Bernasek, "Effect of H_2S on Fe corrosion in CO_2-saturated brine", *Journal of Material Science*, vol. 44, pp. 6167 - 6181, September 2009.

[49] E. Abelev, T.A. Ramanarayanan, and S.L. Bernasek, "Iron corrosion in CO_2 - Brine at low H_2S concentrations: An electrochemical and surface science study", *Journal of Electrochemical Society*, vol. 156, no. 9, pp. 331 - 339, 2009.

[50] D. Jingen, Y. Wei, L. Xiaorong, and D. Xiaoqin, "Influence of H_2S content on CO_2 corrosion behaviors of N80 tubing steel", *Petroleum Science and Technology*, vol. 29, no. 13, pp. 1387 - 1396, 2011.

[51] LI. Wen-Fei, Z. Yan-Jun, and X. Yan, "Corrosion Behavior of 110S Tube Steel in Environments of high H_2S and CO_2 content", *Journal of iron and steel research*, vol. 19, no. 12, pp. 59 - 65, 2012.

[52] J. Ning, J. Zheng, D. Young, B. Brown, and S. Nesic, "A Thermodynamic Study of Hydrogen Sulfide Corrosion of Mild Steel", *NACE Corrosion Conference and Expo*, 2013.

[53] T. Tanupabrungsun, B. Brown, and S. Nesic, "Effect of pH on CO_2 Corrosion of Mild Steel at Elevated Temperatures", *NACE Corrosion Conference and Expo*, Salt Lake City, 2013.

[54] M.G. Faichuk, S. Ramamurthy, and W.M. Lau, "Electrochemical behaviour of Alloy 600 tubing in thiosulphate solution", *Corrosion Science*, vol. 53, pp. 1383 - 1393, 2011.

[55] M.H. Nazari, S.R. Allahkaram, and M.B. Kermani, "The effects of temperature and pH on the characteristics of corrosion product in CO_2 corrosion of grade X70 steel", *Materials and Design*, vol. 31, pp. 3559 - 3563, 2010.

[56] P.H. Tewari, M.G. Bailey, and A.B. Campbell, "The erosion corrosion of carbon steel in aqueous H_2S solutions up to 120^{o}C and 1.6 MPa pressure", *Corrosion Science*, vol. 19, pp. 573-585, 1979.

[57] A Neville, T Hodgkiess, and J.T Dallas, "A study of the erosion corrosion behaviour of engineering steels for marine pumping applications", *Wear*, vol. 186-187, p. 497, 1995.

[58] S. Arzola, J.M. Flores, R.D. Romero, and J. Genesca, "Electrochemical behaviour of API X70 steel in hydrogen sulphide containing solutions", *Corrosion*, vol. 62, no. 5, p. 433, May 2006.

[59] W. Sun, and S. Nesic, "A mechanistic model for H_2S corrosion of mild steel", *NACE Corrosion Conference and Expo*, 2007.

[60] B.R. Tian, and Y.F. Cheng, "Electrochemical Corrosion behaviour of X-65 steel in the simulated oil sand slurry. I: Effects of Hydrodynamic condition", *Corrosion Science*, no. 50, pp. 773 - 779, 2008.

[61] X. Tang, X.Y. Xu, and Y.F. Cheng, "Electrochemical corrosion behavior of X-65 steel in the simulated oil-sand slurry. II: Synergism of erosion and corrosion", *Corrosion Science*, vol. 50, pp. 1469-1474, 2008.

[62] J. Feyeri et al., "Erosion-Corrosion of carbon steels in a laboratory: Three phase flow", *Corrosion*, vol. 64, no. 2, pp. 175-186, February 2008.

[63] U. Lotz, and J. Postlethwaite, "Erosion-corrosion in disturbed two phase liquid/particle flow", *Corrosion Science*, vol. 30, pp. 95-106, 1990.

[64] W.P. Jepson, "The effect of flow characteristics on sweet corrosion in high-pressure, three phase, oil/water/gas horizontal pipeline", *Prevention of pipeline corrosion conference*, 1994.

[65] A.K. Vuppu, W.P. Jepson, and U. Ohio, "The effect of temperature in sweet corrosion of horizontal multiphase carbon steel pipelines", in *SPE Asia pacific oil and gas conference*, Australia, 1994.

[66] M. Gopal, A. Kaul, and W.P. Jepson, "Mechanisms contributing to enhanced corrosion in three phase slug flow in horizontal pipes", *Corrosion Conference*, 1995.

[67] C. Kang, R. Wilkens, and W.P. Jepson, "The effect of slug frequency on corrosion in high pressure, inclined pipelines", in *The NACE international Annual Conference and Exposition*, 1996.

[68] W.P. Jepson and S. Bhongale, "Effect of temperature, pressure and oil composition on corrosion rate in horizontal multiphase slug flow", I/UCRC Corrosion in multiphase systems engineering, Ohio, USA, 1996.

[69] R. Zhang, M. Gopal, and W.P. Jepson, "Development of a mechanistic model for predicting corrosion rate in multiphase oil/water/gas flows", *Corrosion*, 1997, p.

601.

[70] S.E. Hernandez, S. Hernandez, H. Rincon, and J.R. Vera, "Flow induced CO_2 and H2S corrosion studies using dynamic field tester in crude oil wells", *Corrosion*, vol. 58, no. 10, p. 881, October 2002.

[71] B. Brown, K.L. Lee, and S. Nesic, "Corrosion in multiphase flow containing small amounts of H_2S", *Corrosion*, 2003.

[72] B. Brown, S.R. Parakala, and S. Nesic, "CO_2 corrosion in the presence of trace amounts of H_2S", *Corrosion Conference*, Houston, 2004.

[73] M.A. Habib, R. Ben-Mansour, H.M. Badr, and M.E. Kabir, "Erosion and penetration rates pf a pipe protruded in a sudden contraction", *Computers and Fluids*, vol. 37, pp. 146-150, 2008.

[74] B. Brown, D. Young, and S. Nesic, "Localized corrosion in and H_2S/CO_2 environment", *17th International Corrosion Congress*, 2009.

[75] A. Mohammad Nor, M.F. Suhor, M.F. Mohamed, M. Singer, and S. Nesic, "Corrosion of Carbon Steel in High CO_2 Environment: Flow Effect", in *NACE Corrosion Conference and Expo*, 2011.

[76] M.F. Suhor, M.F. Mohamed, M.A. Nor, M. Singer, and S. Nesic, "Corrosion of Mild Steel in High CO_2 Environment: Effect of the $FeCO_3$ Layer", in *NACE Corrosion Conference and Expo*, 2012.

[77] (2014, February) Institute for Corrosion and Multiphase Technology. [Online]. http://www.corrosioncenter.ohiou.edu/facilities/h2scorrosionloop.asp

[78] (2014, February) Erosion Corrosion Research Center. [Online]. http://www.ecrc.utulsa.edu/research.html

[79] (2014, February) Fontana Corrosion Center. [Online]. http://www.matsceng.ohio-state.edu/~frankel/fcc/research.htm

[80] (2014, February) Curtin University. [Online]. http://corrosion.curtin.edu.au/research/

[81] J. Villarreal, D. Laverde, and C. Fuentes, "Carbon-Steel corrosion in multiphase slug flow and CO_2", *Corrosion Science*, no. 48, pp. 2363 - 2379, 2006.

[82] G. Schmitt, "Effect of elemental sulfur on corrosion in sour gas systems", *Corrosion*, vol. 47, no. 4, pp. 285-308, April 1991.

[83] Z.A. Foroulis, "Electrochemical behaviour and corrosion of iron in aqueous sulfidic solution", *Material Corrosion*, vol. 6, no. 31, pp. 463 - 470, 1980.

[84] B. Mishra, S. Al-Hassan, D.L. Olson, and M.M. Salama, "Development of a predictive model for activation-controlled corrosion of steel in solutions containing CO_2", *NACE Corrosion Conference*, Houston, Texas, 1997, pp. 852 - 859.

[85] F. Farelas, B. Brown, and S. Nesic, "Iron Carbide and its Influence on the Formation of Protective Iron Carbonate in CO_2 Corrosion of Mild Steel ", *NACE Corrosion Conference and Expo*, Salt Lake City, 2013.

[86] G. Schmitt, "Effect of elemental sulphur on corrosion in sour gas systems", *Corrosion*, vol. 4, no. 47, pp. 258 - 308, 1991.

[87] M. Mullet, S. Boursiquot, and M. Abdelmoula, "Surface chemistry and structural properties of mackinawite", *Geochim. Cosmochim. Acta*, vol. 5, no. 66, pp. 829 - 836, 2002.

VITAE

Name	Muhammad Nauman Zafar
Nationality	Pakistani
Date of Birth	September 9th, 1989
Email	zafar.nauman@gmail.com
Address	Core-C, Research Institute, KFUPM, Dhahran, KSA
Academic Background	B.E Mechanical Engineering
	National University of Sciences and Technology (NUST)
	EME Campus, Rawalpindi, Pakistan

Publications:

- Effect of $Na_2S_2O_3$ and CO_2 in oil/water emulsions on corrosion resistance of SA-543 & X65 steels. (Submitted)
- Investigating the corrosion resistant of SA-543 & X65 steels in an emulsion containing H_2S and CO_2 using novel emulsion flow loop. (Submitted)
- Investigation of oil-in-water emulsion corrosion using H_2S and CO_2 in vertical flow. (Submitted)
- Effect of H_2S and CO_2 in oil-in-water emulsion corrosion. *NACE Corrosion 2014*, San Antonio, USA, March 2014.

- Corrosion behavior of SA-543 & X65 steels when exposed to oil-in-water emulsions in presence of $Na_2S_2O_3$, CO_2 and NaCl. *15th Middle East Corrosion Conference, Bahrain*, February 2014.
- A novel emulsion flow loop for studying the corrosion of engineering materials in emulsion flow in presence of $Na_2S_2O_3$ and CO_2. *15th Middle East Corrosion Conference, Bahrain*, February 2014.